AD-A094 758 AIR FORCE INST OF TECH WRIGHT-PATTERSON AFB OH SCHOO--ETC F/G 14/2
EFFECT OF TEST RHOMBUS SIZE ON PHOTON CORRELATION LASER VELOCIM--ETC(U)
DEC 80 I HAMID
UNCLASSIFIED AFIT/GAE/AA/80D-7 NL

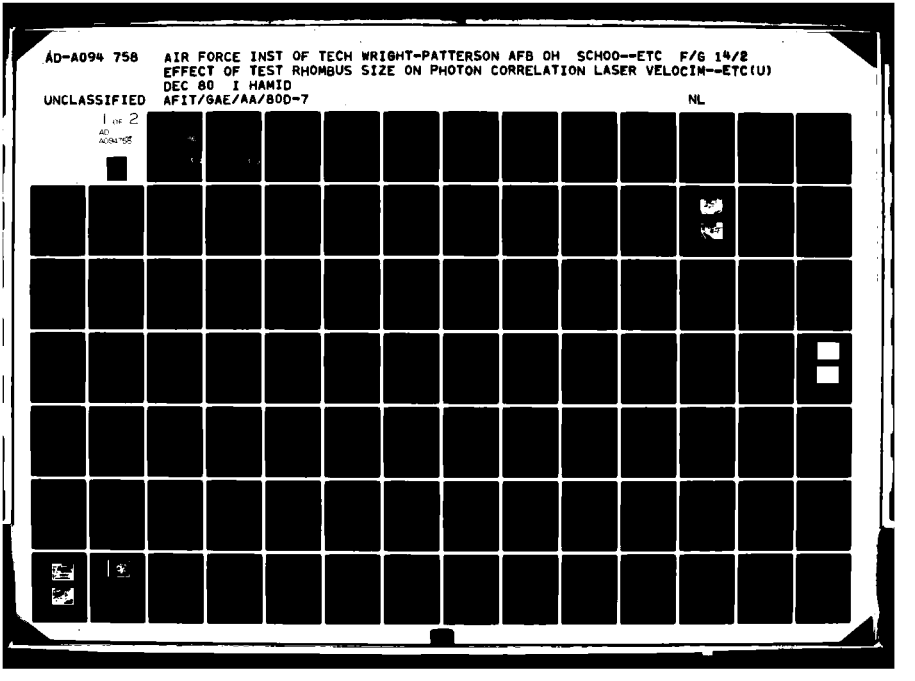

LEVEL II

DEPARTMENT OF THE AIR FORCE

AIR UNIVERSITY (ATC)

AIR FORCE INSTITUTE OF TECHNOLOGY

Wright-Patterson Air Force Base, Ohio

23 JAN 1981

AFIT/GAE/AA/80D-7

APPROVED FOR PUBLIC RELEASE AFR 190-17.

Laurel A. Lampela

LAUREL A. LAMPELA, 2Lt, USAF
Deputy Director, Public Affairs

Air Force Institute of Technology (ATC)
Wright-Patterson AFB, OH 45433

Accession For	
NTIS GRA&I	☑
DTIC TAB	☐
Unannounced	☐
Justification	
By	
Distribution/	
Availability Codes	
Dist	Avail and/or Special
A	

EFFECT OF TEST RHOMBUS SIZE ON PHOTON CORRELATION LASER VELOCIMETER DATA

THESIS (10)

Insha Hamid
Flt. Lt. PAF

AFIT/GAE/AA/80D-7

11 Nov 80

(12) 126

Approved for public release; distribution unlimited

12225

AFIT/GAE/AA/80D-7

EFFECT OF TEST RHOMBUS SIZE ON PHOTON CORRELATION LASER VELOCIMETER DATA

THESIS

Presented to the Faculty of the School of Engineering

of the Air Force Institute of Technology

Air Training Command

in Partial Fulfillment of the

Requirements for the Degree of

Master of Science

by

Insha Hamid, B.E.

Flt. Lt. PAF

Graduate Aeronautical Engineering

December 1980

Preface

This study was conceived to critically evaluate the effects of test rhombus size on the Laser Velocimeter data by measuring velocity and turbulence intensity in a plane free jet and to compare the results with published data and theory. In the past hot-wire or hot-film anemometers provided the principal means of measuring flow velocities and velocity correlation functions. These mechanical probes will undoubtedly continue to be important in experimental fluid mechanics, but their limitations and artificial disturbances in the flow make new measuring techniques worthy of careful considerations. The Laser Velocimeter system offers distinct and substantial advantages over alternative methods for measurements in particular flow situations.

During the course of this study, a number of people helped me and their cooperation and cheerful attitude turned this work into an enjoyable venture. I wish to thank my thesis advisor, Dr. Harold E. Wright, who contributed a great deal to my understanding of the subject and equipment at various stages. His encouragement and enthusiasm certainly helped me in expelling the fear of the unknown. Dr. William C. Elrod, Capt. (Dr.) George D. Catalano, Mr. William Baker, Mr. Harold Leroy and Mr. Carl Short provided valuable assistance at various stages and helped me finish on time. I am grateful to all of these benefactors and am glad to have the opportunity to acknowledge their debt in this preface.

Above all, I wish to express a full sense of gratitude to my wife, Asiya, for her indulgence, patience and understanding.

Insha Hamid

Contents

Contents (Cont'd)

List of Figures

List of Figures (Cont'd)

List of Tables

List of Symbols

Symbol		Units
b	Jet half-width	cm
b_o	Jet half-width at the nozzle exit plane	cm
C_{scat}	Scattering cross-section	
D_I	Focused beam diameter	mm
d_m	Diameter of measuring control volume	mm
d_ω	Solid angle	steradian
g	Acceleration due to gravity	m/sec^2
h	Planck's constant	mW-sec
I	Intensity of scattered light	mW/m^2
I_o	Beam intensity	mW/m^2
N_{ph}	Number of fringes observed by PM tube	
N_s	Number of scattered photons	
n	Number of fringes	
n_s	Number of scattered photons per unit time	
P_a	Atmospheric pressure	kg_f/cm^2

List of Symbols (Cont'd)

Symbol		Units
P_c	Chamber pressure	kg_f/cm^2
P_L	Laser power	mW
P_o	Total pressure	kg_f/cm^2
P_s	Power scattered by a small particle	mW
Q_{scat}	Scattering efficiency factor	
r_o	Beam radius (at $1/e^2$)	mm
r_p	Particle radius	mm
S	Fringe spacing	μm
T_c	Chamber temperature	°K
T_o	Total temperature	°K
U	Local mean velocity in X-direction	mps
u	Perturbation velocity in X-direction	mps
U_{cen}	Center-line velocity	mps
U_{cor}	Mean velocity in the potential core	mps
v	Perturbation velocity in Y-direction	mps

List of Symbols (Cont'd)

Symbol		Units
X	Axial coordinate axis in the direction of primary flow	cm
X_{PC}	Length of potential core	cm
y	Coordinate axis in the horizontal plane normal to X-axis	cm
$y_{\frac{1}{2}}$	Distance from the center-line of the jet the the point where $U = \frac{1}{2} U_{cen}$	cm
$\Delta\tau$	Time spent by a particle in measuring control volume	sec
η	Turbulence intensity	
η_c	Efficiency of light collecting system	
η_q	Quantum efficiency	
μ	Refractive index	
ν	Signal frequency	sec^{-1}
ν_D	Doppler frequency	sec^{-1}
ρ	Density of media	kg_m/cm^3
ψ	Stream function	m^2/sec
σ	Experimental constant	

List of Symbols (Cont'd)

Symbol		Units
τ_{xy}	Shearing stress in a plane perpendicular to X-Y plane	kg_f/cm^2
θ	Convergence half angle of the laser beam	Degrees
λ	Wave length of incident light	μm

Abstract

This thesis provides an experimental evaluation of the effects of test rhombus size on the photon correlation Laser Velocimeters. It also provides a method and results of laser beam expansion and beam diameter measurements. The study was carried out in the turbulent regime of a plane free jet 1 cm by 10 cm.

The flow field measurements were made at 25 jet widths downstream of the nozzle exit, at M = 0.3, using 0.5, 1.0, 1.1, 3.0, 5.0, 7.0 and 10.0 mm diameter laser beams. The measurements taken were mean velocities and turbulence intensities which were then compared with the theoretical predictions and earlier experimental results.

The Laser Velocimeter System provided accurate results for mean velocities, but was found to be limited at higher turbulence levels (above 20%) for beam diameters up to and less than 5.0 mm.

EFFECT OF TEST RHOMBUS SIZE

ON PHOTON CORRELATION LASER VELOCIMETER DATA

I. Introduction

Background

The use of the Laser Doppler Velocimeter (LDV) for flow measurement was first demonstrated in 1964. Since that time, it has evolved from a novel laboratory instrument into a practical tool for research and industrial use. The LDV's obvious advantage is its ability to make measurements without perturbing the flow under conditions where other instruments provide questionable results or cannot be used at all.

The Malvern Laser Velocimeter system used in this investigation does not require "seeding" of the flow, but can function with normal laboratory air where sufficient natural seeding exists. This investigation is a continuation of a joint research effort of AFWAL/FIMM and AFIT involving the critical evaluation of the photon correlation Laser Velocimeter system.

Previous Work

During the past years, a number of students completed their master's thesis using the Malvern Laser Velocimeter system here at the Air Force Institute of Technology (Refs 2, 5, 7). Their work ranged from the evaluation of LDV for flow diagnostics in a classical two-dimensional jet to the "real world" study of flow inside the inlet

duct of a jet engine. These investigations revealed a good correlation exists between the mean velocity profiles obtained from the LDV and other diagnostic tools, but the LDV system, like the hot wire system, was found to be partially ineffective in highly turbulent flow fields. However, the turbulence intensities revealed a close agreement with other diagnostic tools for turbulence levels between 2% to 30%.

In those earlier studies, a focused laser beam of 1.1 mm diameter was used, giving a small focal volume at the cross-over point of the split beam. No attempt was made in those studies to expand the beam and see the effects on photon correlation with an increased focal volume.

Objectives

The objectives of the investigation were (1) expand the 1.1 mm input laser beam using apertures and beam expanding lenses and measure the diameters of the expanded beams; (2) map a prescribed flow field employing various beam sizes; (3) compare the results of the Laser Velocimeter to theoretical predictions and published results; and (4) evaluate the effectiveness of the test rhombus size on the photon correlation Laser Velocimeter data.

Approach

The present investigation is centered in the determination of the effects of test rhombus size on the photon correlation function of the Laser Velocimeter system. The approach to this study was to use an existing set-up, a classical two-dimensional jet developed by Shepard (Ref 9). This jet is very well documented and the hot wire results obtained by Shepard and Cerullo (Ref 2) have proven to correlate well with the classical predictions. However, the LDV results obtained by

Cerullo show that the system was ineffective at high velocities and high turbulence intensities. In the present study, the flow field at 25 jet width downstream of the nozzle exist, at M = 0.3, was selected for the investigation, using various beam diameters. The effects of increased beam size on the photon correlation would then be documented.

Scope

This paper would include a method of expanding an input laser beam to a specific size by the use of an appropriate aperture and beam expanding lens, and a technique to measure the output beam diameter. The 1.1 mm input laser beam, after passing through aperture (A-6) and beam expanding lens (L-3), would produce various beam sizes by merely changing the focal length of the output beam. Flow field measurements would be made at 25 jet widths downstream of the nozzle exit, at M = 0.3, using 0.5, 1.0, 1.1, 3.0, 5.0, 7.0 and 10.0 mm diameter laser beams. Data obtained from the Laser Velocimeter would be reduced for the mean velocities and turbulence intensitites which would then be compared with the theoretical predictions and earlier experimental results.

This paper would deal critically with two problem areas of Laser Velocimeter systems; namely, limitations on the high velocity measurements due to optical set-up and limitations on the signal output of the system due to lower beam intensities with constant seeding. This first chapter is followed by a chapter on test apparatus. Chapters III, IV andV describe instrumentation, principle of operation and experimental procedure, respectively. Results and their discussion

are outlined in Chapter VI, followed by chapters on conclusions and recommendations. Some analytical solutions, experimental results and experimental data can be found in the appendices.

II. Test Apparatus

The test apparatus used was the existing 1 cm by 10 cm two-dimensional nozzle constructed by Shepard (Ref 9). Later, some internal modifications were made to the system by Cerullo (Ref 2) in order to achieve lower turbulence and a thinner boundary layer at the exit. The apparatus used by Cerullo was not modified for the present study, as it was found suitable for Laser Velocimeter measurements. Figure 1 shows the set-up of the two-dimensional nozzle and its various components.

This particular test bed is very well documented. A great deal of investigation has been carried out by Shepard and Cerullo using a hot wire anemometer and the laser doppler anemometer. The central aim was not to further investigate the flow field of this test bed, but to use LDV from a totally different approach and comapre the results with the earlier experimental results.

Test conditions selected were those which could provide a basis for comparison of results to the earlier studies and still remain within the working limitations of the LDV. Therefore, a nozzle exit Mach number of 0.3 and test plane of 25 jet widths downstream of the nozzle exit were selected for the investigation. This test condition provided exit velocity of 100 mps and Reynold's number (based on jet exit widths) of 6.25×10^4. Figure 2 shows the plane of interest where measurements were taken by the Laser Velocimeter system.

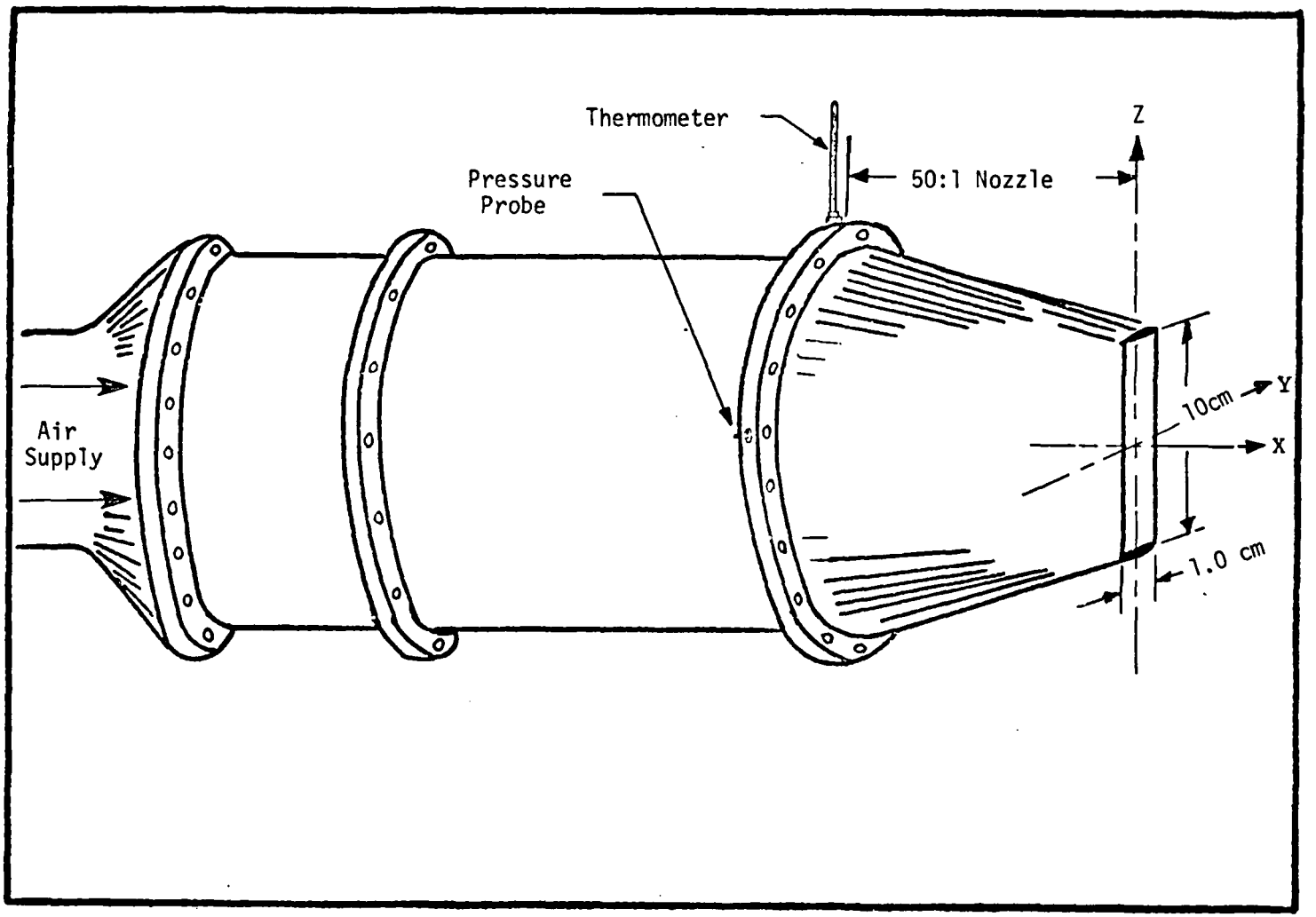

Figure 1. Schematic of Two-Dimensional Nozzle

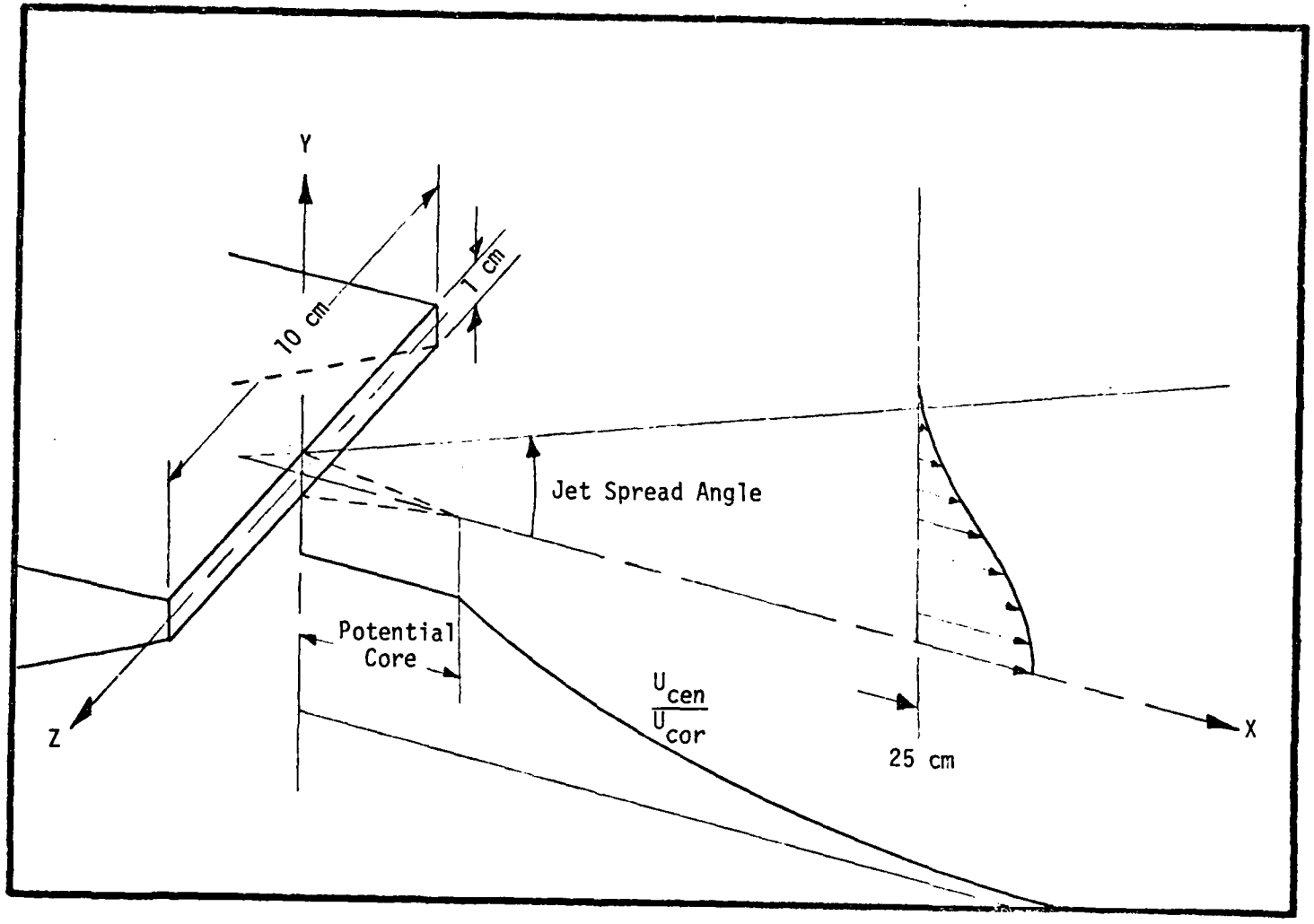

Figure 2. Flow Field Schematic

III. Instrumentation

Instrumentation for data acquisition included Marriam manometer and a thermometer for pressure and temperature observations, respectively, to monitor nozzle exit Mach number. The Laser Velocimeter System was fixed on an optical bench, which in turn was mounted on a traversing mechanism. The discharge nozzle and the components of the LDV system are discussed in the proceding section.

Nozzle

A 100 inch Marriam fluid manometer was used to measure the total pressure in the nozzle chamber and, hence, determine the exit Mach number. A thermometer, positioned in a region of the flow where velocity of the air was negligible, was used to measure the total temperature (Figure 1). In order to maintain a constant pressure in the chamber, the main compressor was run under constant load. A course adjust main valve and a fine adjust bypass valve located at the inlet of the chamber enabled the pressure to be regulated in the chamber.

Laser Doppler Velocimeter

The LDV set-up consisted of a helium-neon laser, a beamsplitter, three mirrors, a 200 mm telephoto lens, a photomultiplier tube, a digital correlator and an oscilloscope. The LDV set-up is shown in Figure 3. Figure 4 provides the pictorial view of the experimental set-up. The LDV was operated in the forward scatter mode. The following is a brief description of the compoennts. A more detailed description of the system can be found in Reference 4.

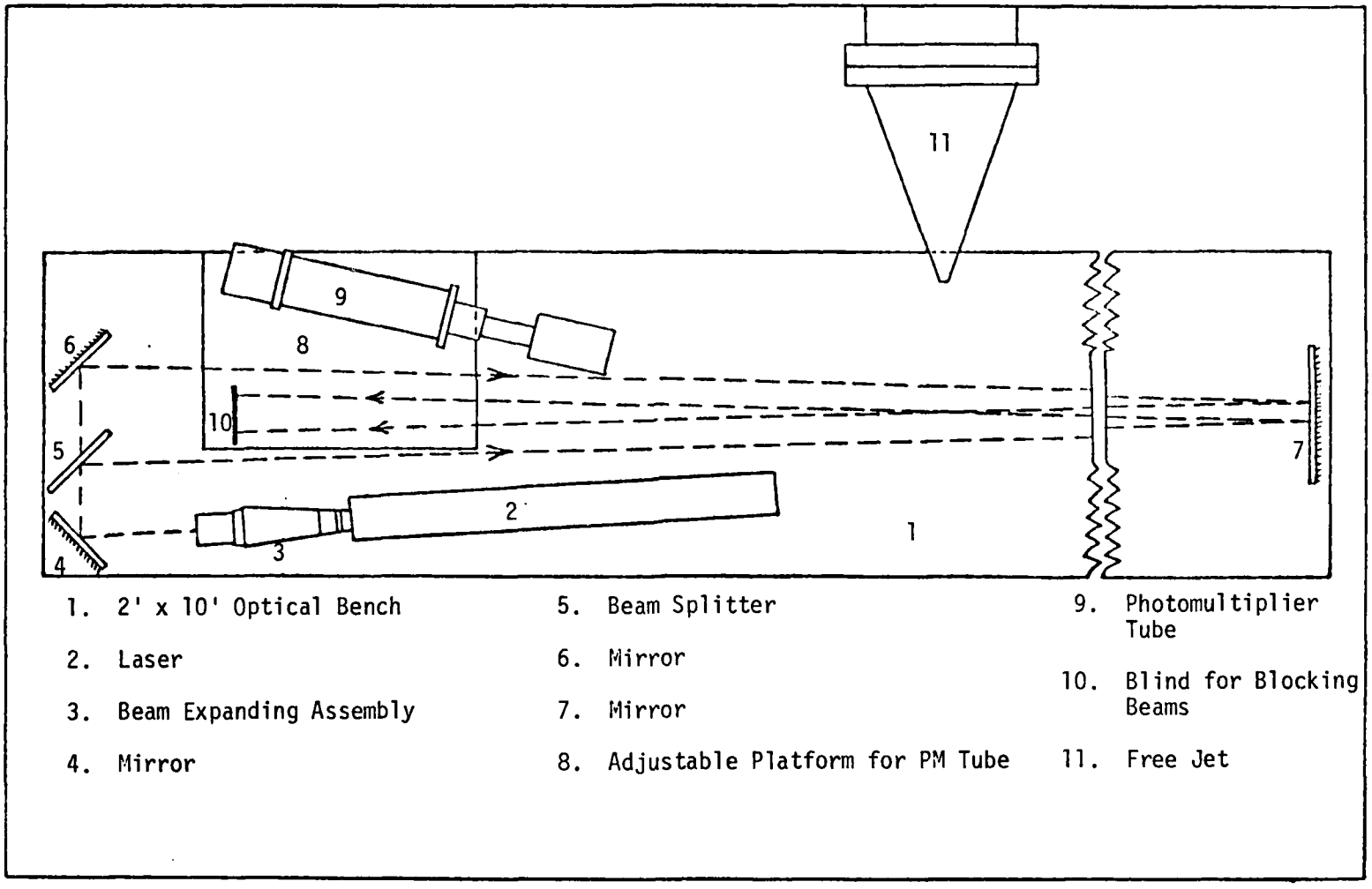

1. 2' x 10' Optical Bench
2. Laser
3. Beam Expanding Assembly
4. Mirror
5. Beam Splitter
6. Mirror
7. Mirror
8. Adjustable Platform for PM Tube
9. Photomultiplier Tube
10. Blind for Blocking Beams
11. Free Jet

Figure 3. Laser Velocimeter Set-up

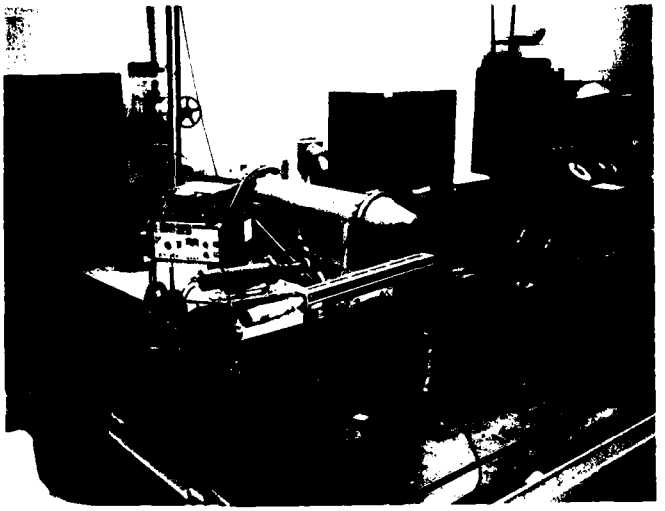

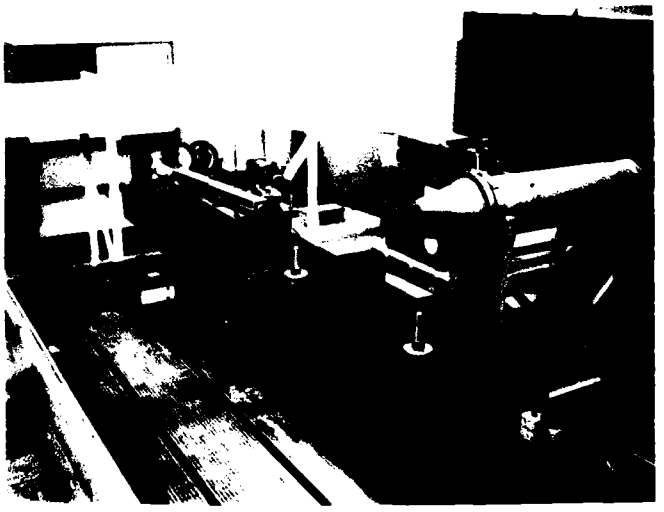

Figure 4. LDV Experimental Set-up

Laser. A Spectra Physics Model 124A helium-neon laser operating at 6328 Å with a nominal output power of 15 mW was used. Incorporated with the laser was a Model 255 DC exciter and together they produced a laser beam of 1.1 mm diameter.

Beamsplitter. A 5 inch diameter beamsplitter was used to split the laser beam into bwo beams of nearly equal power. A beamsplitter support was provided with two micrometer adjustments which provided means to make fine adjustment of the reflected beam in two axes.

Mirrors. Three 5 inch diameter plain mirrors were used for reflecting the beam. Their mounts were also provided with two micrometer adjustment which were used for fine adjustment of the cross-over point of the two beams at the focal spot.

Telephoto Lens. A 200 mm telephoto lens installed with a 9.0 cm spacer was used to align the photomultiplier optics. The lens collected the light scattered by the particles as they moved through the focal volume and focused the light onto a pinhole aperture. A 400 μm pinhole aperture was selected for this investigation which provided a flow control volume diameter of 0.72 mm being observed (Ref 4).

Photomultiplier Tube. The photomultiplier tube was an EMI 9863 KB/100 unit supplied by Malvern Instruments. An EMI PM 25B power supply regulated a constant 1850 volts to the PM tube. The lens system focused the incident light from the focal volume onto the pinhole aperture and via a narrow band spectral filter onto the PM tube cathode. Photons scattered by the moving particles in the focal volume were received at the cathode of the PM tube. These photons

generated the signal which was amplified by the PM tube circuitry and sent the signal to the digital correlator.

The set-up and operation of the PM tube were the most critical. It could very easily be damaged by its inadvertent exposure to direct laser light or any other kind of bright light, when the high voltage supply was switched on. However, a standby mode on the power supply allowed for a low voltage on the grid circuit, avoiding damage to the PM tube while room lights were on. This mode also allowed for instant operation of the PM tube once the full voltage was supplied to it. Another critical and important portion of the set-up was the optimum focusing and alignment of the PM tube for the proper operation of the entire system.

Digital Correlator. The type K7023 Malvern digital correlator system consisted of a high speed (50 nanosecond resolution) digital correlator and a storage unit (Figure 5). This instrument received data from the PM tube, stored and processed it, and developed the autocorrelation function which was developed for this study and displayed on the oscilloscope. As long as the system was in operation, the autocorrelation function was continuously being updated. The autocorrelation function evaluation could be ceased at any time by placing it in the stop mode for obtaining digital values of the function. In the reset mode, the data acquisition and processing could be started afresh.

Oscilloscope. An AN/USM-425(V)1 oscilloscope was used for display of the autocorrelation function from the digital correlator. The sinusoidal curve of the autocorrelation function shown on the screen of the oscilloscope in Figure 5 is the digital autocorrelator

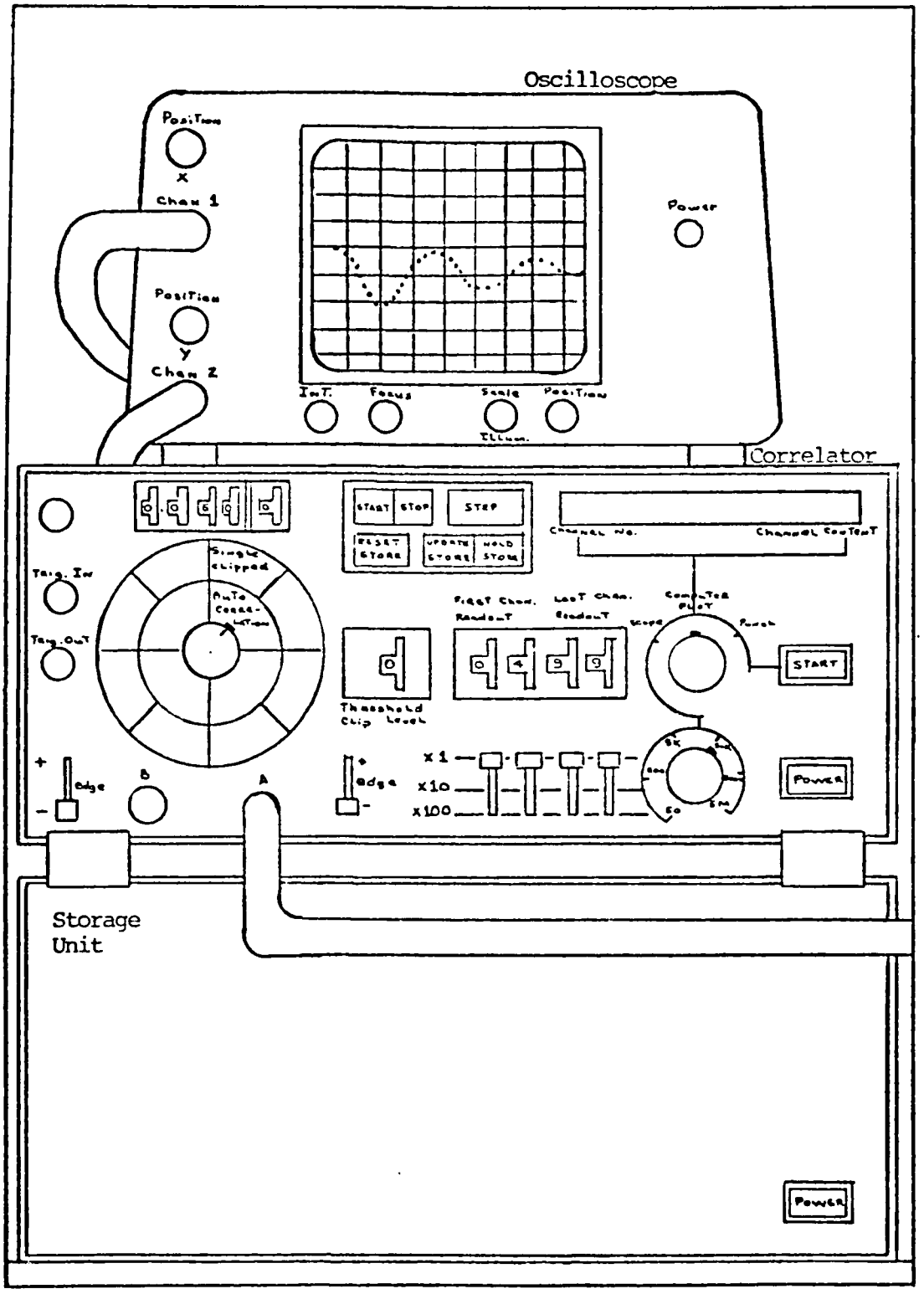

Figure 5. Digital Correlator and Oscilloscope Set-up

display of the PM tube signal. Velocity and turbulence intensity information was extracted from this curve simply by recording the channel number and content of the first minimum, g_1 , the first peak, g_2 , and the second minimum, g_3 . The proceding section describes in detail the operating principle of the system.

IV. Principle of Operation

The purpose of this section is to provide an abbreviated description of principle of the laser velocimeter system and its working equations. Detailed description of installation procedure and operating principles of the LDV is given in Malvern manual (Ref 4) and in Roger's thesis (Ref 7).

The basic principle of the LDV is that it records the time taken by a particle to travel a known distance in the focal volume. This known distance is the spacing between the fringes. Flow particles of the unseeded air are assumed to follow the flow. Therefore, the velocity of those particles computed by the LDV is the flow velocity.

Figure 6 shows various electronic components used for data processing in the LDV. It shows that the two laser beams cross at the point at which the flow measurements are taken. Intersection of two coherent laser beams at a common point form a set of parallel fringes as depicted in Figure 7. This figure indicates the principle of the "interference fringe" model which provides the basis for quantitative analysis of the laser-doppler signal. Fringe spacing, S , can be calculated with the help of the interference model shown in Figure 7.

$$S = \frac{\lambda}{2\sin\theta}$$

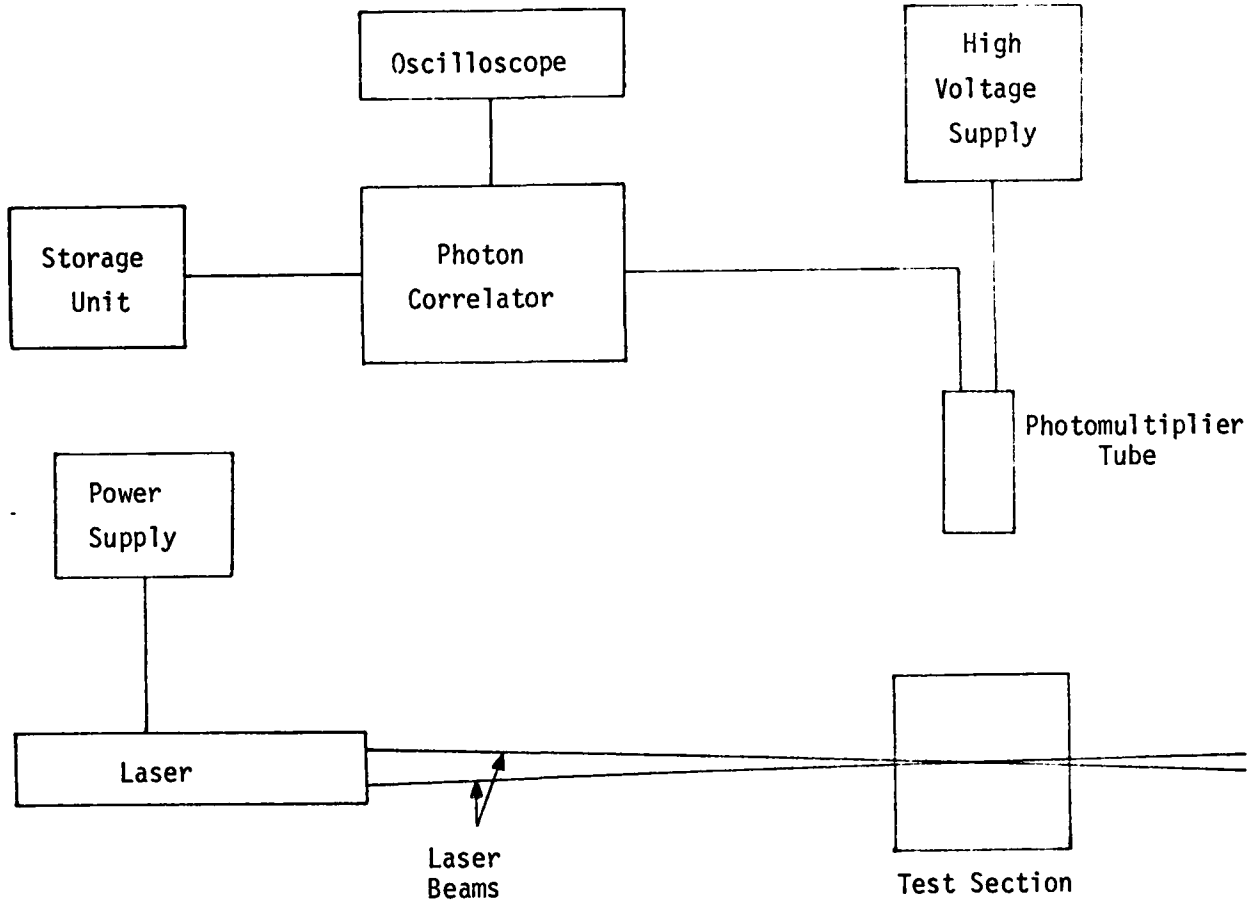

Figure 6. Laser Velocimeter Electronic Data Processing Scheme

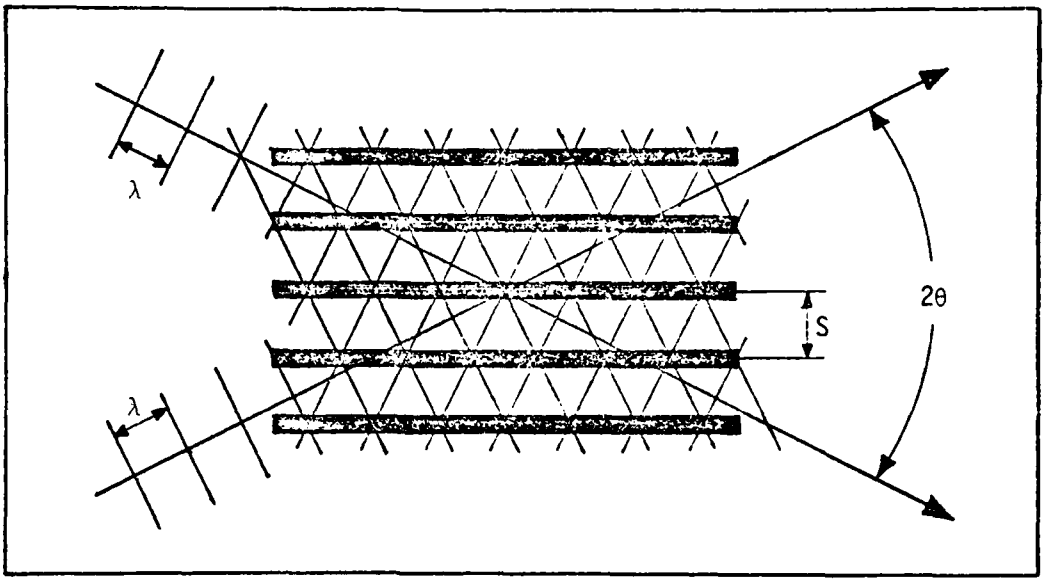

Figure 7. Interference Fringe Model

This value of S is valid for a medium having refractive index of unity. For a medium having refractive index, μ , the fringe spacing would be:

$$S = \frac{1}{2\sin\theta} \frac{\lambda}{\mu} \qquad (1)$$

A cross-section view of the focal volume at the beam intersection point is given in Figure 8. As indicated in this figure, when a number of flow particles pass through the field of spatially varying light intensity (optical fringes), they scatter light in the form of photons in all directions. Portions of these scattered photons are detected by the photomultiplier tube through the pinhole

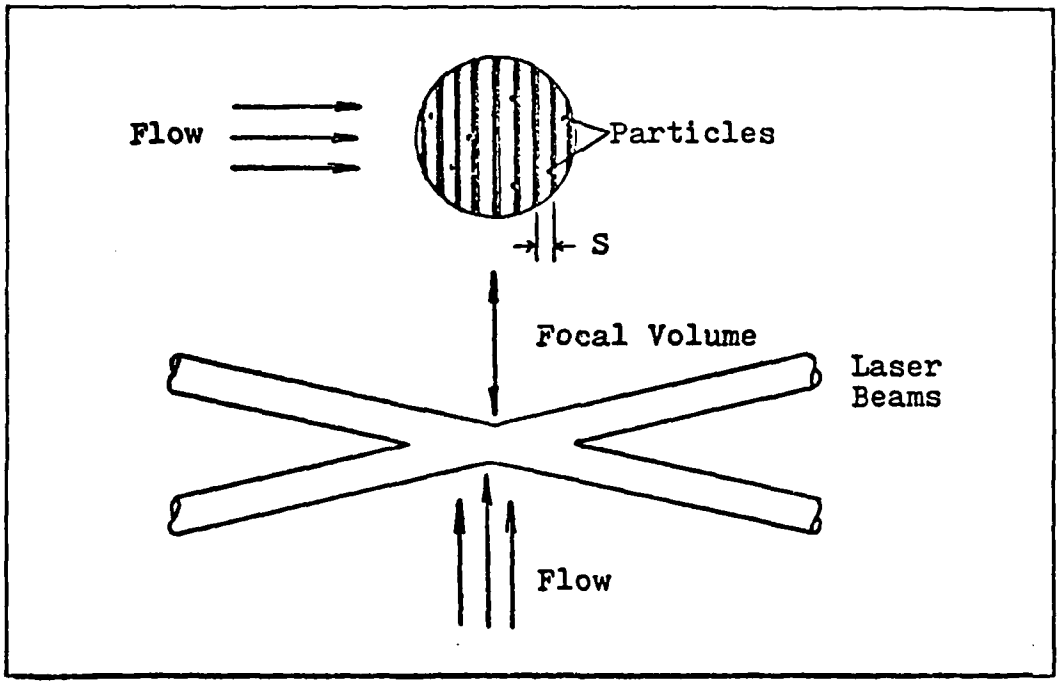

Figure 8. Schematic of Beam Intersection Point

aperture. As this light hits the cathode of the PM tube, it causes a pulse train burst which is then passed onto a high gain amplifier and discriminator for maintaining only the frequency modulation. This signal is then passed onto the digital correlator for further processing.

The digital correlator, in order to extract the periodicity of the pulse train, multiplies the pulse train with many time-delayed versions of itself. The output of the correlator is then fed to the oscilloscope for visual display. Figure 9 shows the display of the autocorrelation function on the oscilloscope. Mean velcoity and turbulence intensity can be extracted out of the autocorrelation function with the help of the following working equations.

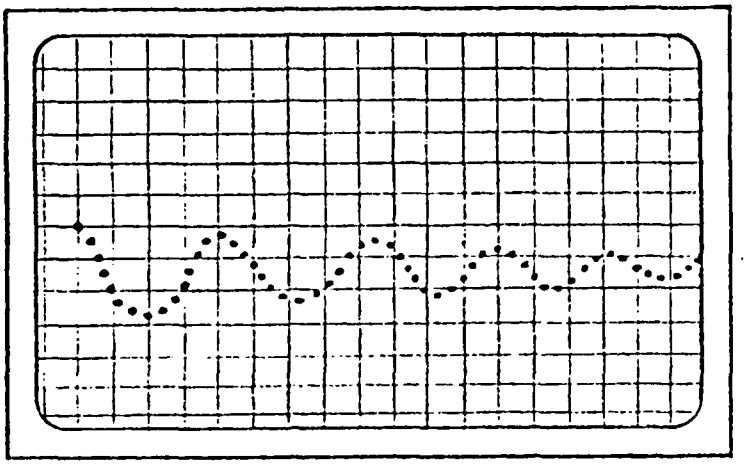

Figure 9. Oscilloscope Display

Working Equations

A detailed description for working equations of mean velocity and turbulence intensity is outlined in Malvern manual (Ref 4) Fringe spacing, S , is given by Eq (1). Beam angle, θ , in terms of geometry of the optics, is given in the sketch below.

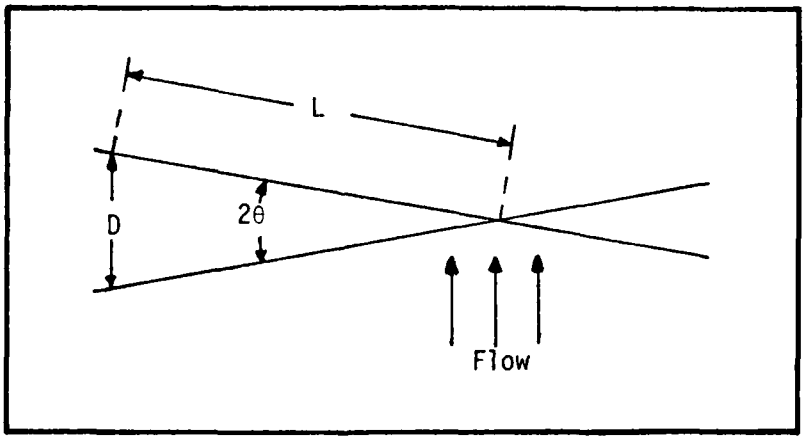

Here, D is the distance, the two beams are apart at any reference surface and L is the distance traveled by a beam from the point

on the reference surface to the focal spot. Then Eq (1) becomes

$$S = \frac{L}{D}\frac{\lambda}{\mu}$$

where

S = fringe spacing

λ = wave length of laser beam = 6.328×10^{-9} m

μ = refractive index of air = 1.0

The correlator time, T , is defined as the time taken by a particle to travel through one fringe spacing (Figure 10). This

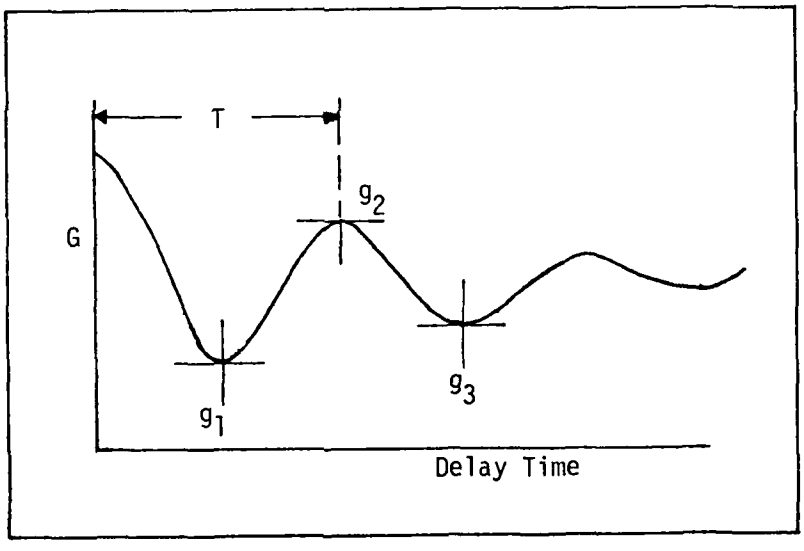

Figure 10. Autocorrelation Function

time, T , can be calculated from the sample time setting on the correlator and channel number of the first peak, g_2.

$$T = (\text{channel number of peak} - 3) \times \text{sample time}$$

Velocity, U, of the flow is then given by

$$U = \frac{S}{T} \tag{2}$$

and the turbulence intensity, η.

$$\eta = \frac{1}{\sqrt{2}\,\pi}\left[(R - 1) + \frac{1}{n^2}\right]^{\frac{1}{2}} \tag{3}$$

where

$n = \frac{r_o}{s}$

r_o = radius of the focused beam

$R = \left(\frac{g_2 - g_1}{g_2 - g_3}\right)$

g_1 = contents of channel corresponding to first minimum

g_2 = contents of channel corresponding to first maximum

g_3 = contents of channel corresponding to second minimum.

Equation (3) is valid for turbulence intensity up to $\eta = 0.2$ or 20% (Ref 4). A detailed development of Eq (3) is contained in Reference 4.

V. Experimental Procedure

The following section presents a brief description of the experimental procedure employed in this investigation.

Test Condition

The nozzle exit velocity was in the compressible flow regime; therefore, applicable tables were used for calculating the required chamber pressure. Velocity in the calming chamber was negligible; hence, pressure and temperature measured in the calming chamber were assumed to be total conditions. For compressible, isentropic flow in a nozzle, the pressure and temperature relations in terms of exit Mach number are given by the following equations:

$$\frac{P_o}{P} = \left(1 + \frac{k-1}{2} M^2\right)^{\frac{k}{k-1}} \tag{4}$$

$$\frac{T}{T_o} = \left(\frac{P}{P_o}\right)^{\frac{k-1}{k}} \tag{5}$$

From Eq (4)

$$M^2 = \frac{U^2}{gkRT} = \frac{2}{k-1}\left[\left(\frac{P_o}{P}\right)^{\frac{k-1}{k}} - 1\right]$$

Replacing T in terms of T_o from Eq (5), and after suitable algebraic manipulation, the exit velocity, U, can be written in the following form:

$$U = \sqrt{2gRT_o \frac{k}{k-1}\left[1 - \left(\frac{P}{P_o}\right)^{\frac{k-1}{k}}\right]} \qquad (6)$$

where

P = P_a atmospheric pressure for $P \geq 0.52828\ P_o$

P_o = $P_c + P_a$

P_c = calming chamber gage pressure

T_o = T_c calming chamber temperature

Equation (4) can be used directly to find total pressure and, in turn, calming chamber pressure for the required exit Mach number, M . Constant pressure in the calming chamber was maintained by adjusting the compressed air by-pass valve, which was vented to the atmosphere, until steady flow at the desired pressure was obtained with the compressor running under a constant load condition.

Optical Alignment

The first step before starting on the alignment of the equipment was to make the test apparatus and traversing mechanism orthogonal to each other, so that the flow measurements in the required direction could be carried out. The next step was to focus the two beams at the center of the jet and at 25 cm downstream of the nozzle exit. This was accomplished by setting the bisector of the angle between the beams parallel to the optical bench and orthogonal to the jet flow. The fine adjustment in focusing the two beams at the focal spot was carried out with the help of the micrometer adjustments provided by the mirror and the beamsplitter mounts.

This was followed by the alignment of the photomultiplier tube optics. According to the distance between the PM tube and the focal volume, a 200 mm telephoto lens and two spacers (9.0 cm) were selected (Ref 4). A piece of transparent paper was placed at the focal spot, and the PM tube was roughly aligned with the focal volume by looking through the polaroid eyepiece. The fine focusing adjustment was carried out by translating the PM tube forward and back on its railing, and adjusting the telephoto lens until the sharpest image of the focal volume was visible through the polaroid eyepiece. The final step was to center the light entering the PM tube onto its pinhole aperture. This was accomplished by viewing the light through an X10 eyepiece and adjusting the X and Y control knobs provided on the mount of the PM tube.

After aligning the optics, a few trial runs were made for the purpose of familiarization before the actual runs with the expanded beam were carried out.

Beam Expansion

The laser beam could be expanded to a fixed diameter with the use of the beam expanding lens and pinhole aperture. A detailed description of the 1.1 mm input laser beam expansion and its diameter measurements is contained in Appendix D. Table I shows the combination of expanding lenses and pinhole apertures, their measured output beam diameters and output laser power.

As discussed in Appendix D, laser power, P_L , is one of the factors which influence the signal-to-noise ratio of the PM tube. Therefore, the use of the telescope was found to be more practical than

TABLE I

Results of Beam Expansion Experiment

Expanding Lens L	Pinhole Aperture A	Output Beam Diameter	Output Laser Power
6	6	12 mm	0.02 mW
3	6	27 mm	13.1 mW
3	4	30 mm	10.0 mW
1	3	50 mm	8.6 mW

changing the beam diameter size by using various lenses and apertures, as this permitted the use of one optical set-up and gave the optimum beam intensity for this investigation. For the present investigation, beam expanding lens L3 and pinhole aperture A6 were selected and the various beam diameters at the focal volume were obtained by merely changing the focal length of the telescope. A second advantage of the system was that the total power in the focal volume was a constant with intensity varying with volume.

Data Acquisition

The objective of this investigation was to map the flow field at the jet exit Mach number of 0.3. The suitability of the LDV to measure velocities depends mainly on the value of the fringe spacing, S , which itself depends on the value of $\frac{L}{D}$. $\frac{L}{D}$, a measure of incidence

angle between the two beams at the cross-over point, was required to be in the order of 24 to measure the flow velocities. This was achieved by reflecting the two beams from a mirror to make them travel a longer distance, L , before crossing at the focal spot (Figure 3). This optical set-up gave $\frac{L}{D} = 23.4$ and $S = 14.81 \times 10^{-6}$ meters and remained such throughout the investigation.

Data were taken which could yield mean velocity and turbulence intensity information. In this study, only the flow in the half jet width was investigated, as this particular jet had already been proven to be axially symmetric (Refs 2, 9).

In order to reduce the data efficiently, computer programs were developed prior to the running of the experiment. Large amounts of data were processed by the CDC 6600 computer and Calcomp Plotter. All the experimental data are presented in *Appendix F. Results* of this investigation are discussed in the next section.

VI. Results and Discussion of Results

The central aim of this study was not to investigate the behavior of the jet, but to evaluate the effects of test rhombus size on the photon correlation laser velocimeter system and compare the results with the existing published data. The test conditions selected for this study were those which could provide a basis for comparison of the results to the earlier studies and still remain within the working limitations of the LDV. Therefore, the flow field measurements were made at 25 jet widths downstream of the nozzle exit, at $M = 0.3$, using 0.5, 1.0, 1.1, 3.0, 5.0, 7.0 and 10.0 mm diameter laser beams.

The results of this investigation are discussed in the following pages. The plots presented are representative of the results obtained with that particular beam diameter. A complete set of data is presented in Appendix F.

All the data were non-dimensionalized as shown on the appropriate plots. The method used was that used by Shepard (Ref 9) and Cerullo (Ref 2), so that a proper comparison with their results could be made.

Center-Line Velocity

The ratio of center-line velocity to jet exit velocity is compared with the following theoretical prediction, Eq (B-7) of Appendix B;

$$\left(\frac{U_{cen}}{U_{cor}}\right)_{\text{at } x=25 \text{ cm}} = 0.6 \qquad (7)$$

where U_{cor} is the jet exit velocity. The experimental results are shown in Table II below.

TABLE II

Results of U_{cen}/U_{cor}

Beam Diameter mm	U_{cor} m p s	U_{cen} m p s	$\frac{U_{cen}}{U_{cor}}$
1.1	97.553	59.244	0.6073
0.5	103.927	63.025	0.6064
1.0	91.924	56.965	0.6197
3.0	87.086	54.855	0.6299
5.0	102.143	59.244	0.5800
7.0	92.394	51.968	0.5625
10.0	81.367	55.890	0.6869

Table II shows that the experimental values remained close to the theoretical predictions (within ± 5%) for laser beam diameters up to 5.0 mm. Beyond 5.0 mm diameter, the results started deviating from the theoretical values. This deterioration in the results at higher beam diameters is due to the fact that the laser beam intensity reduces as the diameter increases, introducing noise in the signal output of the photomultiplier tube. This behavior of the PM tube will be discussed in detail later in this section.

Mean Velocity Similarity

When measurements in a free jet are made across the jet at points where the flow is fully isotropic turbulent, the mean velocities present at different stations in the flow will all reduce to the same curve if properly non-dimensionalized. In order to compare the results to the theoretical curves developed by Tollmien and Gortler (Ref 1), the velocities and the distances from the center were non-dimensionalized by dividing by U_{cen} and $y_{1/2}$, respectively, where $y_{1/2}$ is defined as the distance from the center-line of the jet to the point where the local velocity is 50% of the center-line velocity. Results of mean velocity similarity profiles are presented in Figures 11 through 18.

Figure 11 shows the results of a 1.1 mm unexpanded laser beam. Figures 12 to 18 are the results of the expanded beams ranging from 0.5 mm diameter to 10.0 mm diameter, using beam expanding lens L3 and pinhole aperture A6 as explained earlier. These results show that the experimental values are in good agreement with the theoretical curves up to a laser beam of 7.0 mm diameter. These figures also show that the experimental values are close to the Gortler curve and fall within ± 5% error of the theoretical predictions. These experimental results also agree very well with Shepard's and Cerullo's results.

Figure 17 shows the results of a 10.0 mm diameter beam. This figure seems to be in fairly good agreement with the Gortler curve close to the jet center and with the Tollmien curve close to the jet boundary. But, as shown in Table II, the center-line velocity measured with the 10.0 mm beam is much higher than the theoretical prediction; also, the value of $y_{1/2}$ is higher than the average value of the experiments with

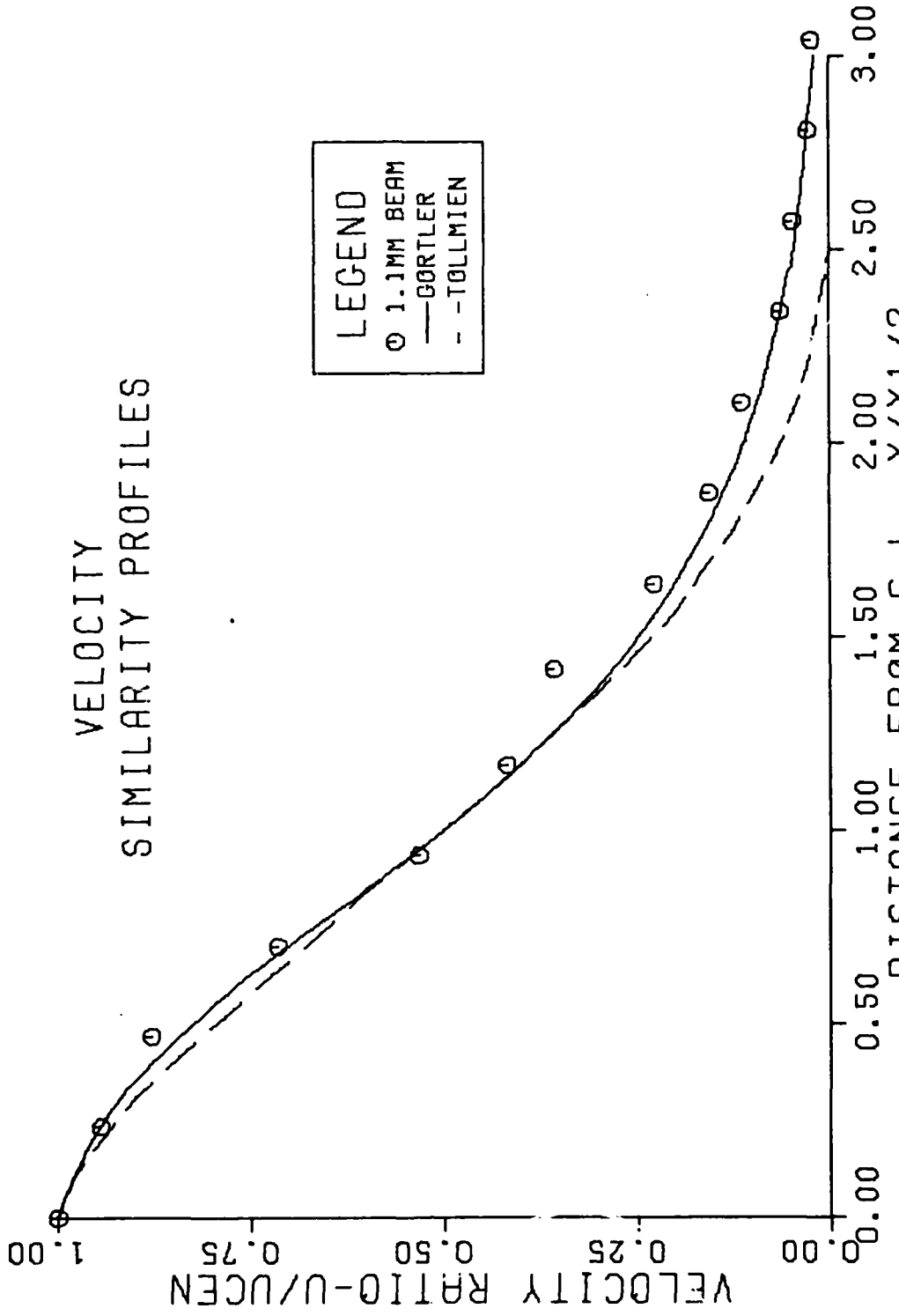

FIG. 11. MEAN VELOCITY SIMILARITY PROFILES USING 1.1 MM BEAM

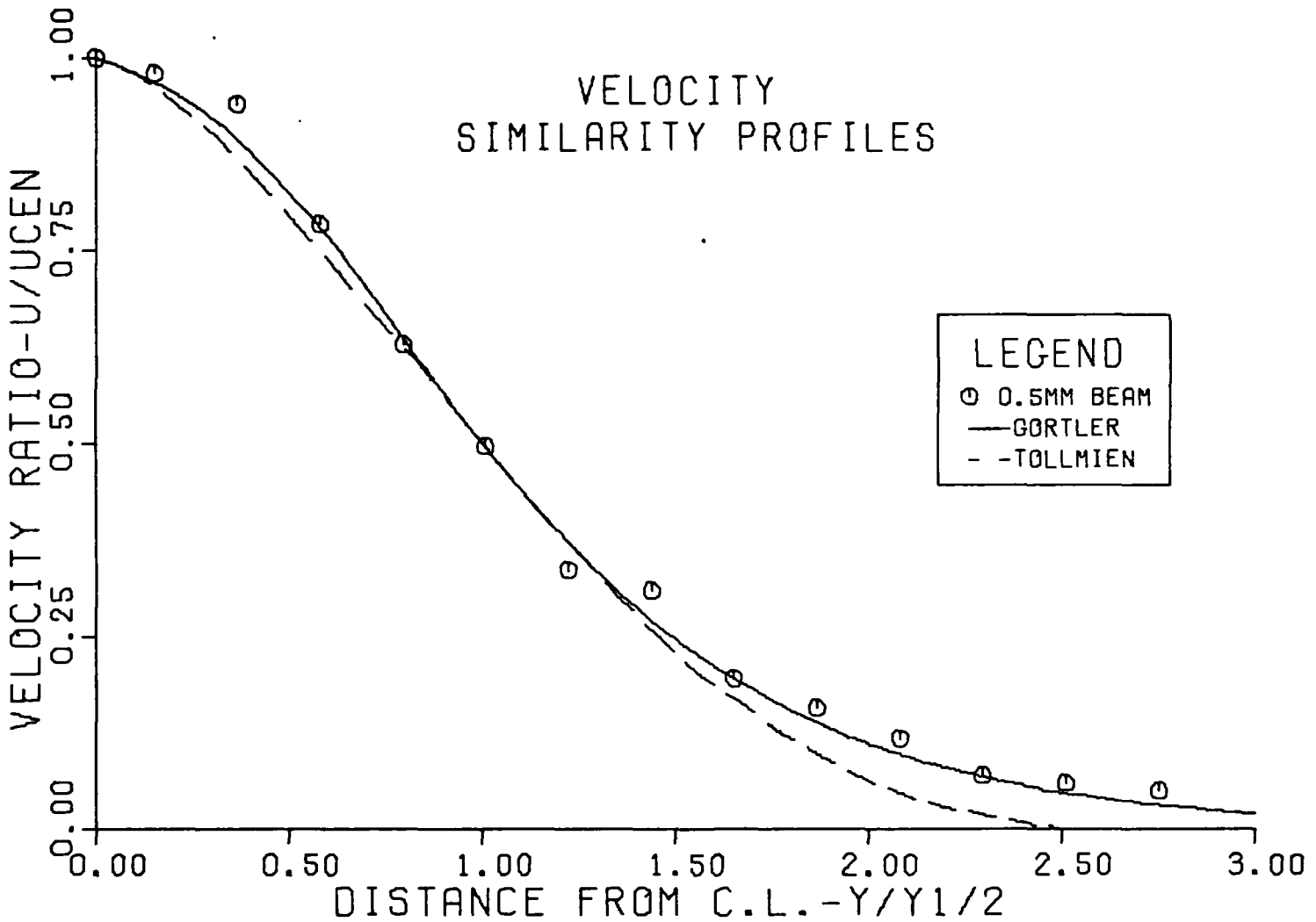

FIG. 12.MEAN VELOCITY SIMILARITY PROFILES USING 0.5 MM BEAM

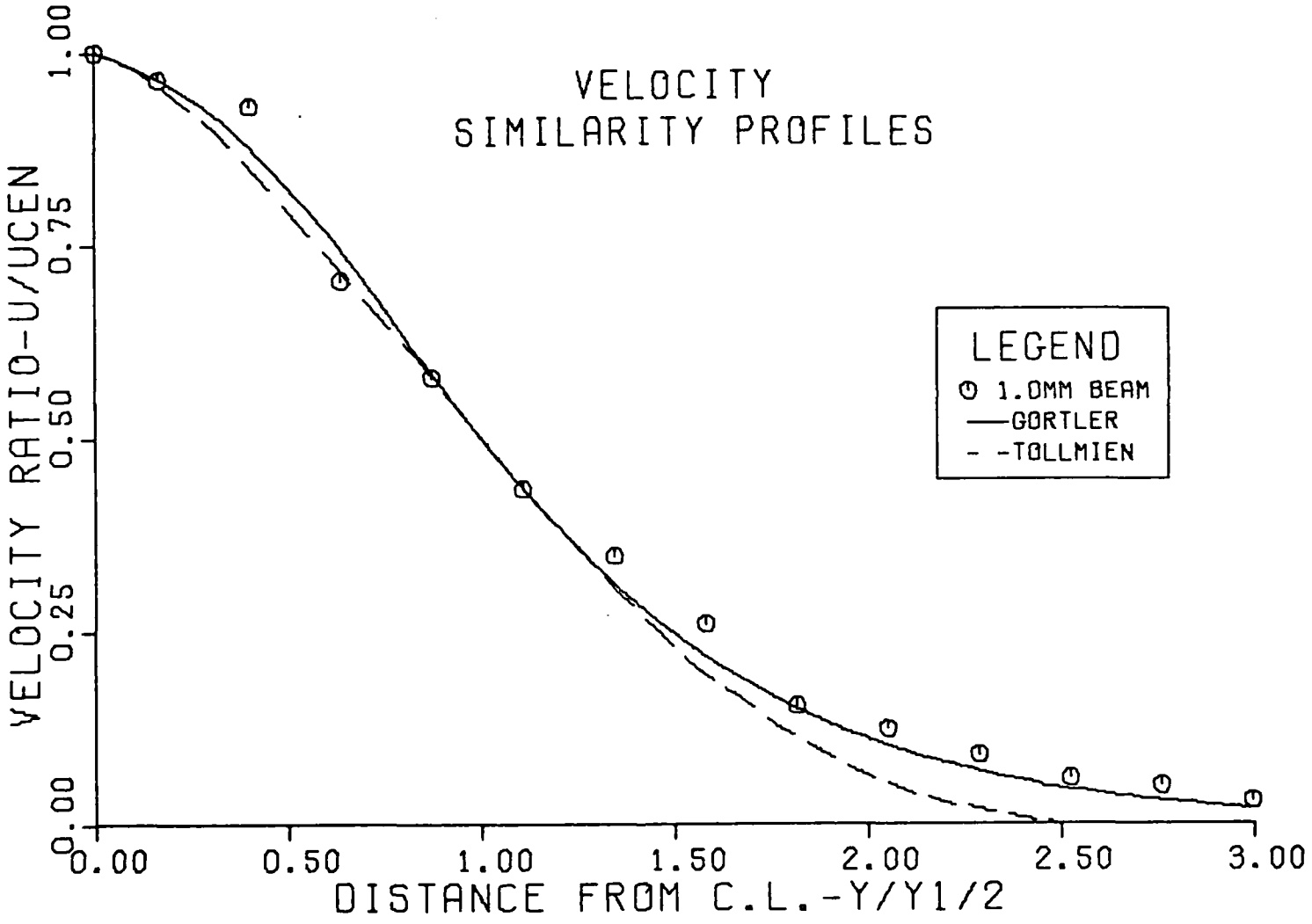

FIG.13. MEAN VELOCITY SIMILARITY PROFILES USING 1.0 MM BEAM

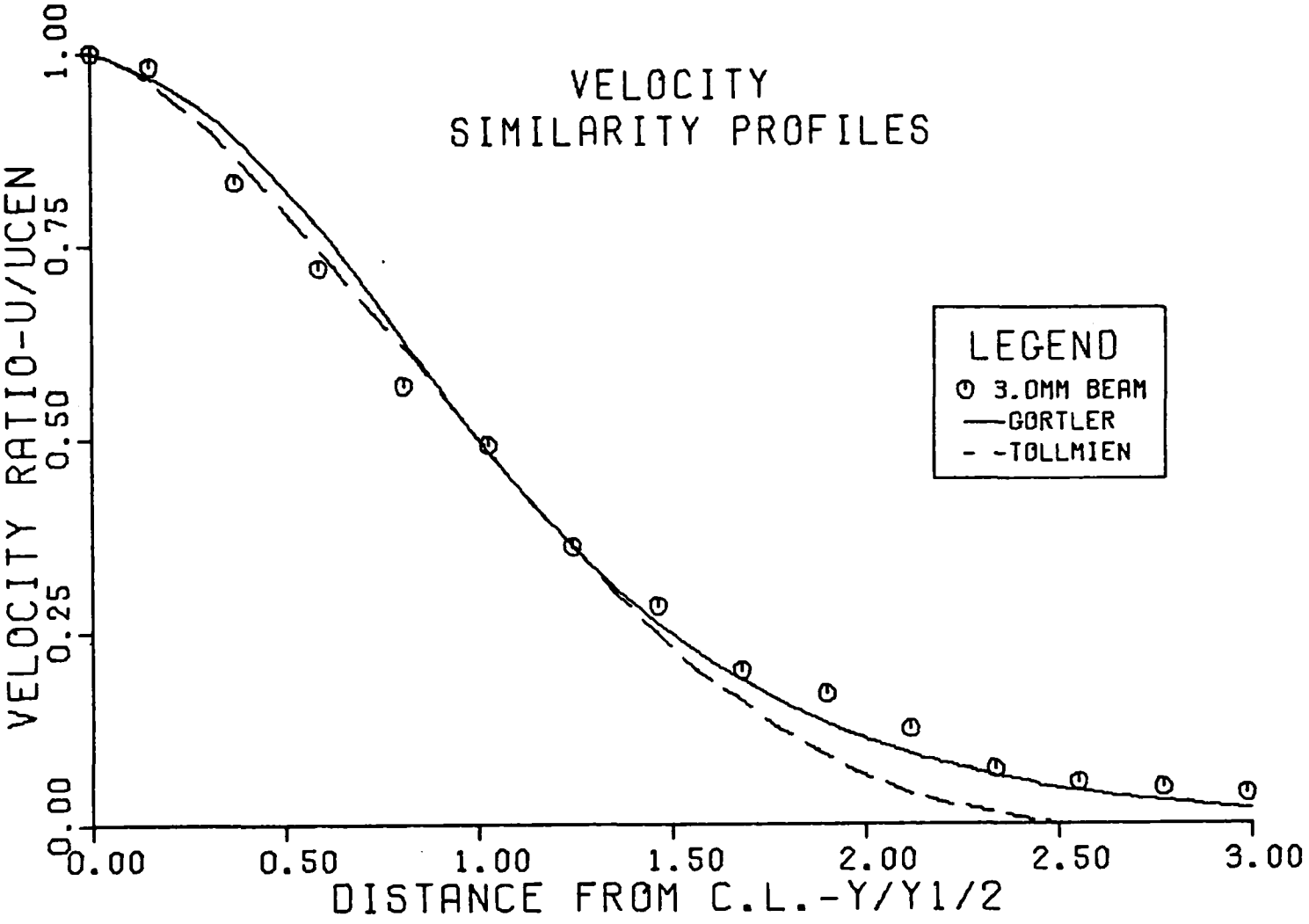

FIG.14. MEAN VELOCITY SIMILARITY PROFILES USING 3.0 MM BEAM

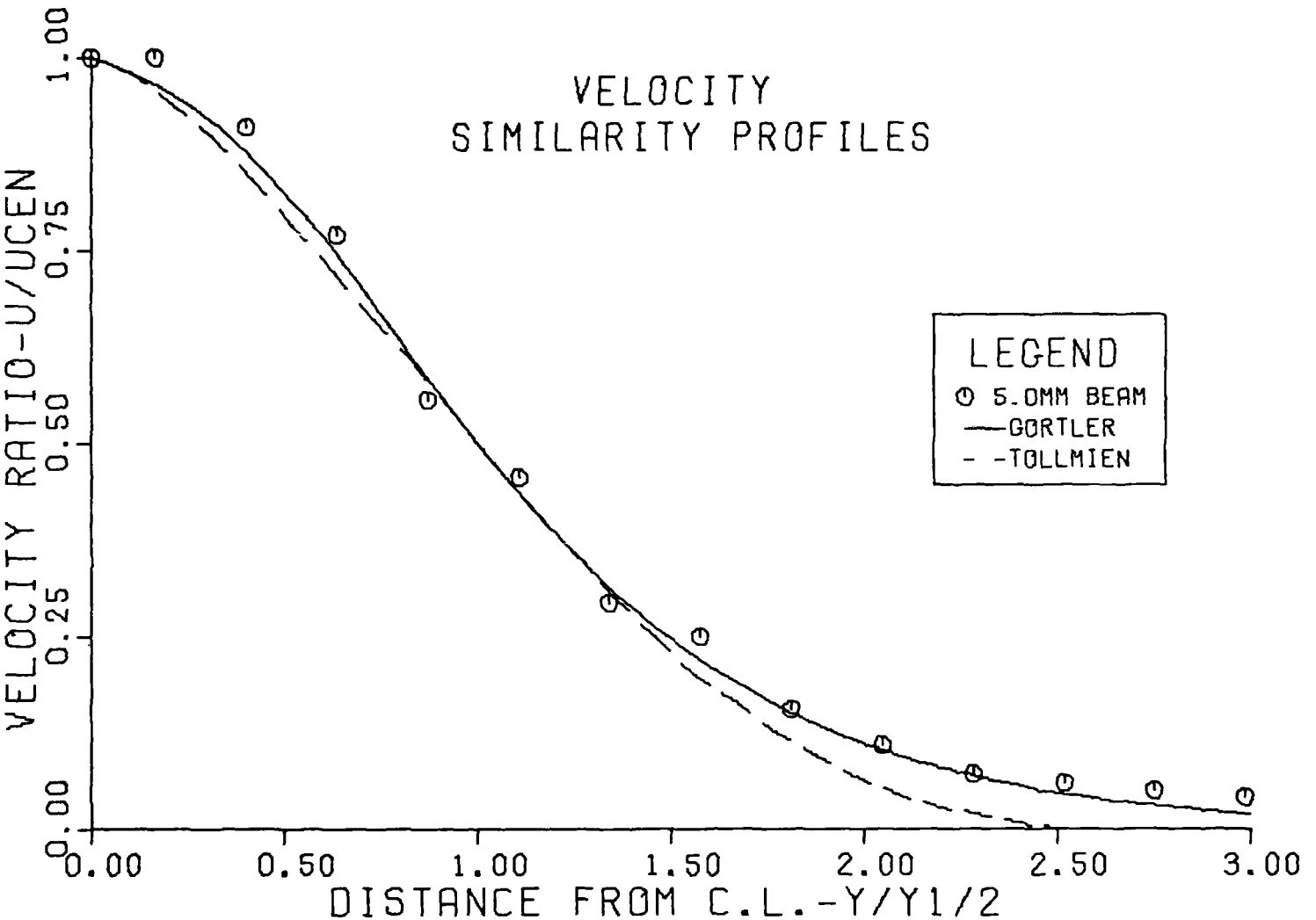

FIG. 15. MEAN VELOCITY SIMILARITY PROFILES USING 5.0 MM BEAM

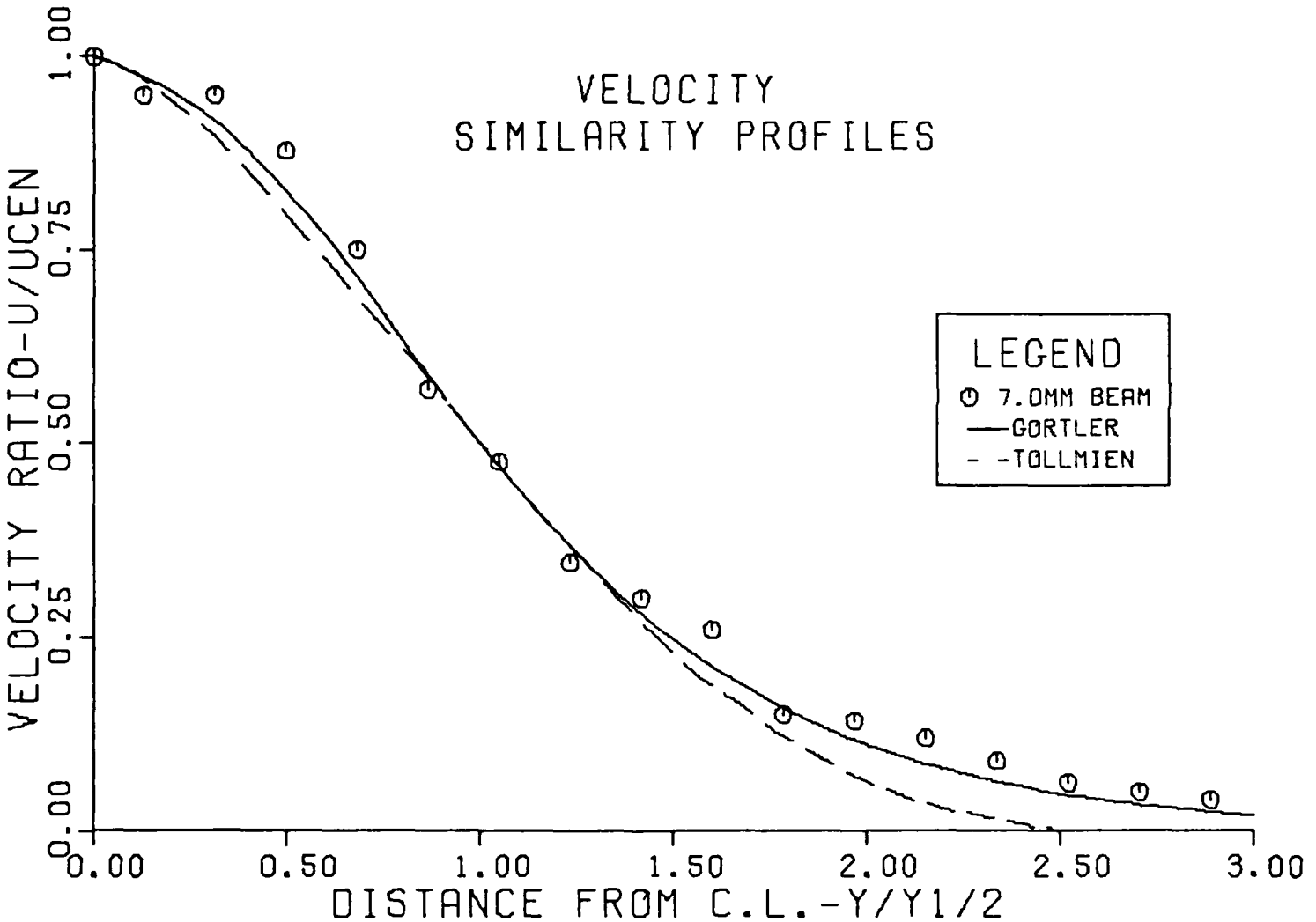

FIG. 16.MEAN VELOCITY SIMILARITY PROFILES USING 7.0 MM BEAM

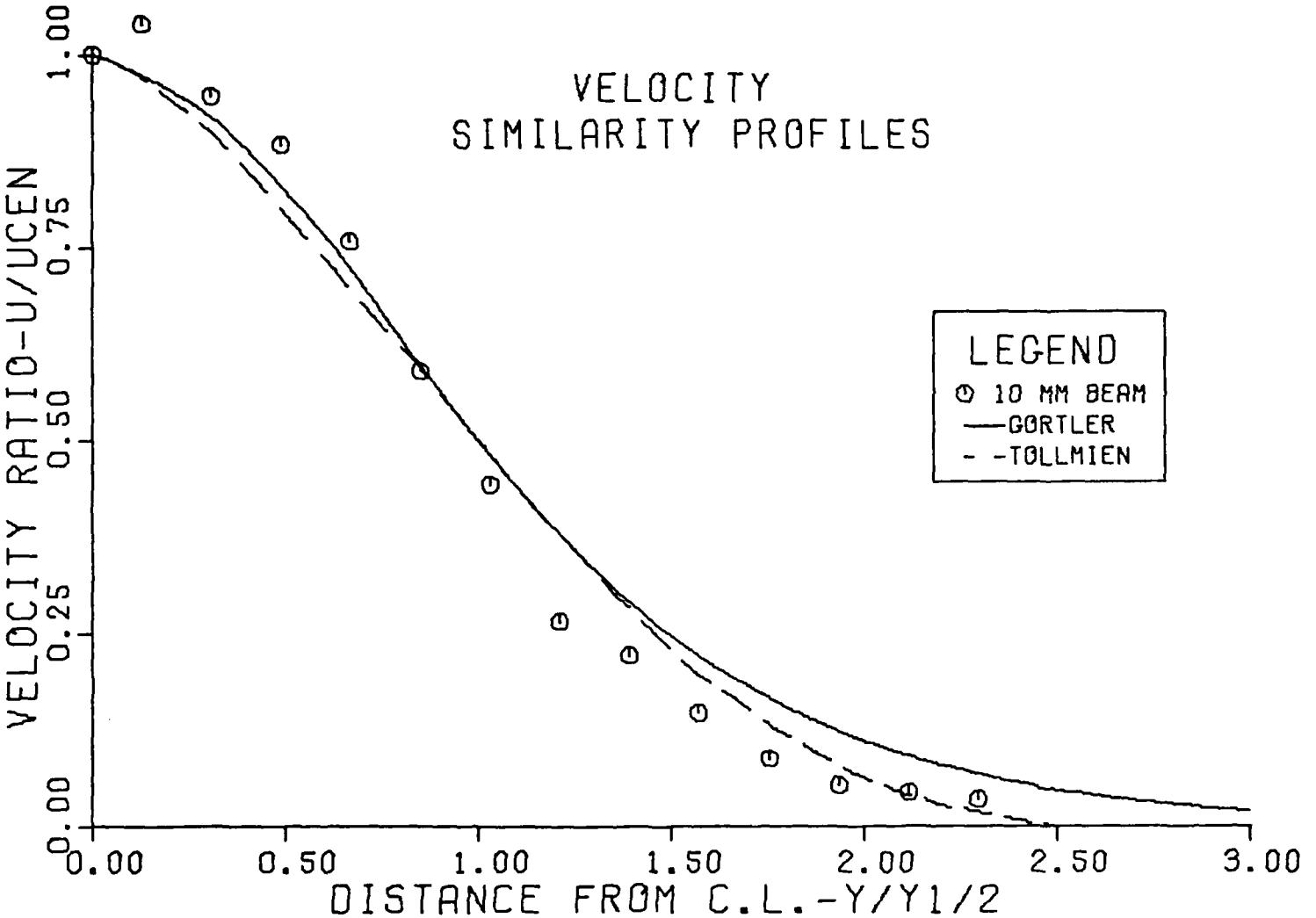

FIG.17. MEAN VELOCITY SIMILARITY PROFILES USING 10. MM BEAM

lower beam diameters. The value of $y_{\frac{1}{2}}$ comes out to be 2.81 cm (1.106 inches) as compared to 2.236 cm (.88033 inches) of the averaged values of experiments involving the lower beam diameters, excluding the 7.0 mm beam results. This average value of $y_{\frac{1}{2}}$ is very close to the one measured by Shepard and Cerullo. The 7.0 mm beam results are also questionable, as the value of $y_{\frac{1}{2}}$ comes out to be 2.762 cm (1.0874 inches) in this case. While plotting the velocity similarity profile, one forces the data to pass through two points; that is, at $\frac{y}{y_{\frac{1}{2}}} = 0$, $\frac{U}{U_{cen}} = 1.0$ and at $\frac{y}{y_{\frac{1}{2}}} = 1$, $\frac{U}{U_{cen}} = 0.5$. This makes the experimental points fall close to the theoretical curve as shown in Figure 17. But once the same results are plotted after non-dimensionalizing the data by the expected values of U_{cen} and $y_{\frac{1}{2}}$, the velocity similarity profile appears to be the one shown in Figure 18. This figure shows that the experimental points are away from the theoretical curve, especially in the vicinity of the center of the jet where velocities are higher.

This behavior of the experiment at higher beam diameter can best be explained by the help of an analytical solution for the laser power requirements derived in Appendix C to this report. Equation (C-11) provides a quantified relation of the output of the photomultiplier tube as a function of the laser power, velocity, optical arrangement and photodetector properties. The output of the PM tube in terms of number of electrons leaving the cathode of the PM tube is given by

$$N_e = 4\eta_q\eta_c \frac{P_L Q_{scat} r_p^2}{D_I^2 h\nu} \frac{N_{ph}}{\nu_D} \qquad (8)$$

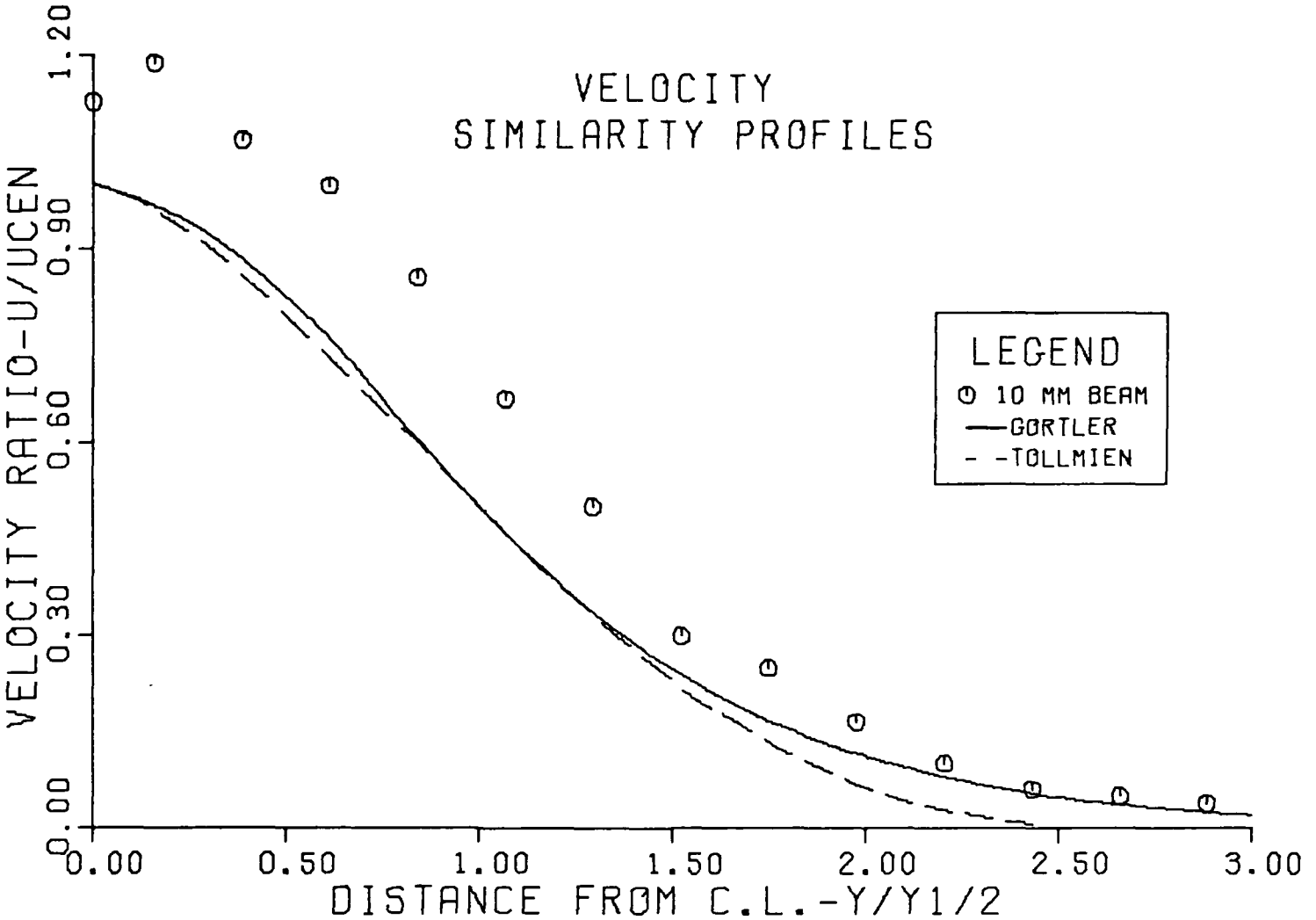

Figure 18. Mean Velocity Similarity Profiles Using 10 mm Beam and Corrected for U_{cen} and $y_{1/2}$

As discussed in Appendix D, the number of electrons, N_e , is a direct measure of the output signal efficiency of the PM tube. The higher the value of N_e , likewise the higher the signal-to-noise ratio. In Eq (8), all the parameters on the right hand side are constants except the focused beam diameter, D_I . This shows that the signal-to-noise ratio is inversely proportional to the square of the focused beam diameter, D_I . This explains the deterioration of the signal-to-noise ratio and, hence, the results at higher beam diameters. Figure 19 shows the output of the correlator with small and large beam diameters at the same point in the flow field.

Another factor which appears on the right hand side of Eq (8) is the signal frequency, ν , which affects the output signal. This signal frequency is the ratio of the particle velocity to the fringe spacing. It indicates that a decrease in the flow velocity would increase the signal-to-noise ratio. This factor is evident in the results as the data with higher beam diameters and at points away from the center-line, where velocities are small, are in conformity with the theoretical results.

The results of mean velocity profiles show a good agreement with the theoretical curves and earlier experiments up to a beam diameter of 5.0 mm. The beam diameters higher than 5.0 mm produced questionable results.

Turbulence Intensity Profiles

The data for turbulence intensities are also non-dimensionalized by y_o , where y_o is the half-width of the jet nozzle at the exit.

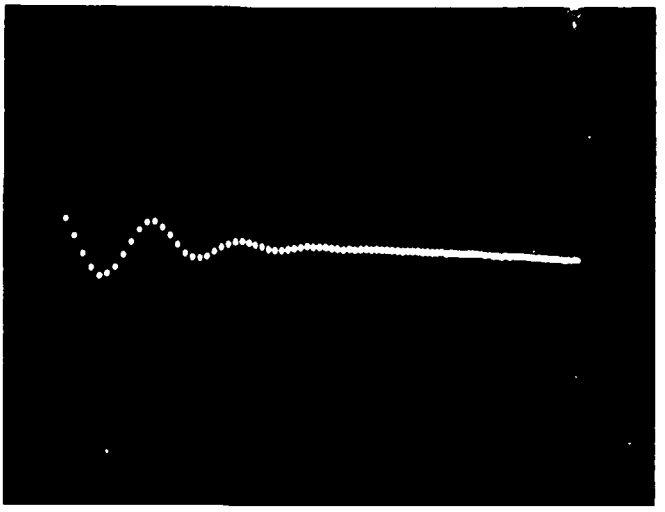

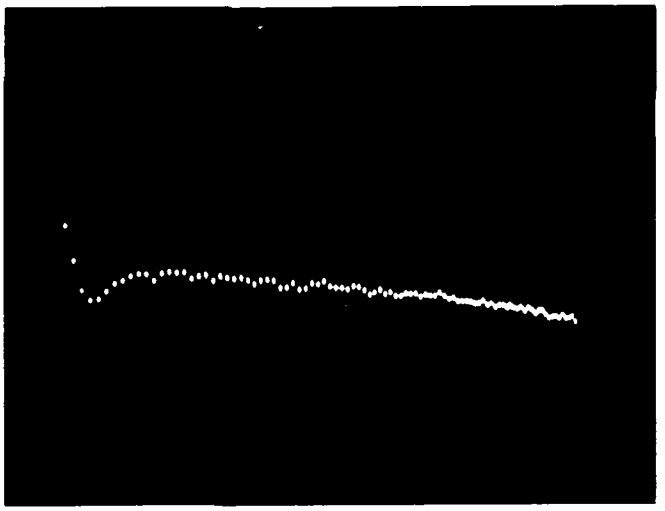

Figure 19. Autocorrelation Function at (a) Small Beam Diameter (1.0 mm), (b) Large Beam Diameter (15.0 mm)

Theoretically, non-dimensionalizing the turbulence intensity profiles should reduce them to one curve regardless of the beam diameter used. The results of an unexpanded 1.1 mm beam and an expanded beam of 3.0 mm diameter are shown in Figures 20 and 21, respectively. The plots for other beam diameters are presented in Appendix E.

All of the turbulence measurements are compared with the Hot Wire results obtained by Cerullo. The Hot Wire results are for an exit Mach number of 0.4. Cerullo carried out measurements at $M = 0.4$, 0.6 and 0.8, and the trend of his turbulence measurements shows that for $M = 0.3$, the Hot Wire turbulence intensity profile should be slightly lower than the one used here for comparison. Figures 20 and 21 show that the turbulence intensity profile generally follows the same trend as that of the hot wire, but nothing can be said positively as these two, and the rest of the plots in Appendix E, do not fall into one similar curve.

Figure 22 shows the turbulence intensity profile by taking the average value of the turbulence intensities for 0.5, 1.0, 1.1, 3.0 and 5.0 mm beam diameters. This figure indicates that for turbulence level up to 20%, results are close to the hot-wire results. These average results show a better correlation with the hot-wire results than the individual results.

For the purpose of comparison, the only data available is that of Cerullo. His turbulence intensity data by the LDV was so erratic that it went off the scale and he did not plot his LDV's results. From the results of this study, it appears that the turbulence intensities in the vicinity of the jet boundary are close to the

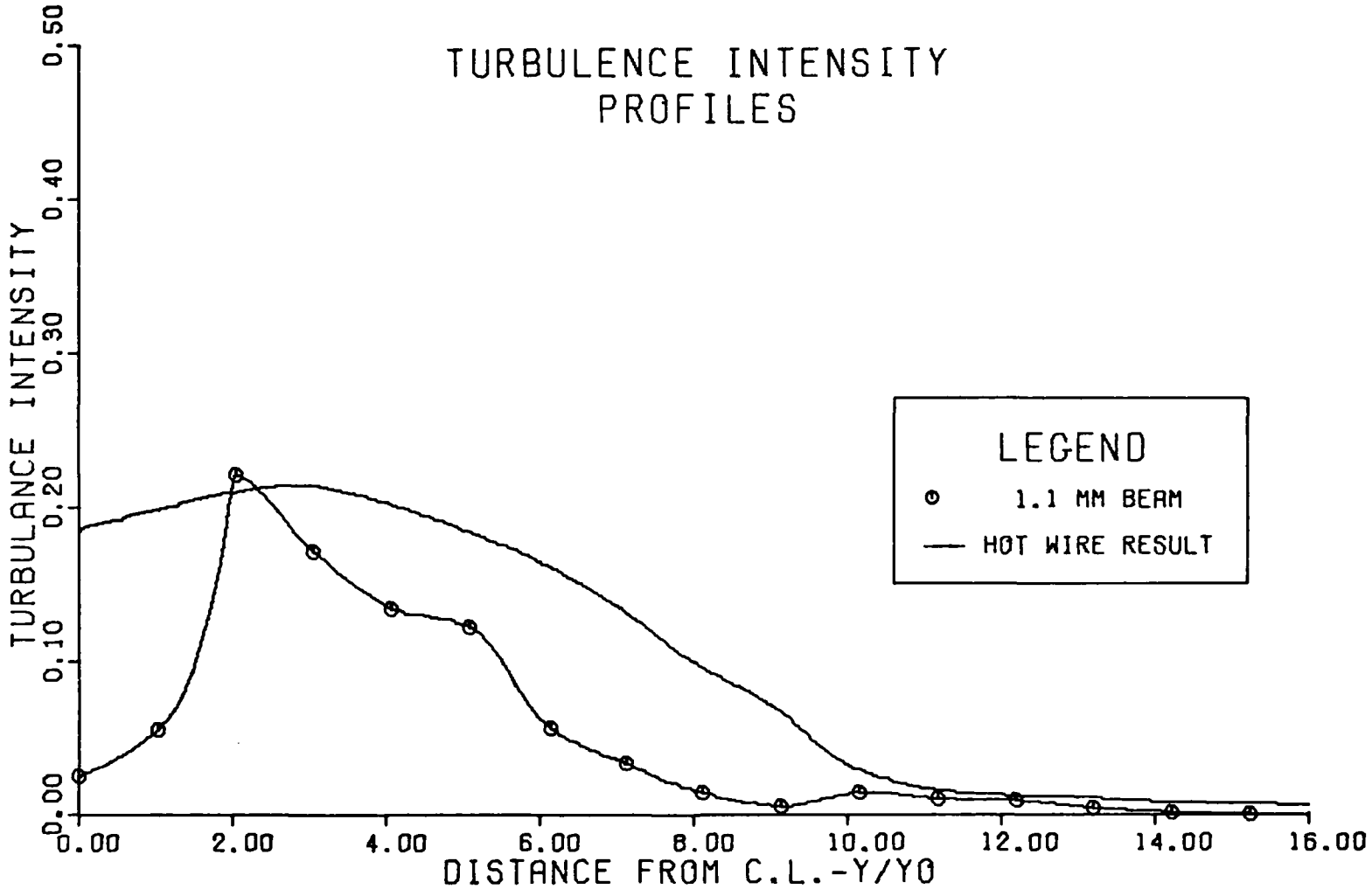

FIG.20. TURBULENCE INTENSITY PROFILES USING 1.1 MM BEAM

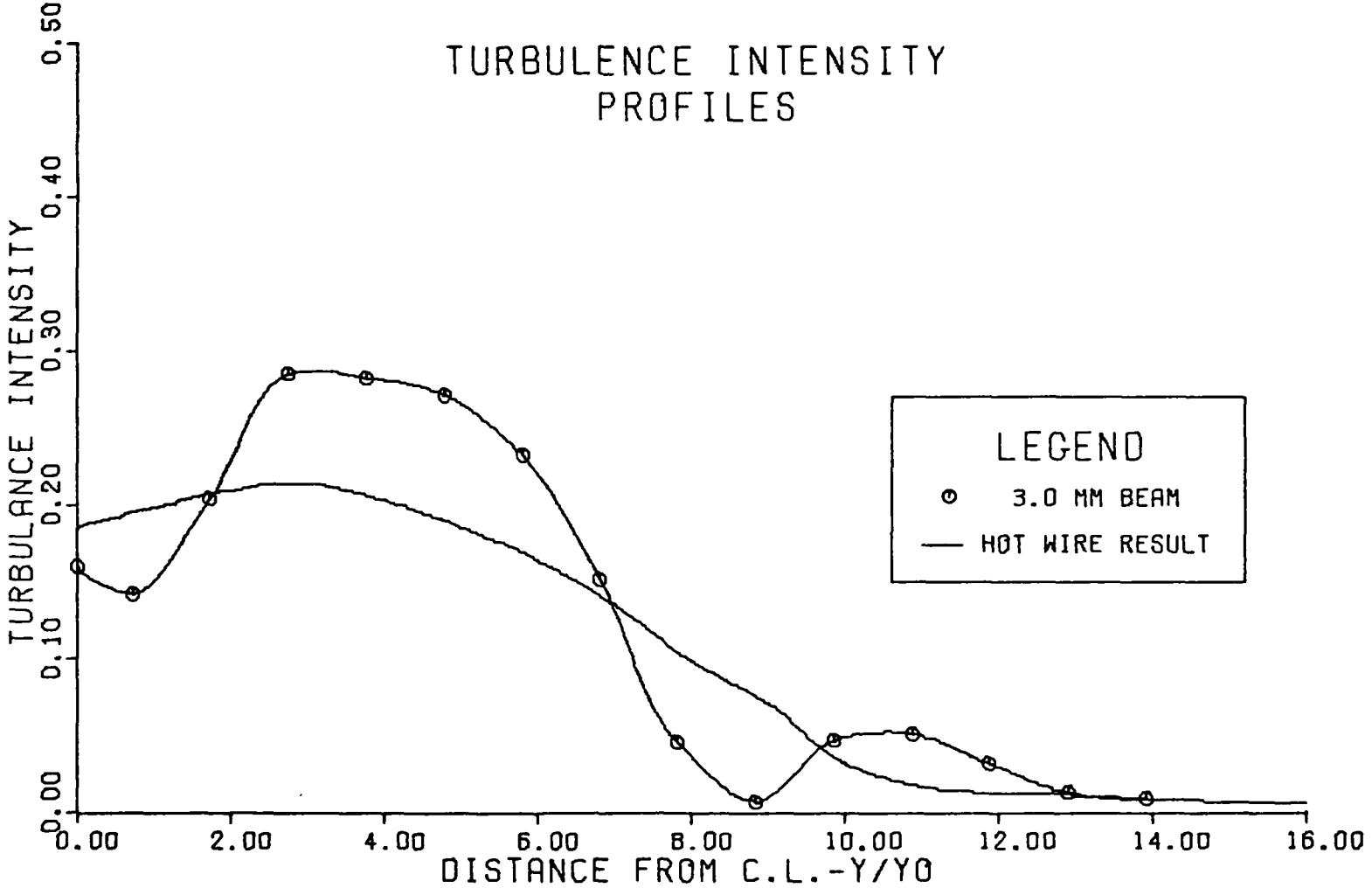

FIG.21. TURBULENCE INTENSITY PROFILES USING 3.0 MM BEAM

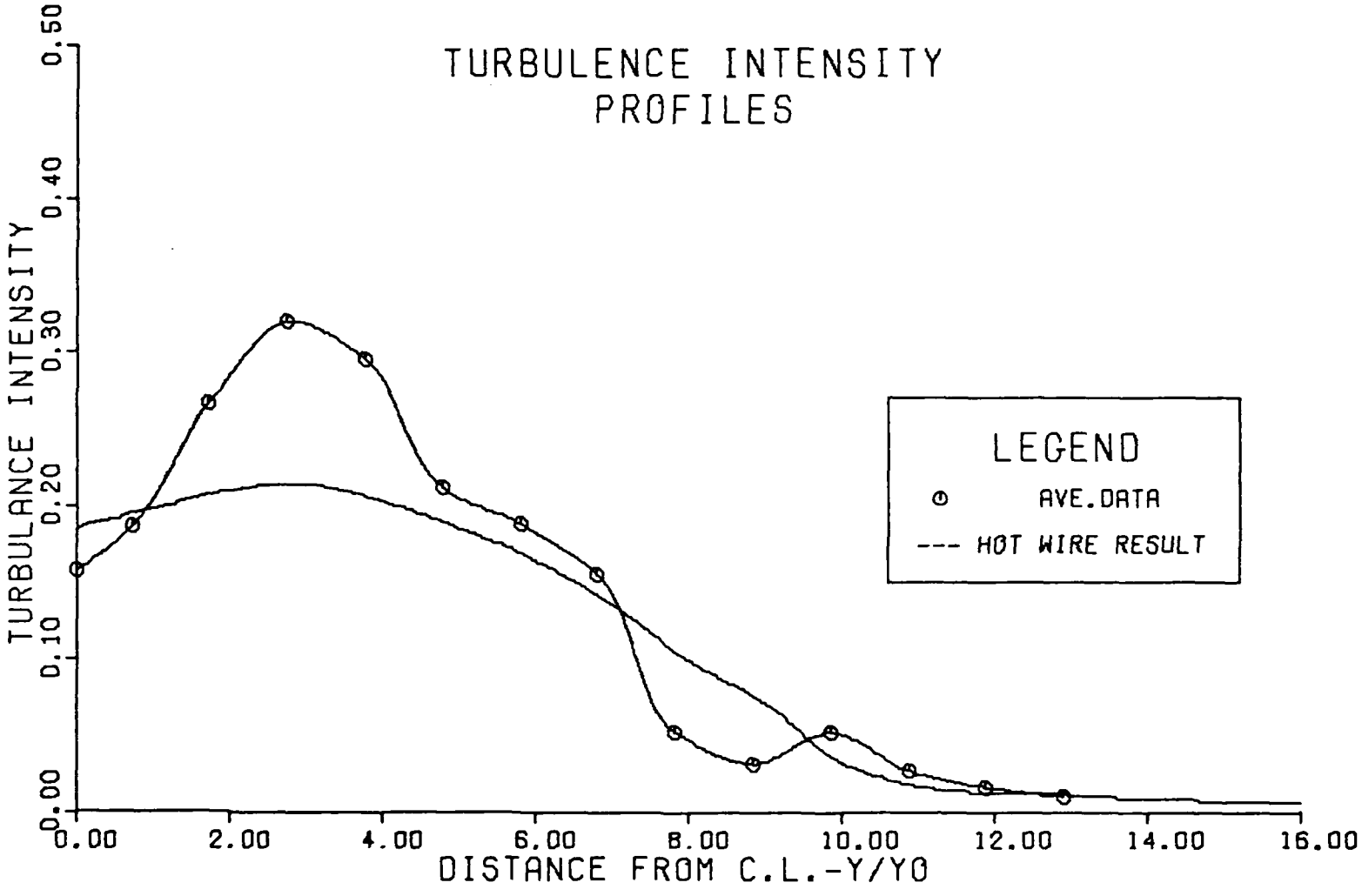

FIG.22. TURBULENCE INTENSITY PROFILES WITH AVERAGE DATA

Hot Wire results. Also, there is an upper limit for validity of the Hot Wire turbulence measurement. At places where turbulence intensity is recorded more than 20%, the results deviate quite a bit from the Hot Wire results. This can be explained by the fact that the formula used for calculating the turbulence intensity is valid only up to turbulence level of 20% (Ref 4). Those values above this limit must be viewed accordingly.

The equation of turbulence intensity is

$$\eta = \frac{1}{\sqrt{2}\,\pi}\left((R-1)+\frac{1}{n^2}\right)^{\frac{1}{2}}$$

A problem of computing the turbulence intensity arose when the R value was less than 1.0. For this investigation, it was assumed that values of R in the range of $R < 1.0$ corresponded to a 0% turbulence intensity. Some concluding remarks on these results are contained in the next section.

VII. Conclusions

As a result of the investigation of the effects of the test rhombus size on the photon correlation laser velocimeter data and limited computer aided data reduction, the following conclusions are drawn:

1. The Laser Velocimeter System, within the framework of the scope of this study, produced good results. The mean velocity results obtained in this investigation for beam diameters up to 5 mm are in conformity with the analytical predictions and consistent with the earlier experimental results. Error in the mean velocity remained below 5% of the theoretical predictions.

2. The LDV system as configured, while quite accurate for mean velocities, did not perform very well in the range of turbulence intensities required. Although some improvement in this area in the present study has been made, the turbulence intensity data above the 20% level is questionable.

3. The effects of the test rhombus size were investigated, and it became evident that the beam sizes could be increased to the working limitations of the LDV system (5 mm diameter), beyond which it reduced the output signal-to-noise ratio of the PM tube and produced questionable results.

4. The averaging of the turbulence intensity results obtained from the multi-readings at a particular station decreases the scatter

in the data and increases the accuracy of the results.

Based on these conclusions, recommendations are made in the next section for extending the use of the system.

VIII. Recommendations

The present LDV system can be used effectively for future study. The following are the recommendations to bring about possible improvements to the system for future investigations.

1. On the basis of the present study, it can be safely stated that the data for the mean velocity and turbulence intensity below the 20% level is accurate and reliable. For the measurements in the region where the turbulence level is more than 20%, a modified method of obtaining the data from the autocorrelation function could be employed by fitting a third order polynomial to the autocorrelation function to correct it for the skewness. This method is outlined in Reference 10, and would involve the use of a phase modulator with the present system.

2. The present system was limited to the nozzle exit Mach number of 0.3. For measuring higher velocities, either a correlator with smaller resolution time would be helpful, or improving the optical set-up by decreasing the incidence angle between the two beams at the cross-over point of the present system would serve the purpose. For improving the optical set-up, it would be very difficult to further increase the size of the optical bench and traverse it along with the equipment across the flow field. Instead, the equipment could be placed at a permanently fixed position at a sufficient distance away from the flow field (giving required incidence angle, θ) and traversing the calming chamber by placing it on a traversing mechanism

and connecting the inlet with the air supply by means of a high pressure flexible hose. This would also eliminate the chances of disturbing the focusing and alignment of the equipment while traversing the optical bench during the experiment.

3. A more detailed evaluation of the effects of test rhombus size could be made by the use of higher size pinhole apertures in the PM tube. This would increase the scanning area of the focal volume observed by the PM tube and would also improve the signal-to-noise ratio. But with higher size pinhole apertures, utmost precaution must be taken with small beam sizes, as it might allow excessive light to enter the PM tube and damage it.

4. A phasemodulator with larger crystals to accommodate larger beam diameter would extend the system to measure higher turbulence levels.

5. To evaluate scatter in the data and thus enhance the quality of the data, multi-readings at each station should be accomplished. This can now be made possible with recent delivery of the automatic data acquisition and processing system to the Department of Aeronautics and Astronautics.

Bibliography

1. Abramovich, G.N. The Theory of Turbulent Jets. Cambridge MA: The M.I.T. Press, 1963.

2. Cerullo, N.G. An Experimental Evaluation of a Laser Velocimeter by the Study of Turbulence in a Plane Free Jet at High Subsonic Velocities. M.S. Thesis. Wright-Patterson Air Force Base OH: Air Force Institute of Technology, June 1979.

3. Durst, F., Melling, A. and Whitelaw, J.H. Principles and Practice of Laser-Doppler Anemometry. Academic Press, Inc. (London) Ltd., 1976.

4. Malvern Instruments, Ltd. Operating and Installation Manual. Spring Lane Trading Estate, Malvern Link, Worcestershire WR14 1AL, England.

5. Morris, S.L. A Diagnostic Study of Flow in the Wake of a Circular Disk Using a Photon Correlation Laser Velocimeter. M.S. Thesis. Wright-Patterson Air Force Base OH: Air Force Institute of Technology, March 1980.

6. Pai, S.I. Fluid Dynamics of Jets. Von Norstrand Company, Inc., Canada, 1954.

7. Rogers, H.J.V. Velocity Profiles in a Long Inlet Duct Employing a Photon Correlation Laser Velocimeter Without Seeding. M.S. Thesis. Wright-Patterson Air Force Base OH: Air Force Institute of Technology, December 1979.

8. Schlichting, H. Boundary Layer Theory. Seventh Edition. McGraw-Hill Book Company, Inc. New York, 1979.

9. Shepard, W.K. Turbulence Measurements in a Plane Free Jet at High Subsonic Velocities. M.S. Thesis. Wright-Patterson Air Force Base OH: Air Force Institute of Technology, December 1974.

10. Walterick, R.E. An Experimental Investigation of the Near Wake of a Circular Cylinder. M.S. Thesis. Wright-Patterson Air Force Base OH: Air Force Institute of Technology, September 1980.

APPENDIX A

Theory of Free Turbulence in Two Dimensional Jet (Refs 1, 8)

Theoretical solution to two dimensional turbulent free jet flow was first given by W. Tollmien who used Prandtl's old mixing length theory (Ref 1). In 1943, Prandtl proposed a new theory of free turbulence with the main assumption that the coefficient of turbulent viscosity, not the mixing length, is constant over a cross section of the jet (Ref 1). He proposed that the dimensionless velocity profiles at various cross sections of the flow of the jet are similar.

H. Goertler used Prandtl's new theory and arrived at much simpler solutions to the two dimensional turbulent jet (Ref 1). In the present research, experimental data on the velocity has been compared with the Tollmien and Goertler velocity profiles. The following represent Goertler's solution to the two dimensional turbulent jet.

The equation of motion for the two dimensional steady isobaric flow of an incompressible fluid can be represented in the following form:

$$u \frac{\partial u}{\partial x} + v \frac{\partial u}{\partial y} = 1/\rho \frac{\partial \tau_{xy}}{\partial y} \qquad \text{(A-1)}$$

where τ_{xy} is the shearing stress acting in a plane perpendicular to the x-y plane.

According to Prandtl's new theory, shearing stress in a submerged jet is given by

$$\tau_{xy} = \rho \chi b (U) \frac{\partial u}{\partial y}$$

and

$$\varepsilon = \chi b U$$

where ε is the virtual kinematic viscosity, χ an empirical constant, b is the half width of the jet, and U is the center-line velocity.

Substituting the value of τ_{xy} in A-1 momentum equation reduces to

$$u \frac{\partial u}{\partial x} + v \frac{\partial u}{\partial y} = \varepsilon \frac{\partial^2 u}{\partial y^2} \qquad \text{(A-2)}$$

and equation of continuity

$$\frac{\partial u}{\partial x} + \frac{\partial v}{\partial y} = 0 \qquad \text{(A-3)}$$

In two dimensional jets, the center-line velocity is inversely proportional to the square root of the distance x and jet width is directly proportional to the distance x . This gives the relation

$$U = \frac{n}{\sqrt{x}} \qquad \text{(A-4)}$$

and

$$b = a x$$

where n and a are constants.

Taking a fixed characteristic distance s from the origin, the point center-line velocity and jet width would be

$$U_s = \frac{n}{\sqrt{s}}$$

and

$$b_s = a\, s$$

Taking the ratios respectively, one can write

$$U = U_s \sqrt{\frac{s}{x}}$$

and

$$b = b_s \frac{x}{s}$$

Similarly,

$$\varepsilon_s = \chi\, b_s\, U_s$$

$$\varepsilon = \varepsilon_s \frac{b}{b_s} \frac{U}{U_s} = \varepsilon_s \sqrt{\frac{x}{s}}$$

Replacing this value in Eq (A-2), one obtains

$$u \frac{\partial u}{\partial x} + v \frac{\partial u}{\partial y} = \varepsilon_s \sqrt{\frac{x}{s}} \frac{\partial^2 u}{\partial y^2} \qquad \text{(A-5)}$$

Let us define a new variable η such that

$$\eta = \sigma \frac{y}{x}$$

$$\frac{d\eta}{dx} = -\sigma \frac{y}{x^2} \quad \text{and} \quad \frac{d\eta}{dy} = \frac{\sigma}{x}$$

Here, σ is a free constant which is evaluated experimentally.

At this stage, one assumes the existence of a stream function ψ which is of the form:

$$\psi = \frac{U_s \sqrt{sx}\, F(\eta)}{\sigma}$$

such that

$$\frac{\partial \psi}{\partial x} = -v \quad \text{and} \quad \frac{\partial \psi}{\partial y} = u$$

This stream function satisfies the equation of continuity (A-3). Evaluating the values of u and v from this stream function, one obtains

$$u = \frac{\partial \psi}{\partial y} = \frac{U_s \sqrt{sx}\, F'(\eta)}{\sigma} \cdot \frac{d\eta}{dy}$$

$$u = U_s \sqrt{\frac{s}{x}}\, F' \qquad \text{(A-6)}$$

Similarly,

$$v = -\frac{\partial \psi}{\partial x} = \frac{U_s \sqrt{\frac{s}{x}}}{\sigma} \left[\frac{\sigma y}{x} F' - \frac{1}{2} F\right] \qquad \text{(A-7)}$$

From Eq (A-6) one evaluates:

$$\frac{\partial u}{\partial x} \quad , \quad \frac{\partial u}{\partial y} \quad \text{and} \quad \frac{\partial^2 u}{\partial y^2}$$

Substitute these results and values of u and v from Eqs (A-6) and (A-7), respectively, in the original momentum equation (A-2). After simplification, the momentum equation reduces to the form:

$$\frac{1}{2} F'^2 + \frac{1}{2} F F'' + \frac{\varepsilon_s \sigma^2}{U_s s} F''' = 0 \qquad \text{(A-8)}$$

Since ε_s contains free constant χ, one can write σ:

$$\sigma = \frac{1}{2}\sqrt{\frac{U_s s}{\varepsilon_s}}$$

This reduces the above differential equation to

$$\frac{1}{2} F'^2 + \frac{1}{2} F F'' + \frac{1}{4} F''' = 0 \qquad \text{(A-9)}$$

Integrating Eq (A-9) once, one obtains

$$\frac{1}{2} F F' + \frac{1}{4} F'' = C_1$$

or

$$2 F F' + F'' = C_2$$

Integrating the second time, one obtains

$$F^2 + F' = C_2\eta + C_3 \qquad \text{(A-10)}$$

These two constants of integration can be evaluated with the aid of the two boundary conditions; that is, at $y = 0$ and $y = \pm \infty$, at $y = 0$, $\psi = 0$ and $u = U$. That is, at $\eta = 0$, $F = 0$ and $F' = 1$; at $y = \pm \infty$, $u = 0$; that is, at $\eta = \pm \infty$, $F' = 0$.

These boundary conditions give the following values of C_2 and C_3:

$$C_2 = 0 \quad \text{and} \quad C_3 = 1$$

Then Eq (A-10) takes the final form:

$$F^2 + F' = 1 \qquad \text{(A-11)}$$

This is the familiar differential equation for the two dimensional laminar jet with the solution

$$F = \tanh(\eta) \qquad \text{(A-12)}$$

The velocity ratio is given by Eq (A-6)

$$\frac{u}{U_s\sqrt{\frac{s}{x}}} = \frac{u}{U} = F'$$

Therefore,

$$\frac{u}{U} = \operatorname{sech}^2(\eta)$$

The value of the single empirical constant σ was determined experimentally by H. Reichardt, who found $(\sigma = 7.67)$.

Goertler also made another assumption that $u = \frac{1}{2} U$ at $y = y_{1/2}$. These results, along with the Tollmien solution, are plotted in Figure 23, which forms a basis for comparison between the theoretical and experimental results in this research for the mean velocity.

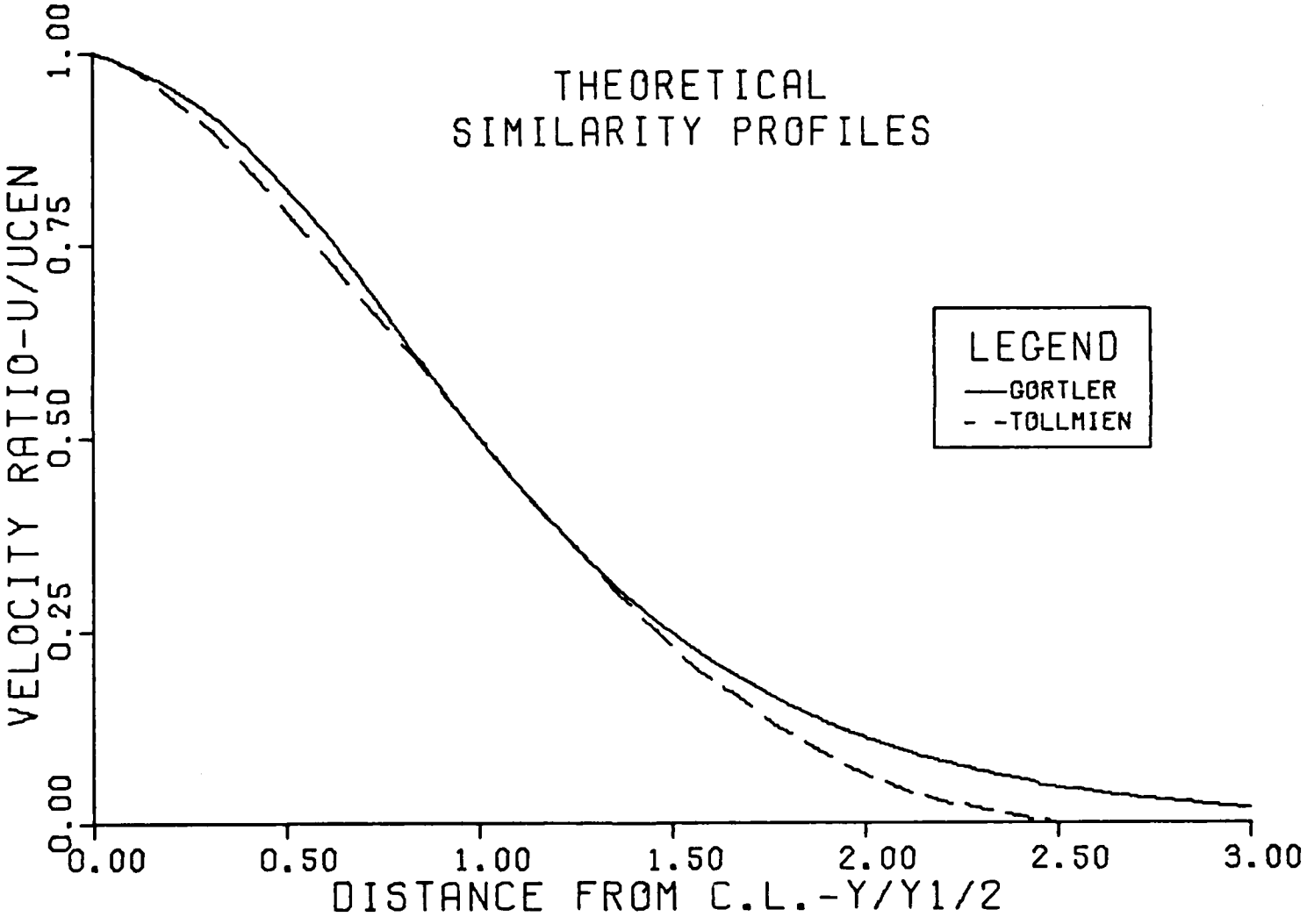

FIG. 23.THEORETICAL MEAN VELOCITY SIMILARITY PROFILES

APPENDIX B

Evaluation of Center-Line Velocity At a Fixed Distance From the Exit (Ref 1)

In this work, ratio of center-line velocity to the exit velocity has been frequently compared with the theoretical result. The following represent theoretical relation between the ratio of center-line velocity to the core velocity and distance from the exit plane of the jet.

Starting with Eq (A-4) of Appendix A, which shows that the center-line velocity in two dimensional jets is inversely proportional to the square root of the distance x from the exit plane,

$$U_{cen} = \frac{n}{\sqrt{x}} \tag{B-1}$$

where n is a constant.

In a free plane jet, momentum remains constant. Using the equation of conservation of momentum

$$\rho \int_0^\infty u^2 dy = \rho U_{cor}^2 b_0 = \text{constant} \tag{B-2}$$

where U_{cor} is the exit velocity and b_0 is one half jet width at the exit ($b_0 = 0.5$ mm) . Multiplying and dividing the left side of the equation by U_{cen}^2

$$U_{cen}^2 \int_0^{\infty} \left(\frac{u}{U_{cen}}\right)^2 dy = U_{cor}^2 b_0 \qquad \text{(B-3)}$$

Now, making a change of variable to evaluate the integral, put

$$\phi = y/ax \rightarrow dy = axd\phi$$

where $F'(\phi) = \frac{u}{U_{cen}}$

at $y = 0 \rightarrow \phi = 0$

(Ref 1:Table 2.3)

and $y = \infty \rightarrow \phi = 2.4$

Then Eq (B-3) reduces to

$$\frac{U_{cen}}{U_{cor}} = \frac{1}{\sqrt{\frac{a_x}{b_0} \int_0^{2.4} F'^2(\phi)\, d\phi}} \qquad \text{(B-4)}$$

The value of the integral can be found from tabular data of Table 2.3 of Reference 1.

$$\int_0^{2.4} F'^2(\phi)\, d\phi = 0.685$$

The resulting equation from Eq (B-4) would be

$$\frac{U_{cen}}{U_{cor}} = \frac{1.2}{\sqrt{\frac{a_x}{b_0}}} \qquad \text{(B-5)}$$

The value of the constant a which closely fitted the Cerullo's experimental results (Ref 2) is

$$a = 0.08$$

Other values of the constant a , based on the experimental results range from 0.09 to 0.12 for plane jets and 0.066 to 0.076 for round jets (Ref 1).

Setting $a = 0.08$ and $b_0 = 0.5$ cm , one can calculate the length of potential core for this jet. In potential core

$$U_{cen} = U_{cor}$$

Then, length of potential core is

$$x_{pc} = \frac{1.44\ b_0}{a}$$

$$x_{pc} = 9.0 \text{ cm} \qquad \text{(B-6)}$$

Since, in this report, all data were taken at 25.0 cm from the jet exit, putting $x = 25.0$ would give the theoretical value of U_{cen} / U_{cor} .

$$\left(\frac{U_{cen}}{U_{cor}} \right)_{\text{at } x = 25 \text{ cm}} = 0.6 \qquad \text{(B-7)}$$

APPENDIX C

Power Requirement for L.D.V. (Ref 3)

During the course of the present study, it became evident that the availability of sufficient radiation power was of practical importance to Laser-Doppler Anemometry. Here effort is made to derive an analytic expression for the required laser power as a function of velocity, optical arrangement and photodetector properties.

It was shown by Van de Hulst (1957) that the intensity, I, of scattered light at a point a large distance R from the particle may be expressed as

$$I = \frac{I_o F(\theta,\phi)}{K^2 R^2} \qquad (C\text{-}1)$$

where $K = 2\pi/\lambda$ and I_o is the beam intensity. Total light power, P_s, scattered by a small particle can be obtained by integrating Eq (C-1) over the surface of a sphere of radius R and taking the solid angle element to be $d\omega$:

$$P_s = \int_s I R^2 \, d\omega \qquad (C\text{-}2)$$

where $d\omega = \sin\theta d\theta d\phi$

$$P_s = \frac{I_o}{K^2} \int_s F(\theta,\phi)\sin\theta d\theta d\phi \qquad (C\text{-}3)$$

Equation of total scattered power, P_s , may be rewritten employing the scattering cross-section, C_{scat} , and the scattering efficiency factor, Q_{scat} .

$$P_s = I_o C_{scat} = (\pi r_p^2 Q_{scat}) I_o \qquad (C\text{-}4)$$

where

$$C_{scat} = \int_s \frac{1}{K^2} F(\theta,\phi) \sin\theta d\theta d\phi$$

is called the scattering cross-section and represents an area the particle seems to occupy to remove the total power, P_s , from a light beam of intensity, I_o , and

$$Q_{scat} = \frac{C_{scat}}{\pi r_p^2}$$

is another integral quantity that has been used to quantify light scattering from particles is the so-called scattering efficiency which is the ratio between the scattering cross-section and the cross-section of the particles.

Here beam intensity, I_o , can be written in terms of laser power, P_L , and focused beam diameter, D_I .

$$I_o = \frac{4 P_L}{\pi D_I^2} \tag{C-5}$$

Assuming that the light intensity inside the measuring control volume is constant, the total number of scattered photons per unit time can be computed to be

$$n_s = \frac{P_s}{h\nu} = \frac{4 P_L C_{scat}}{\pi D_I^2 h\nu} \tag{C-6}$$

or

$$n_s = \frac{4 P_L Q_{scat} r_p^2}{D_I^2 h\nu}$$

The particle spends only a very short time inside the measuring control volume. This time interval, $\Delta\tau$, can be expressed in terms of diameter, dm , of measuring control volume, velocity, U , of particle, number of fringes, N_{Ph} , observed by the photomultiplier tube and fringe spacing, s :

$$\Delta\tau = \frac{dm}{U} = \frac{N_{Ph} S}{U} \tag{C-7}$$

Here $\nu_D = U/S$ is the Doppler frequency. Replacing this quantity in Eq (C-7), one obtains

$$\Delta\tau = \frac{N_{Ph}}{\nu_D} \tag{C-8}$$

Then, within this time interval $\Delta\tau$, N_s number of photons will be scattered in all directions.

$$N_s = n_s \Delta\tau = \frac{4 P_L Q_{scat} r_p^2}{D_I^2 h\nu} \frac{N_{Ph}}{\nu_D} \qquad \text{(C-9)}$$

Equation (C-9) gives the total number of photons scattered per particle in all directions. Only a small portion of the scattered photons will reach the photomultiplier tube due to finite collection efficiency of the light collecting system. Then the number of scattered photons collected at the photomultiplier tube would be

$$N_{sc} = \eta_c N_s \qquad \text{(C-10)}$$

where η_c is the efficiency of the light collecting system. Equation (C-10) gives the total number of photons detected by the photomultiplier tube per particle. The number of electrons leaving the cathode of the photomultiplier tube is given by multiplying the number of collected photons, N_{sc} , with the quantum efficiency, η_q

$$Ne = \eta_q N_{sc} = 4\eta_q \eta_c \frac{P_L Q_{scat} r_p^2}{D_I^2 h\nu} \frac{N_{Ph}}{\nu_D} \qquad \text{(C-11)}$$

Equation (C-11) gives a quantified relation of the number of electrons per particle arriving at the cathode of the photomultiplier tube. There is a minimum number of electrons required to ensure signal

detectability. The higher the number of electrons per particle, the higher the signal-to-noise ratio will be and the Eq (C-11) shows the main parameters that influence the accuracy of Laser-Doppler measurements.

In the present study, almost all the parameters were constants on the right hand side of the Eq (C-11), except focused beam diameter, D_I . In the above relation the number of electrons, Ne , or in other words signal-to-noise ratio, is inversely proportional to the square of the focused beam diameter, D_I . This explains the deterioration of signal-to-noise ratio or the output of the photomultiplier tube as the beam diameter increases. An increase in signal-to-noise ratio can be expected by employing the following techniques:

(a) Increasing particle size, r_p , and hence increasing scattering efficiency at the expense of velocity measuring error.

(b) Increasing the illumination in the measuring control volume by decreasing the dimensions of the focal spot.

(c) Increasing the efficiency, η_c , of the light collecting system.

(d) Increasing power, P_L , of the laser.

(e) Decreasing the particle velocity and, hence, the signal frequency, ν .

APPENDIX D

Beam Diameter Measurement

This investigation was centered at the effects of test rhombus size on the photon correlation laser velocimeter system. This required a method of expanding the 1.1 mm diameter laser beam to various sizes. This appendix deals with the technique of expanding the laser beam and method of measuring the beam diameter. Results of some sample cases would then be presented at the end of the appendix. Figure 24 shows a pictorial view of the experimental set-up used for measuring beam diameter. Following represents the various components used in this experiment and their functions.

Laser. A 15 mW Spectra Physics Model 124A helium-neon laser in conjunction with a Model 255 DC exciter was used to produce a single laser beam of 1.1 mm in diameter.

Expanding Lenses. Three different sizes of expanding lenses, L1, L3 and L6, were used having diameters of 1.1 mm, 2.4 mm and 7.4 mm with focal length of 3.9 mm, 8.5 mm and 25.9 mm, respectively. Figure 25 shows a picture of this expanding lens.

Pinhole Aperture. Three different sizes of pinhole aperture, A3, A4 and A6, were used having aperture diameters of 6.8 μm, 10.0 μm and and 22.0 μm, respectively. These are small, round holes in a thin metal disk, which are used for spatial filtering of laser beam to optimize beam uniformity, and for other diffraction applications. Figure 25 shows a picture of pinhole aperture.

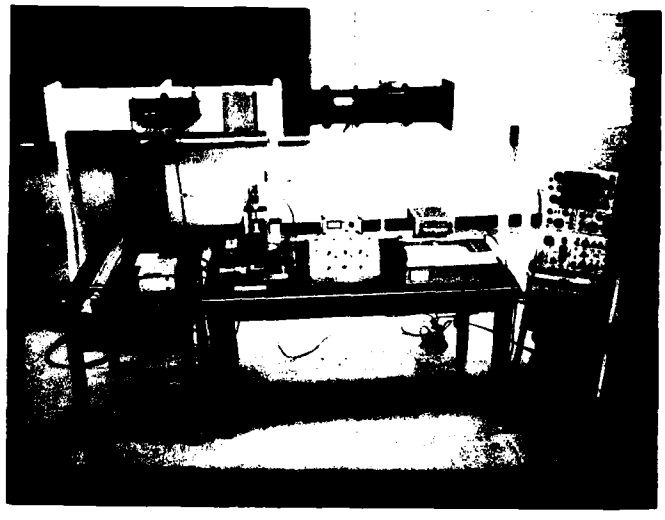

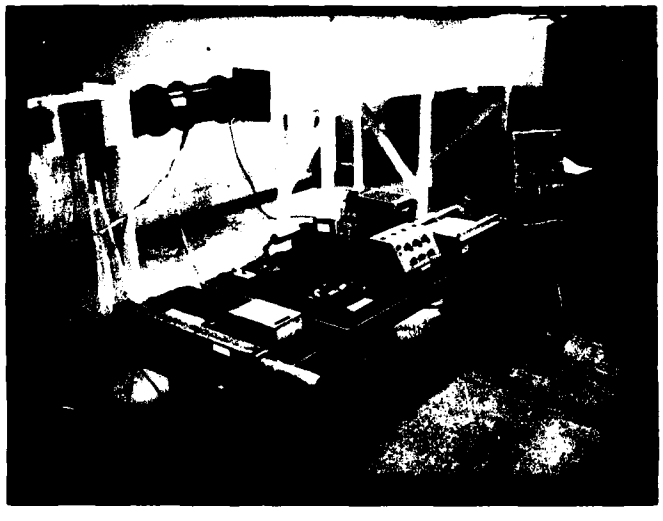

Figure 24. Experimental Set-up for Beam Diameter Measurements

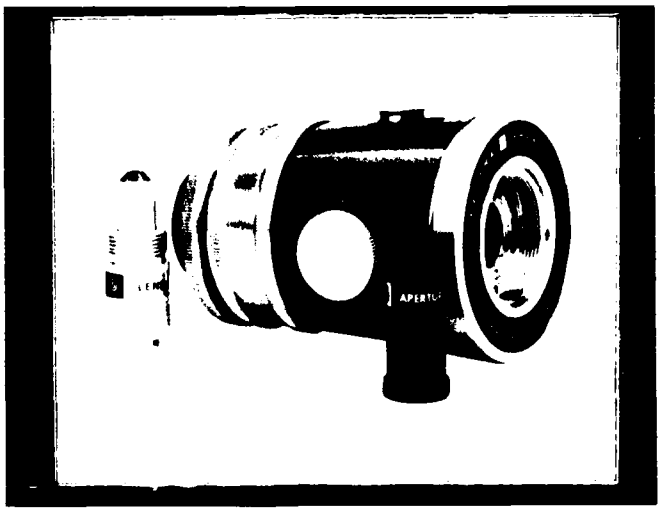

Figure 25. Expanding Lens, Pinhole Aperture and Spatial Filter.

Spatial Filter. Spectra Physics Model 332 spatial filter utilizes a precision pinhole and expanding lens (Figure 25) to eliminate spatial noise, producing a smooth Gaussian intensity profile across the collimated beam from a Model 336 telescope. Model 332 spatial filter contains a knob for aperture adjustment in the x-axis. Two knobs on the side are provided for aperture adjustments in the Y and Z directions. It can be mounted directly to the laser with 1"-32 thread.

Collimating Lens. Spectra Physics Model 336 beam expanding telescope was used for producing a collimated beam diameter up to 50 mm from the laser. It can be mounted directly to Model 332 spatial filter. When used with Model 332, it produces a spatially filtered output beam with smooth Gaussian energy distribution. Figure 26 shows a diagram of Model 336 mounted on Model 332 spatial filter. Its focal length varies from 2 meters to infinity.

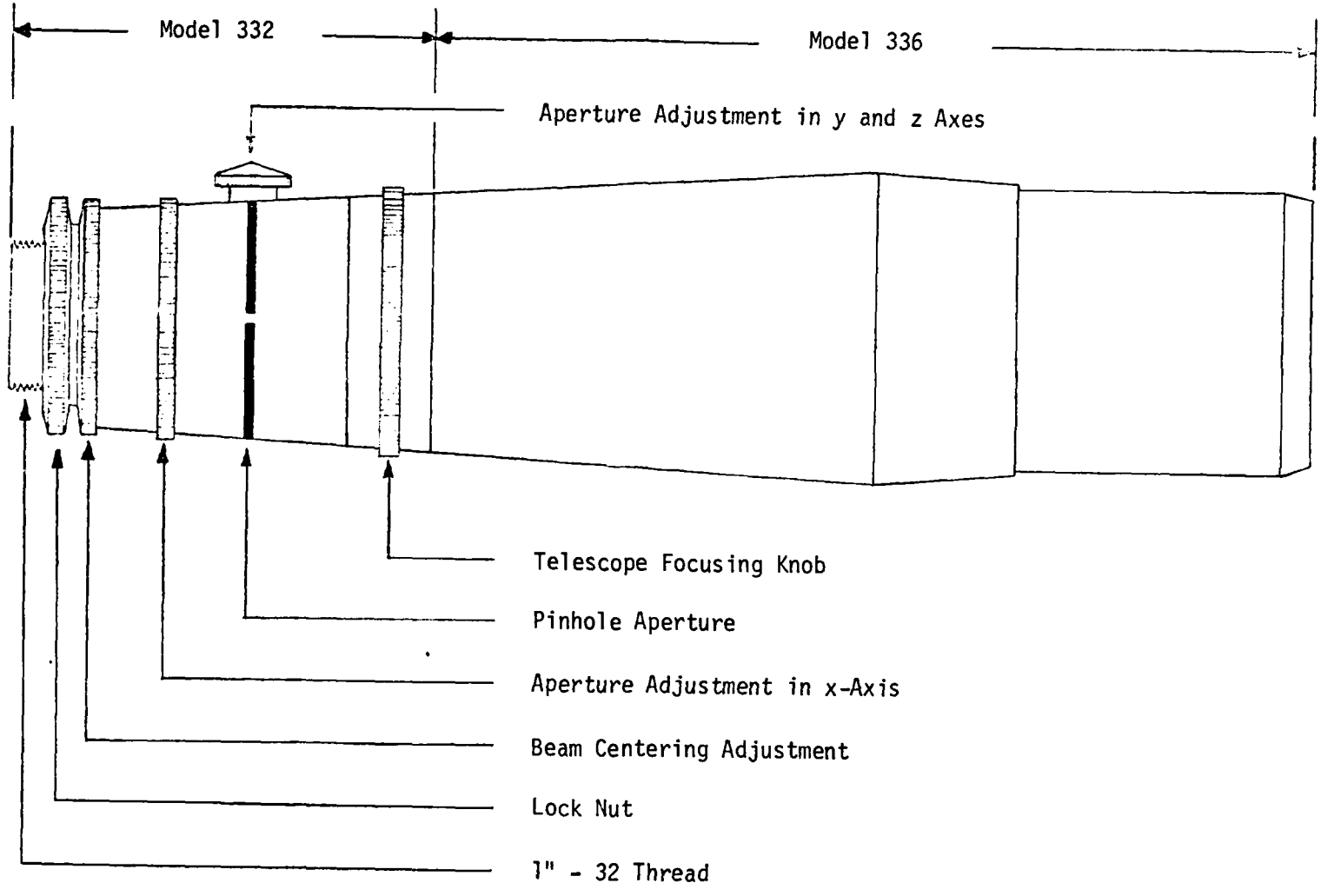

Figure 26. Laser Beam Expanding Assembly

Power Meter. Spectra Physics Model 401C power meter, along with a sensing head, was used for measuring laser output power up to 100 mW full scale. Figure 27 shows the diagram of power meter and sensing head. A recorder output is located on the front panel, through which the output of the power meter can be directly connected to the recorder.

Traversing Mechanism. A two-dimensional traversing mechanism having 12.0 cm of travel in both horizontal and vertical directions was used for traversing the sensing head across the beam. The sensing head was mounted on a plate of traversing mechanism which in turn could move in two directions with the aid of two reversible electric motors. Two slide-pin resistors were mounted on the traversing mechanism for recording the travel of sensing head in either direction on the X-Y recorder.

Control Unit for Traversing Mechanism. This control unit provided electric current to the two motors of the traversing mechanism on pressing the respective selection button. A directional (forward or rear) control switch and motor's speed control switch were provided for regulating the direction and speed of each motor.

DC Power Supply. Hewlett Packard DC power supply was used to provide the DC voltage to the slide-pin potentiometer mounted on the traversing mechanism. The output from the potentiometer, which corresponded to the travel of sensing head, was then fed to the X-Y recorder.

Amplifier. Tektronix type 555 dual-beam oscilloscope was used for amplification of the output signal from the power meter. This amplified signal was then fed to the X-Y recorder.

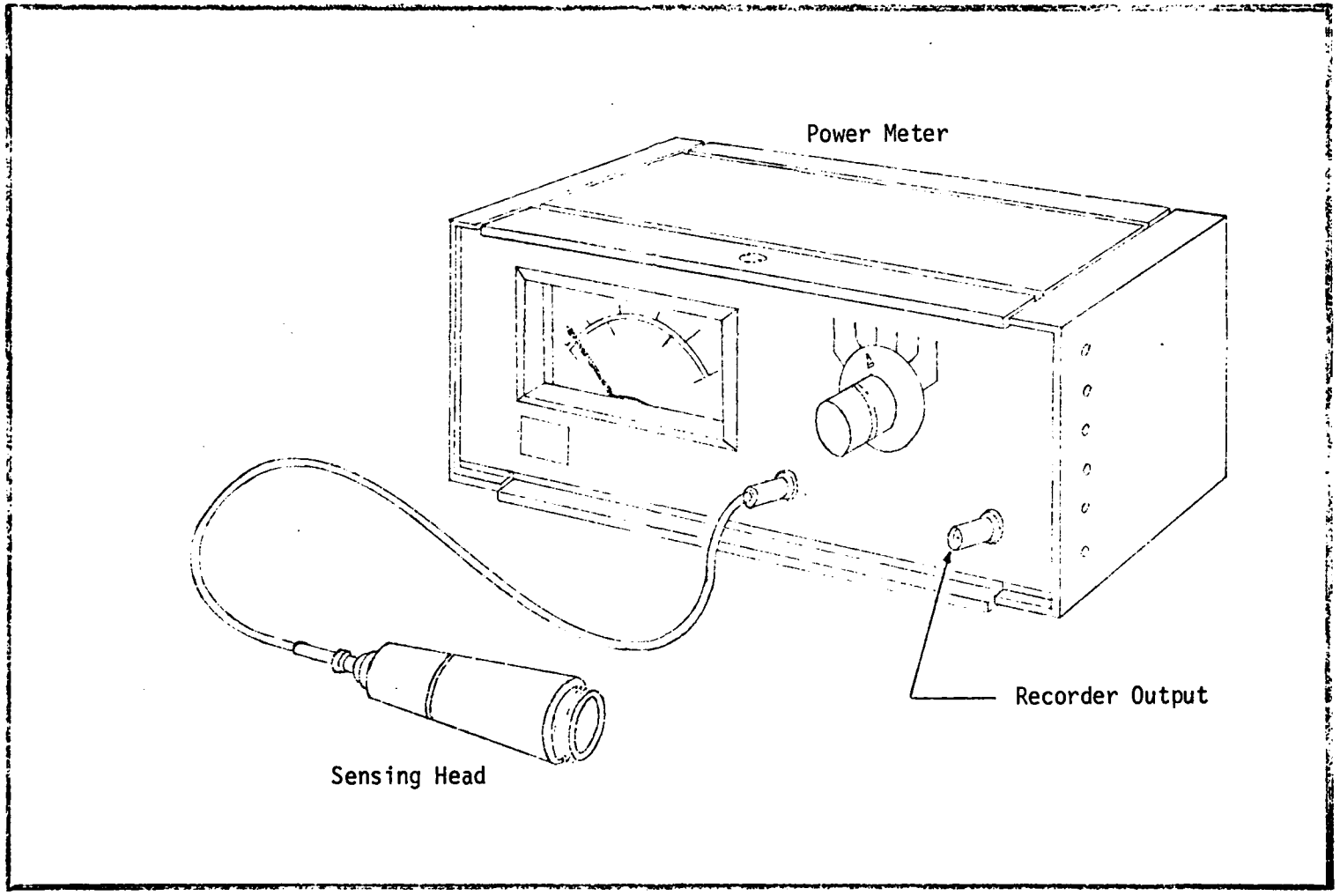

Figure 27. Power Meter and Sensing Head

X-Y Recorder. Electro Instrument Model 320 X-Y recorder was used for plotting the beam intensity profiles across the beam diameter. These plots were then used for determining the beam diameter.

Procedure. Interchangeable Spectra Physics optics (expanding lenses and pinhole apertures), when used with Model 332 and 336, provided an easy way of expanding a laser beam to fixed output beam diameter. Two charts shown in Figure 28 provide a guide line for selecting an appropriate expanding lens (L number) to achieve desired output beam diameter for a given input beam diameter. The other chart is used for the selection of aperture (A number) for a chosen lens and input beam diameter. The three lenses and three apertures provided the necessary combinations to form four different output beam diameters.

These combinations, along with their approximate output beam diameters, are given in Table III.

TABLE III

Lens and Aperture Combinations

Lens L	Aperture A	Approximate Output Beam Diameter
6	6	11 mm
3	6	27 mm
3	4	30 mm
1	3	50 mm

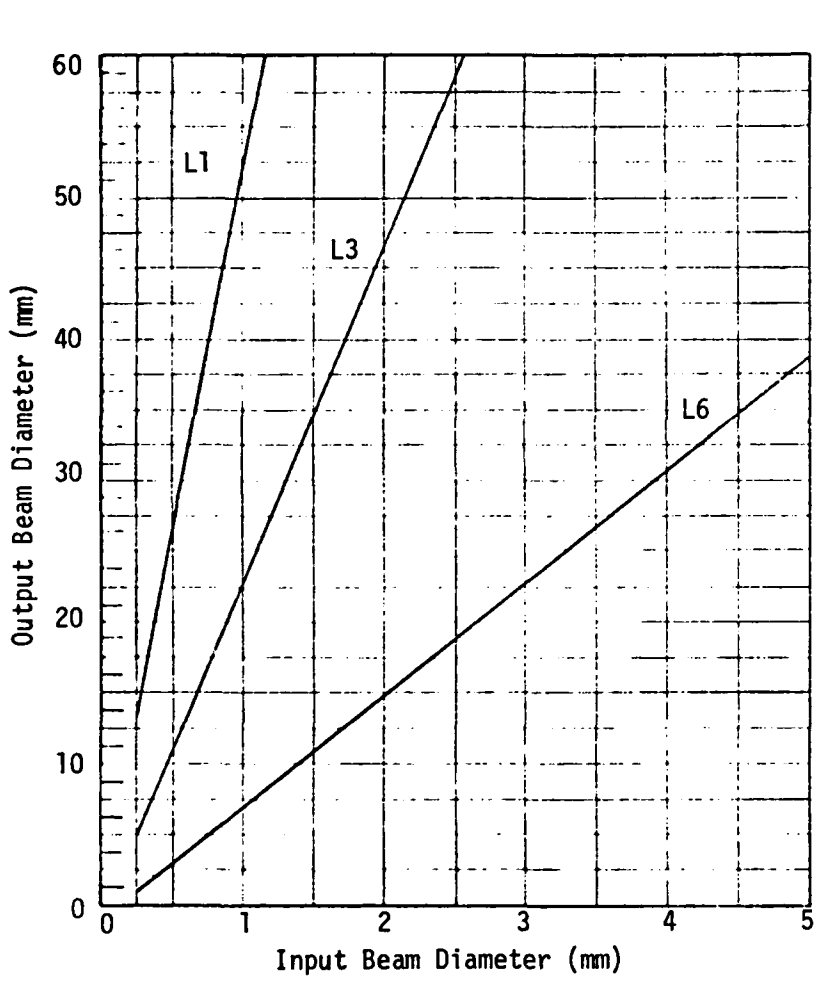

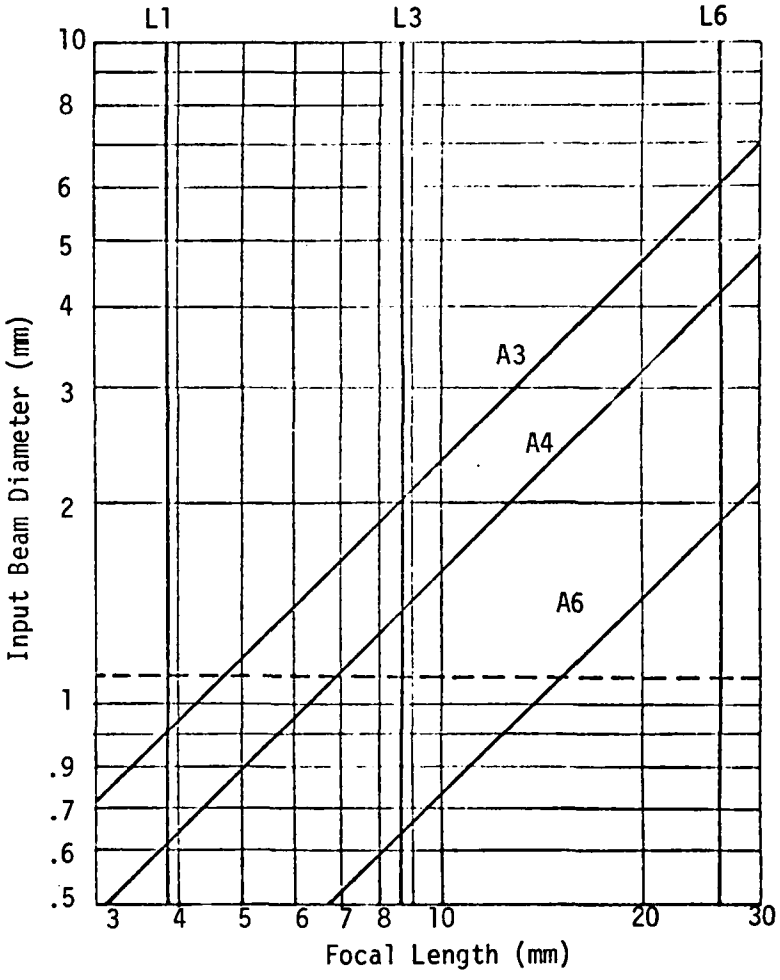

Figure 28. Guide for Selecting Beam Expanding Lens and Pinhole Aperture

Principle of Operation. Spectra Physics beam expanding assembly, when used with appropriate lens and aperture, expands the input beam to a specified diameter. This outgoing beam is spatially filtered to produce smooth Gaussian energy distribution. A typical energy distribution curve of a Gaussian beam is shown in Figure 29 . Here, peak intensity, I_o , is at the center of the beam. Beam edges are defined at the point where intensity, I , is equal to I_o/e^2 where I_o is the maximum intensity. Distance, D , is then defined as the beam diameter.

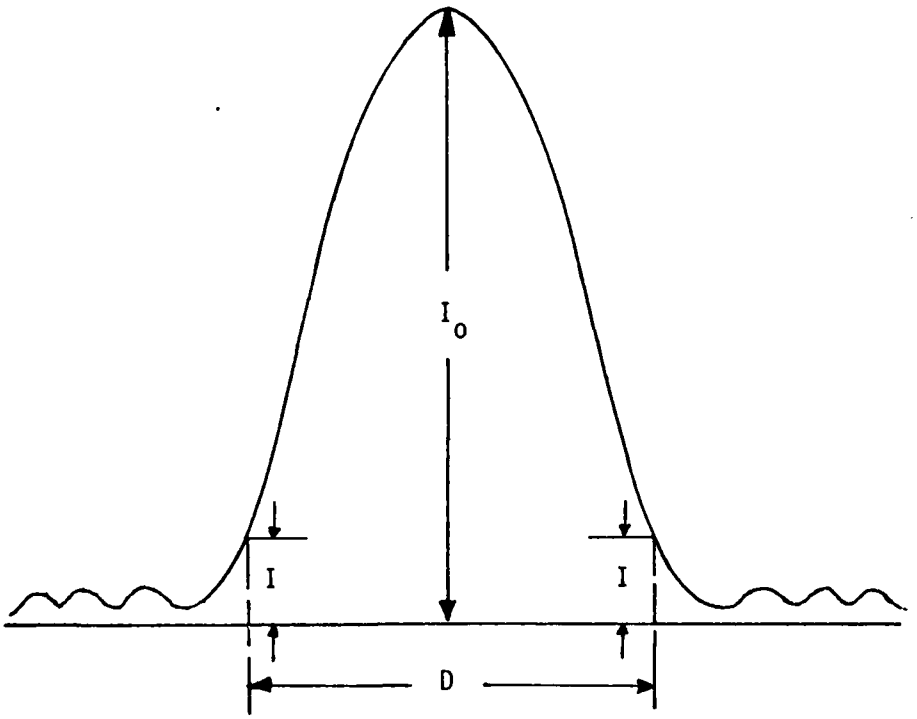

Figure 29. Intensity Profile of a Gaussian Beam

Results. Four different combinations of beam expanding lenses and apertures, as given in Table III, were used for expanding the 1.1 mm laser beam. For each output beam, four different traverses were made. Two traverses were made in horizontal and vertical directions across the

beam without using any pinhole aperture in front of the sensing head. The other two traverses were made in the same directions, but using 600 μm pinhole aperture in front of the sensing head. Use of this pinhole reduced the measuring area and gave more detailed intensity profile of the beam. Results of these measurements are presented in Figure 30 to Figure 43 at the end of this appendix. Expanded beam diameter from a particular lens and aperture combination was determined by taking the average of four values obtained from four different traverses. Experimental values of measured beam diameters are given in Table IV below.

TABLE IV

Results of Beam Diameter Measurements

Lens L	Aperture A	Experimental Output Beam Diameter
6	6	12 mm
3	6	27 mm
3	4	30 mm
1	3	50 mm

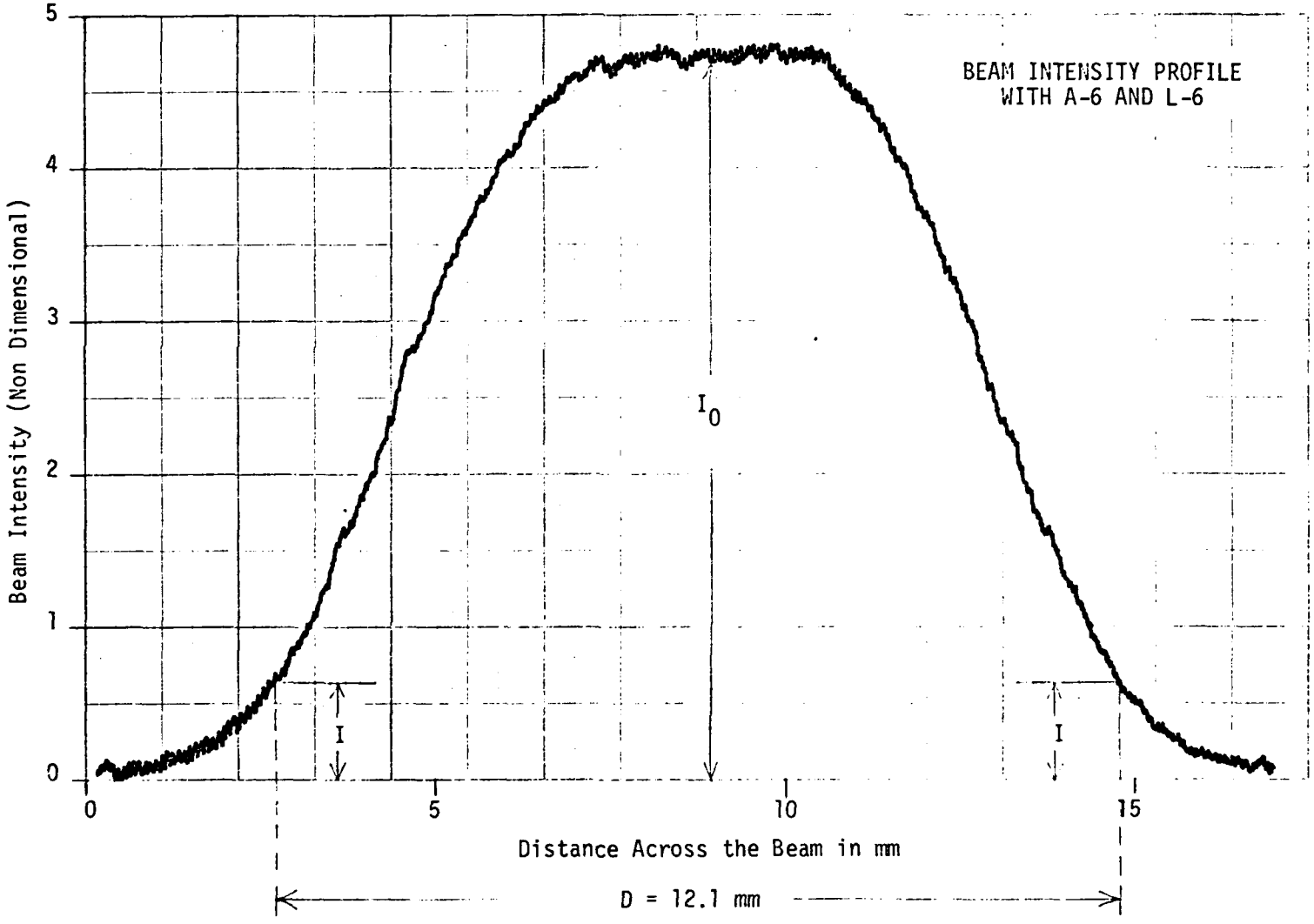

Figure 30. Beam Diameter Without Pinhole in Horizontal Traverse

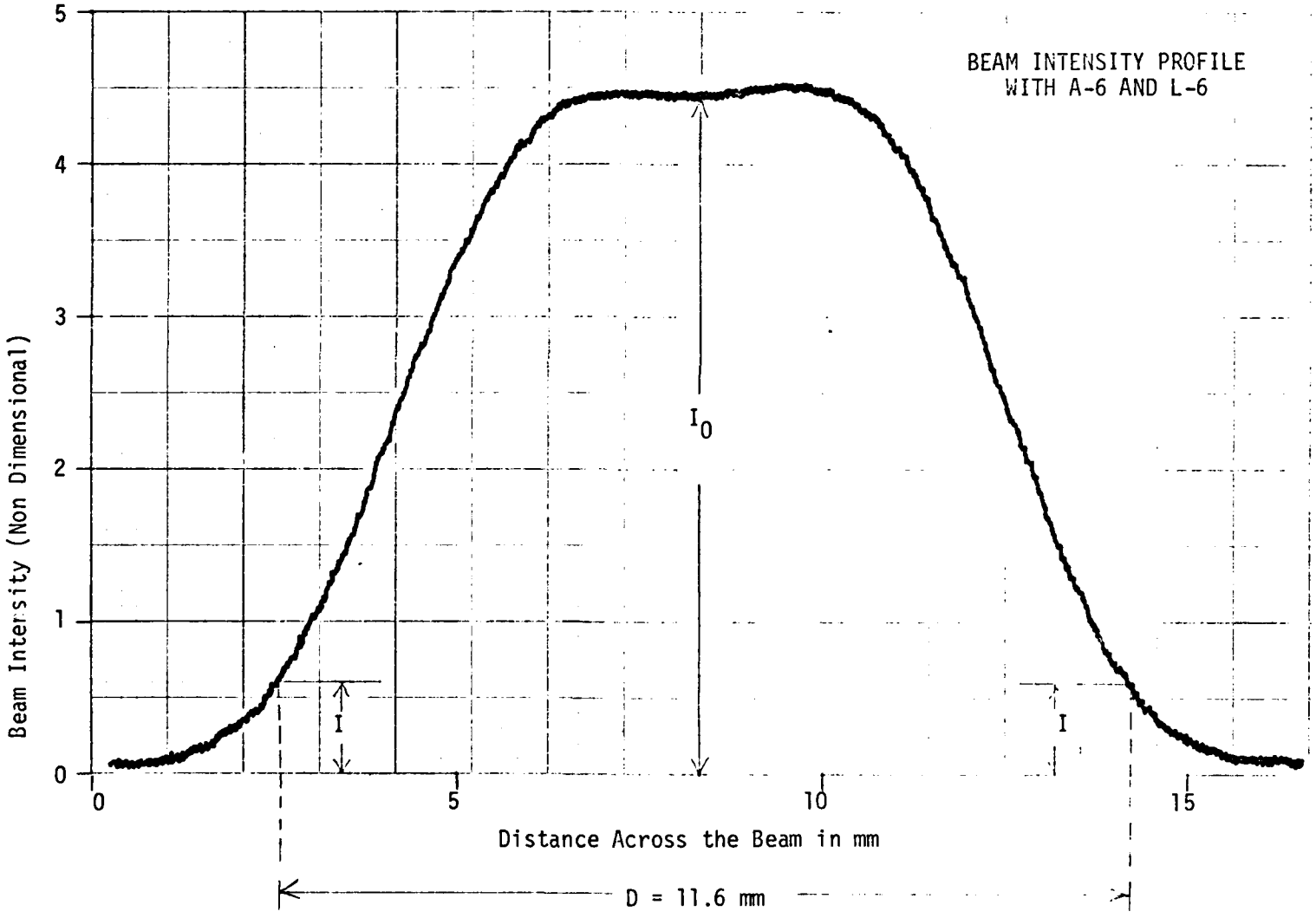

Figure 31. Beam Diameter Without Pinhole in Vertical Traverse

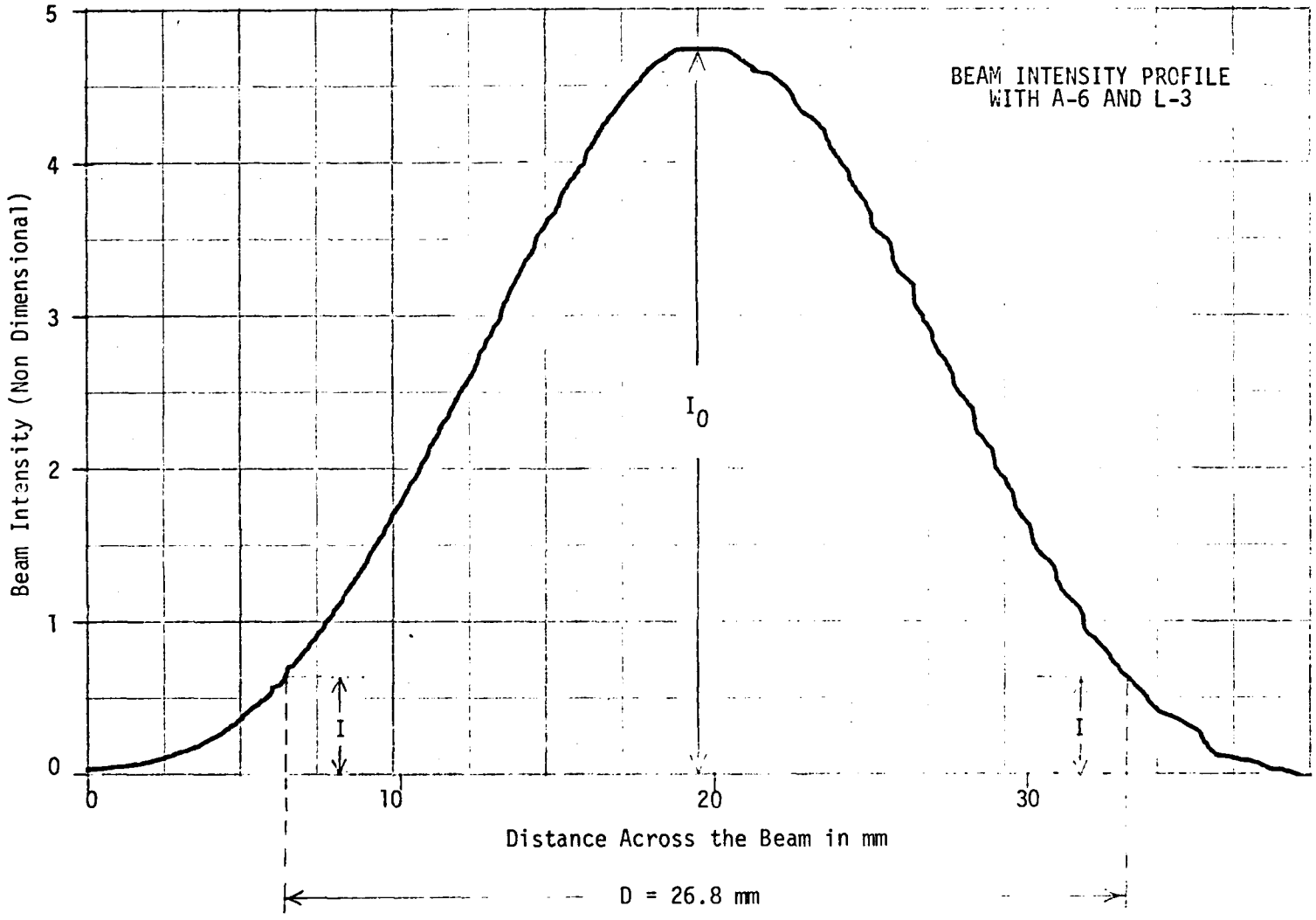

Figure 32. Beam Diameter Without Pinhole in Horizontal Traverse

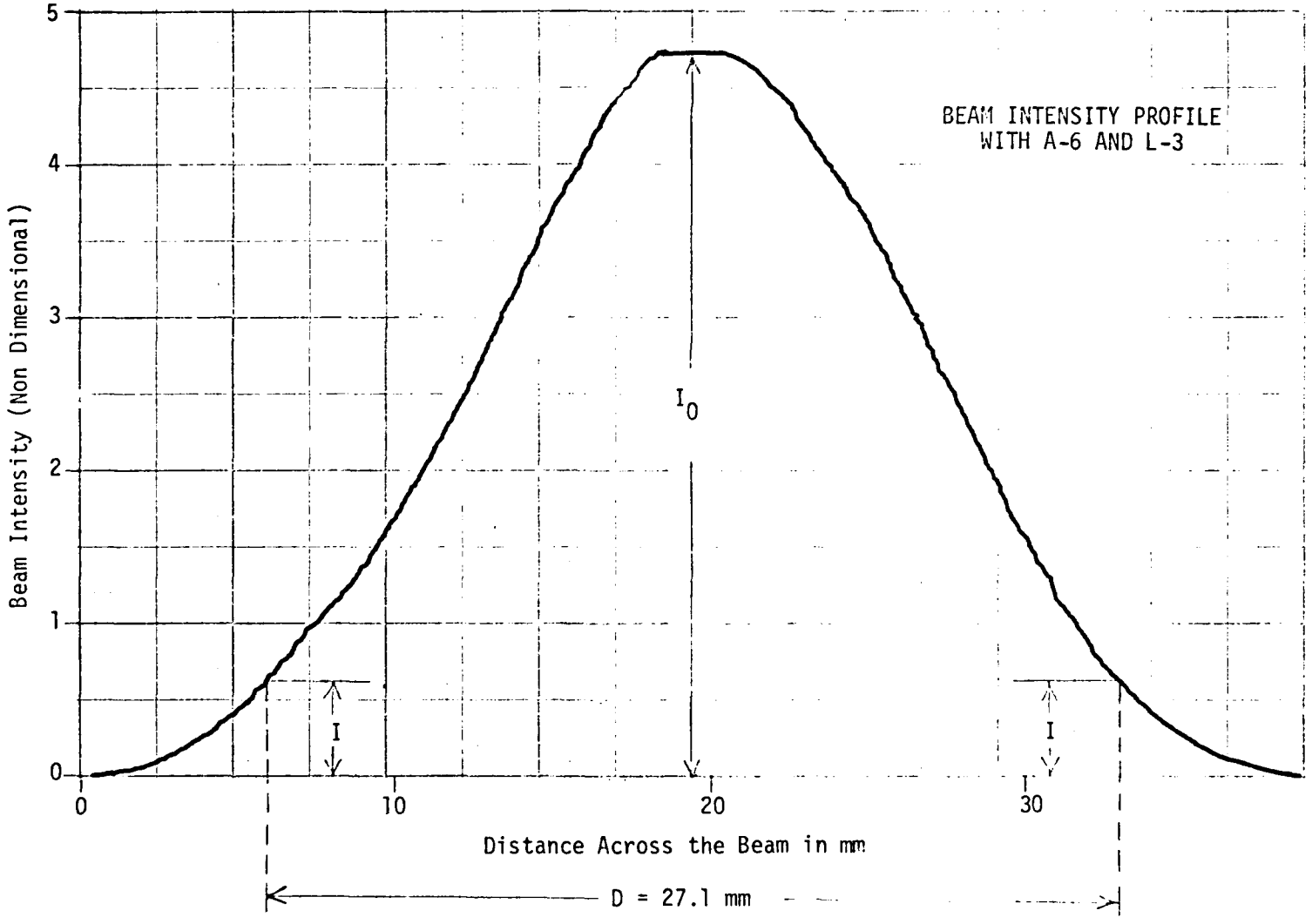

Figure 33. Beam Diameter Without Pinhole in Vertical Traverse

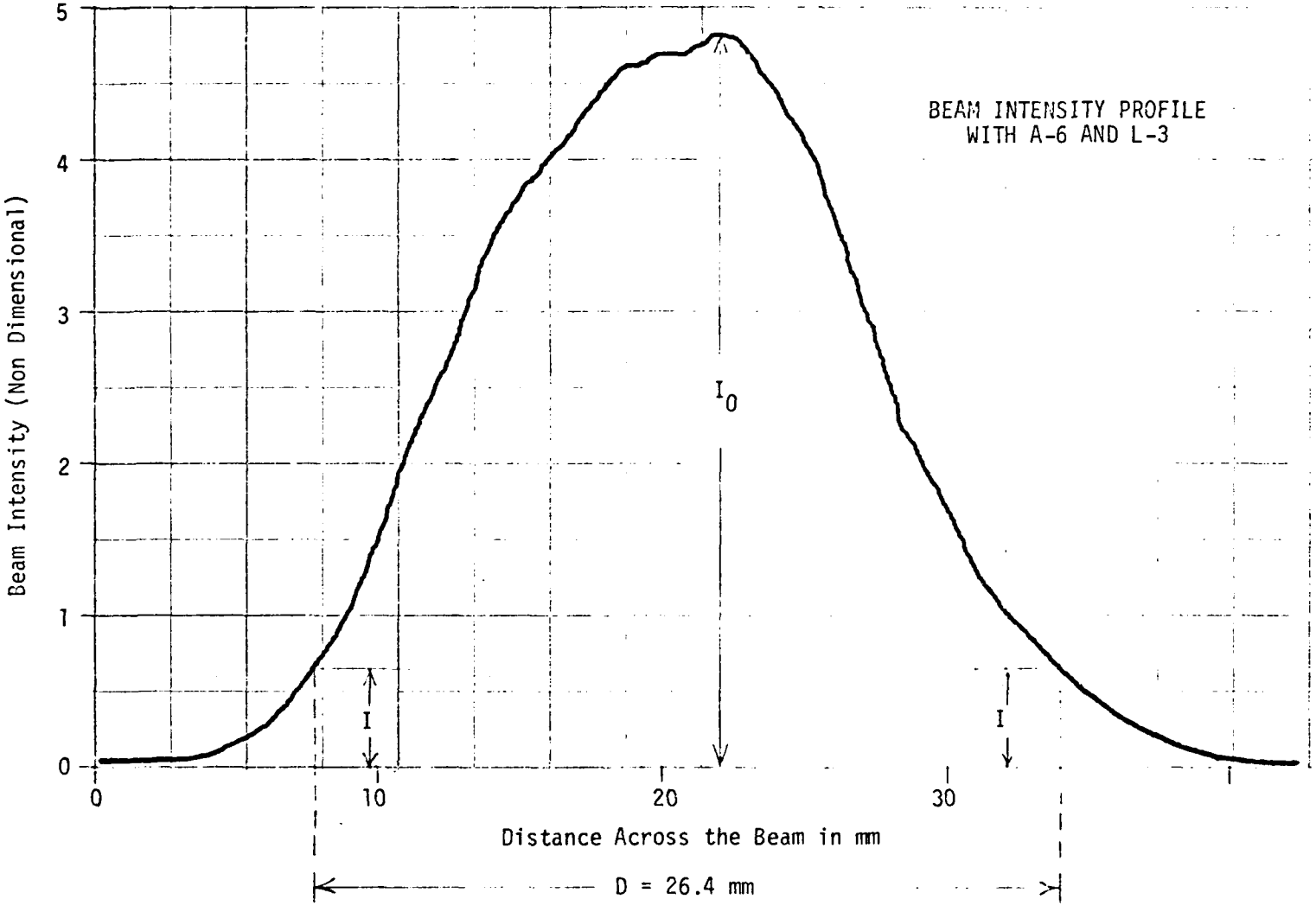

Figure 34. Beam Diameter With Pinhole in Horizontal Traverse

AD-A094 758 AIR FORCE INST OF TECH WRIGHT-PATTERSON AFB OH SCHOO--ETC F/G 14/2
EFFECT OF TEST RHOMBUS SIZE ON PHOTON CORRELATION LASER VELOCIM--ETC(U)
DEC 80 I HAMID
UNCLASSIFIED AFIT/GAE/AA/80D-7 NL

2 OF 2
AD
A094758

END
DATE FILMED
3 81
DTIC

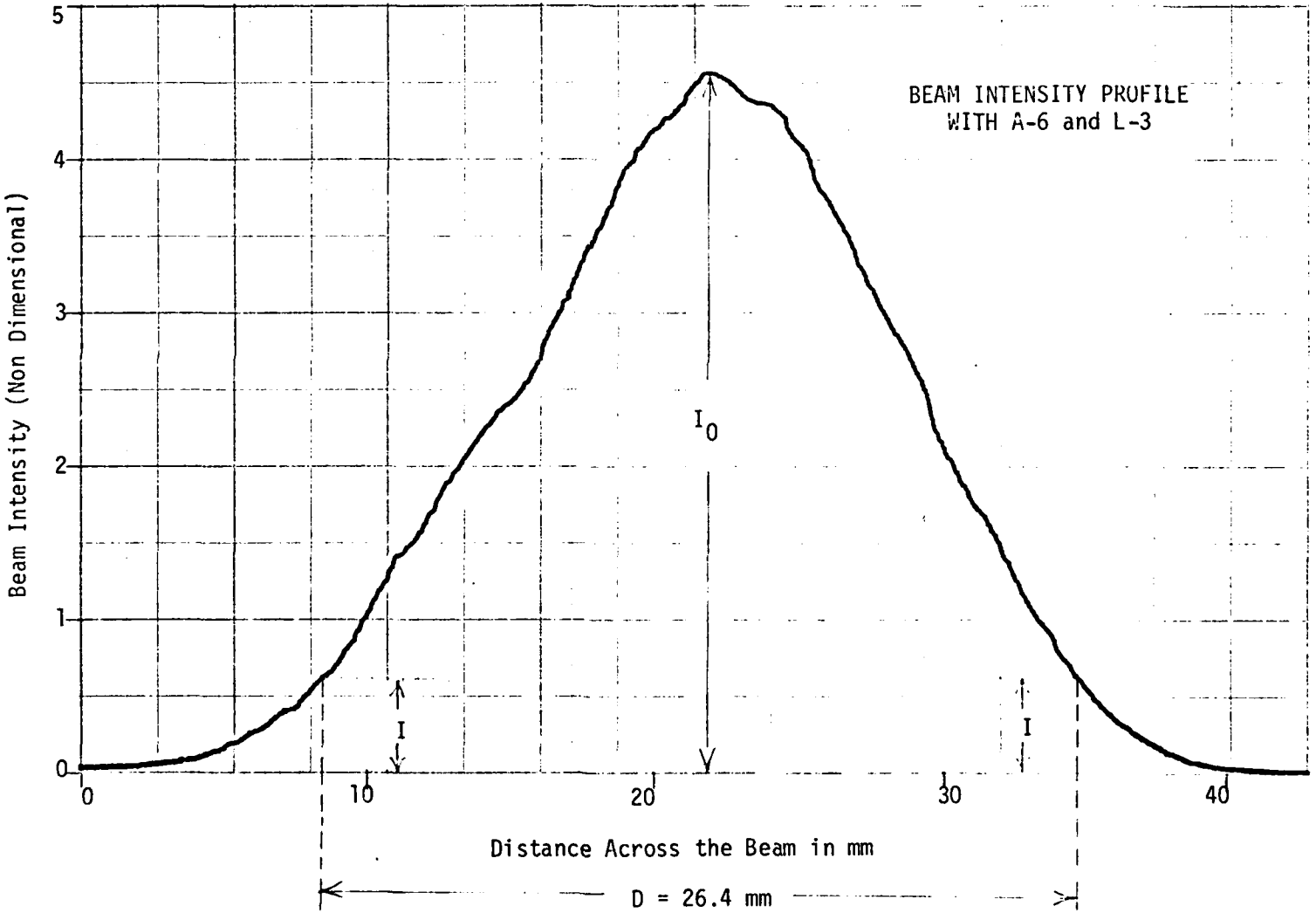

Figure 35. Beam Diameter With Pinhole in Vertical Traverse

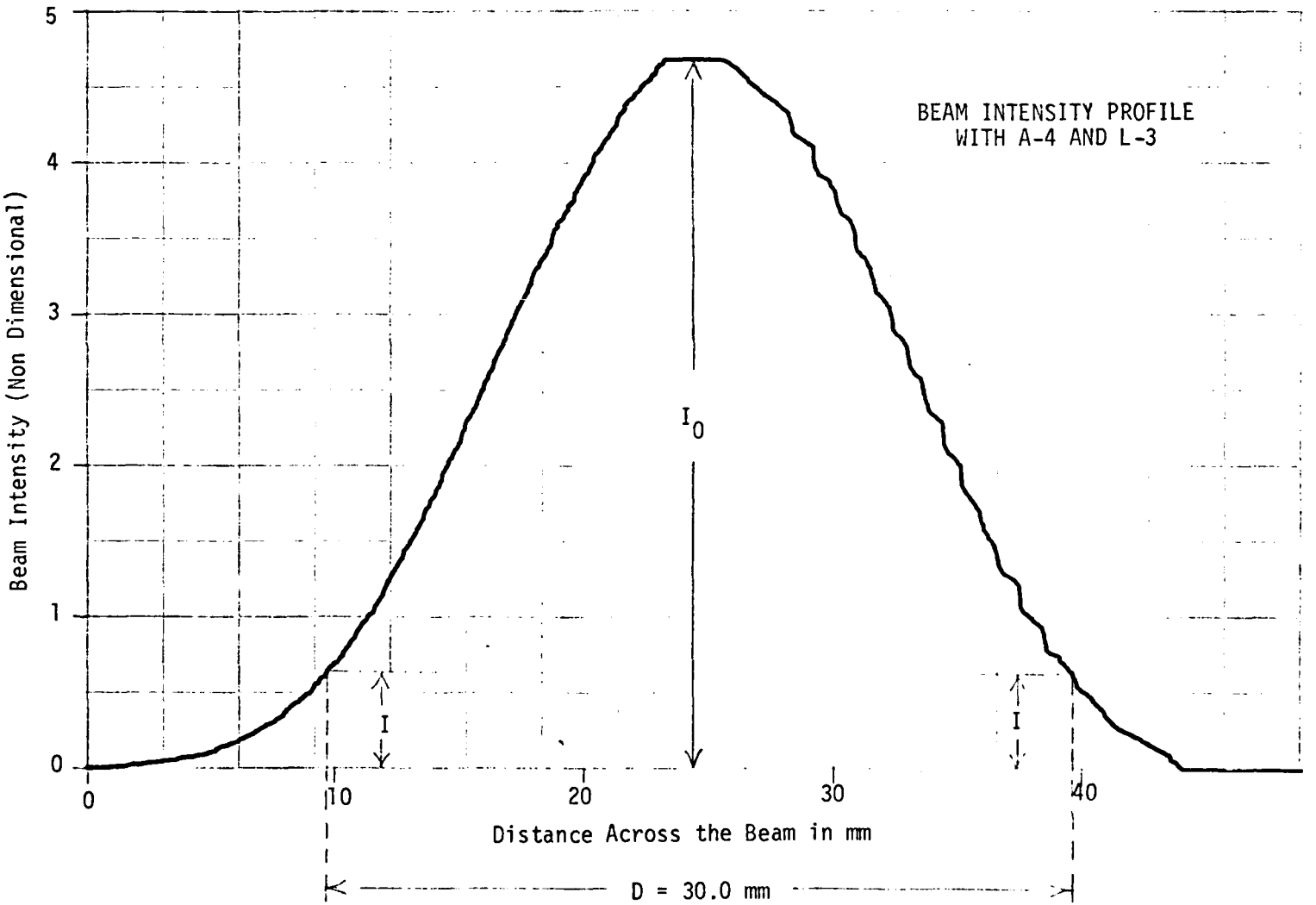

Figure 36. Beam Diameter Without Pinhole in Horizontal Traverse

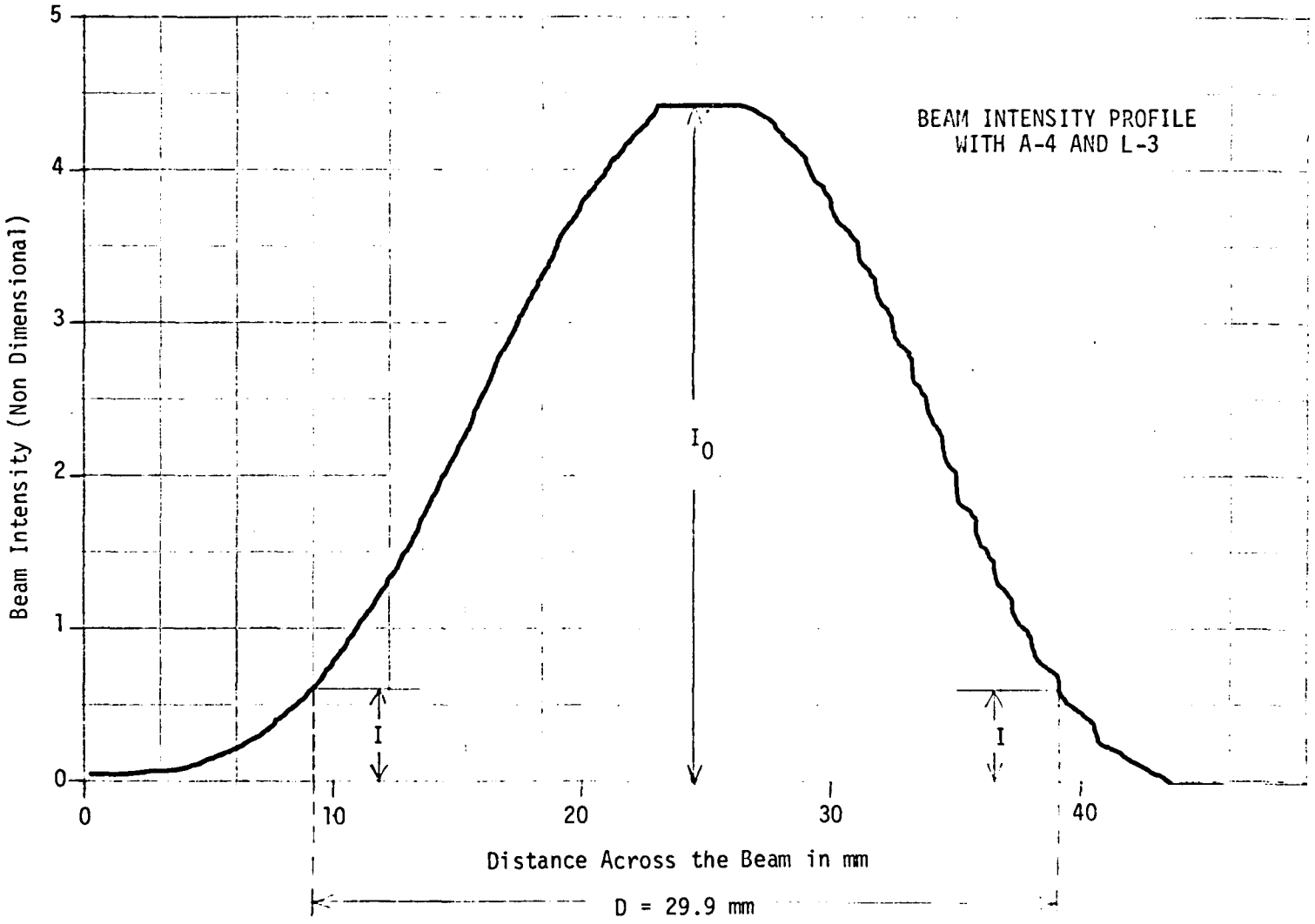

Figure 37. Beam Diameter Without Pinhole in Vertical Traverse

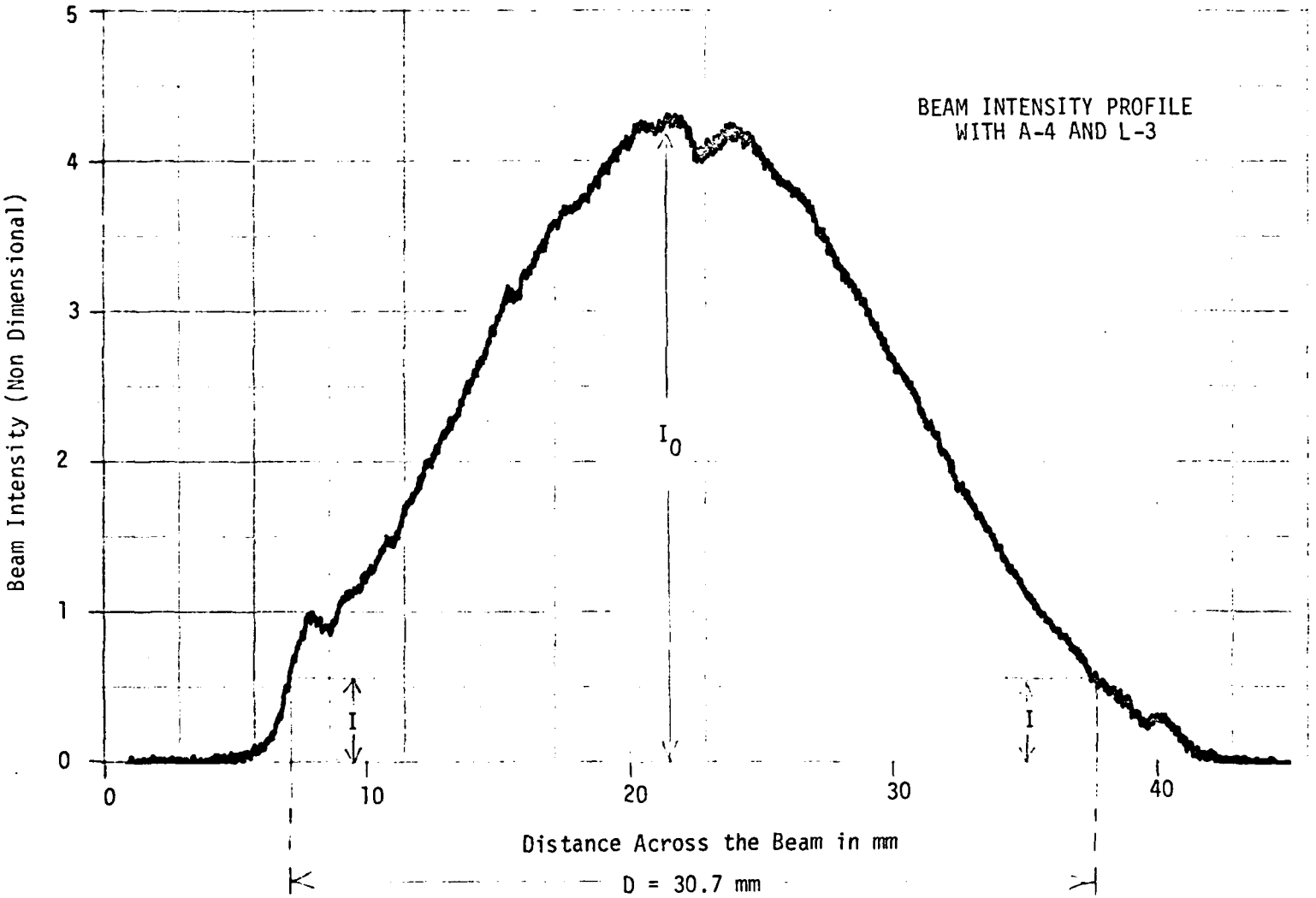

Figure 38. Beam Diameter with Pinhole in Horizontal Traverse

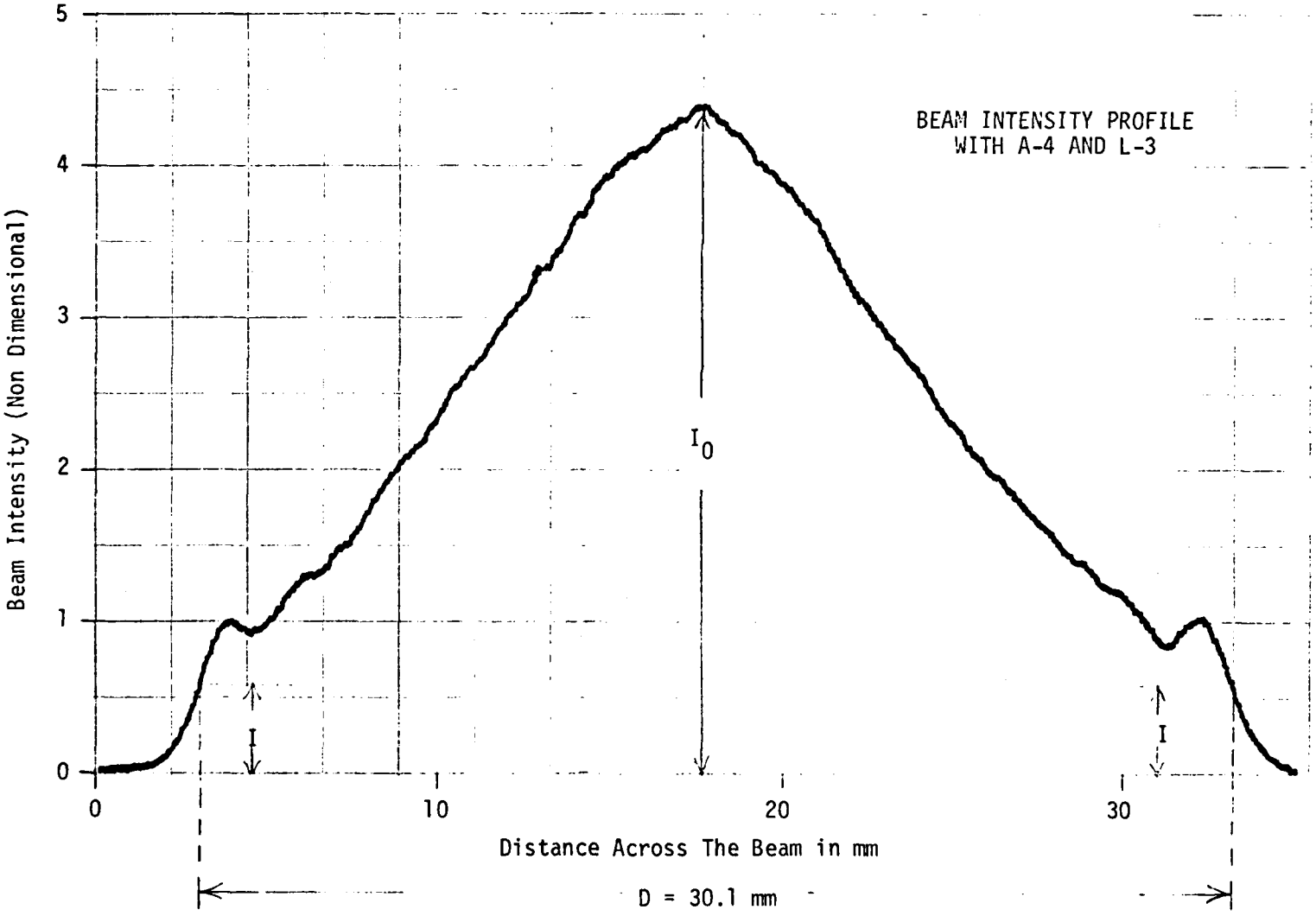

Figure 39. Beam Diameter With Pinhole in Vertical Traverse

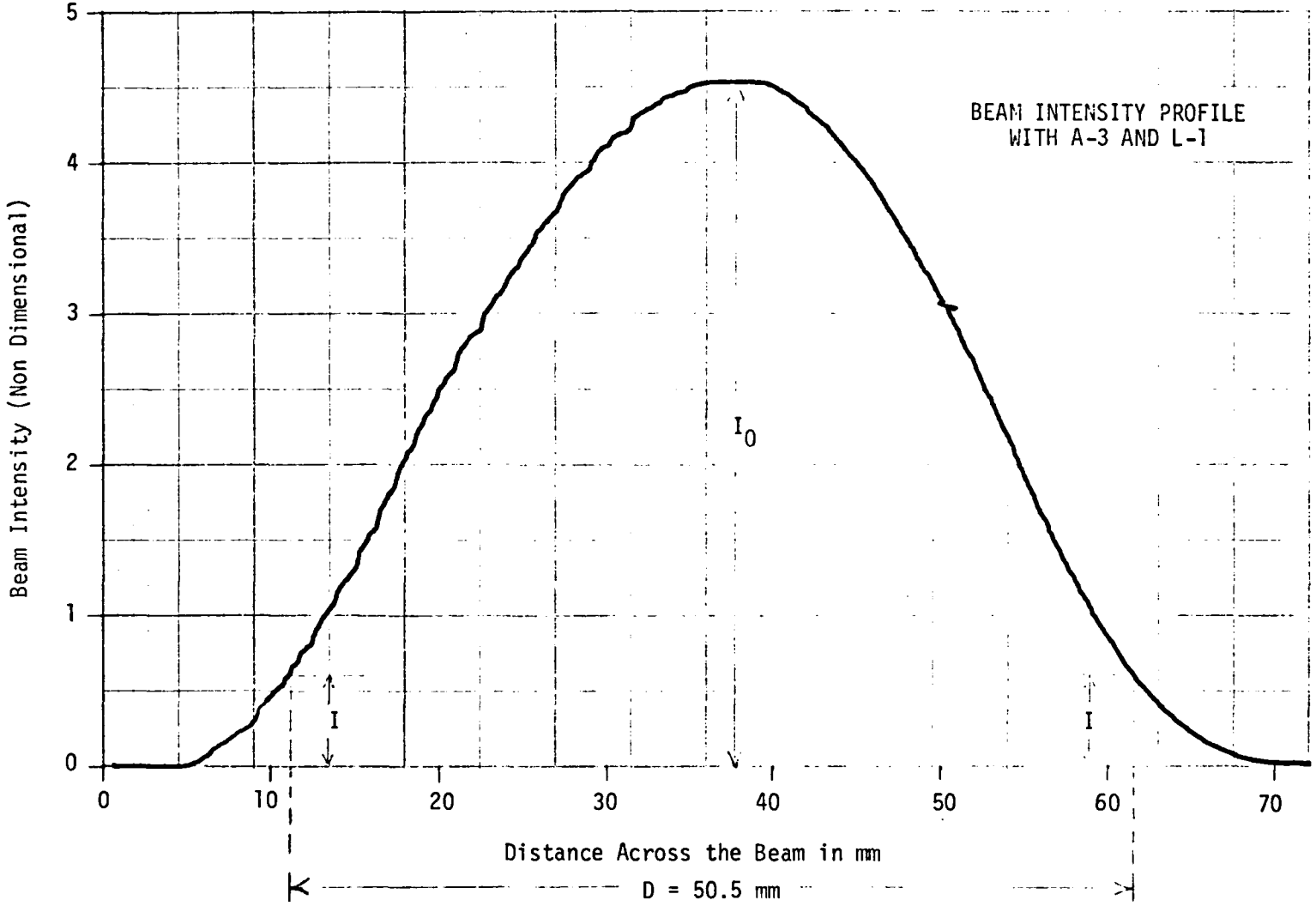

Figure 40. Beam Diameter Without Pinhole in Horizontal Traverse

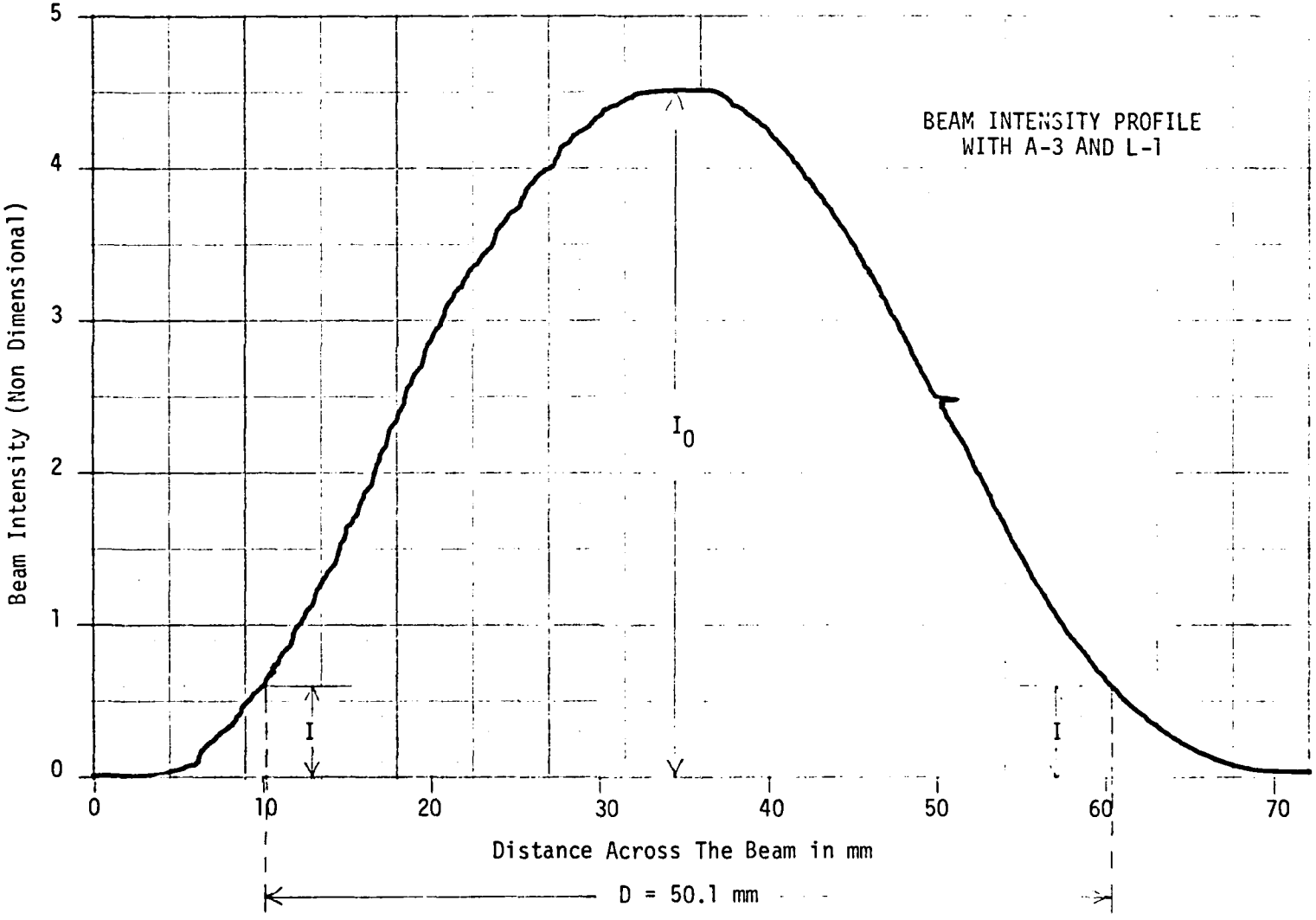

Figure 41. Beam Diameter Without Pinhole in Vertical Traverse

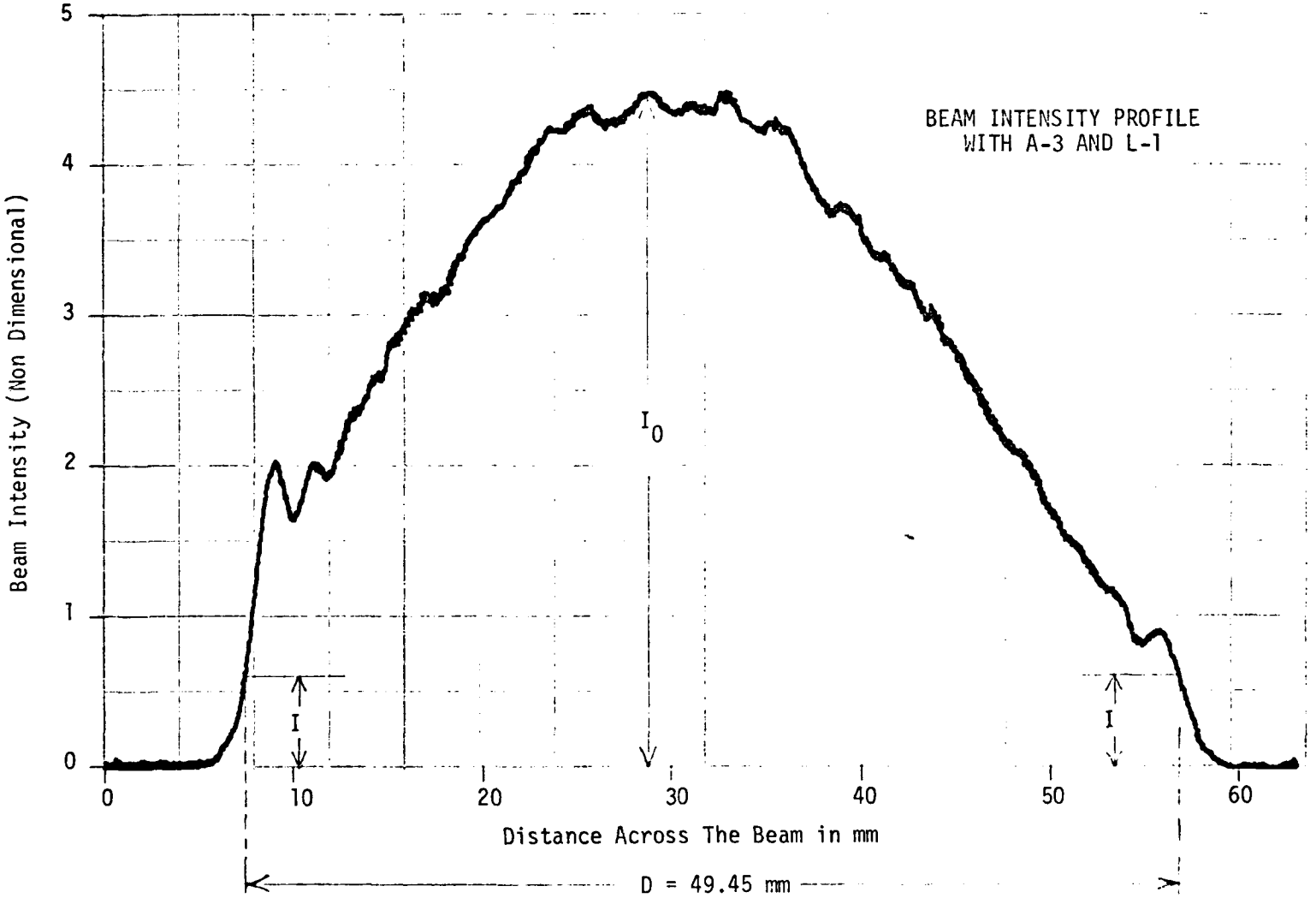

Figure 42. Beam Diameter With Pinhole in Horizontal Traverse

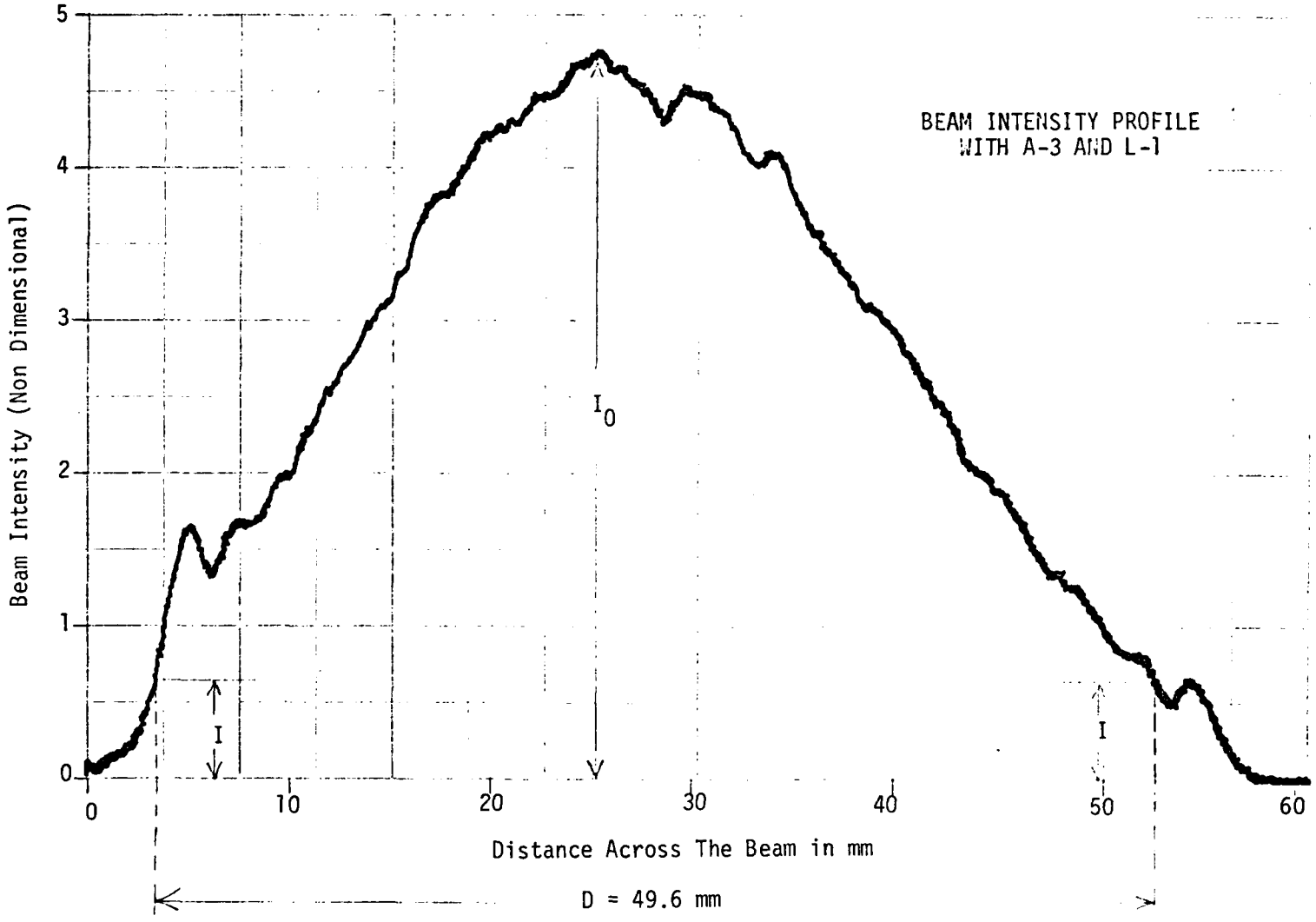

Figure 43. Beam Diameter With Pinhole in Vertical Traverse

APPENDIX E

Experimental Results of Turbulence Intensity

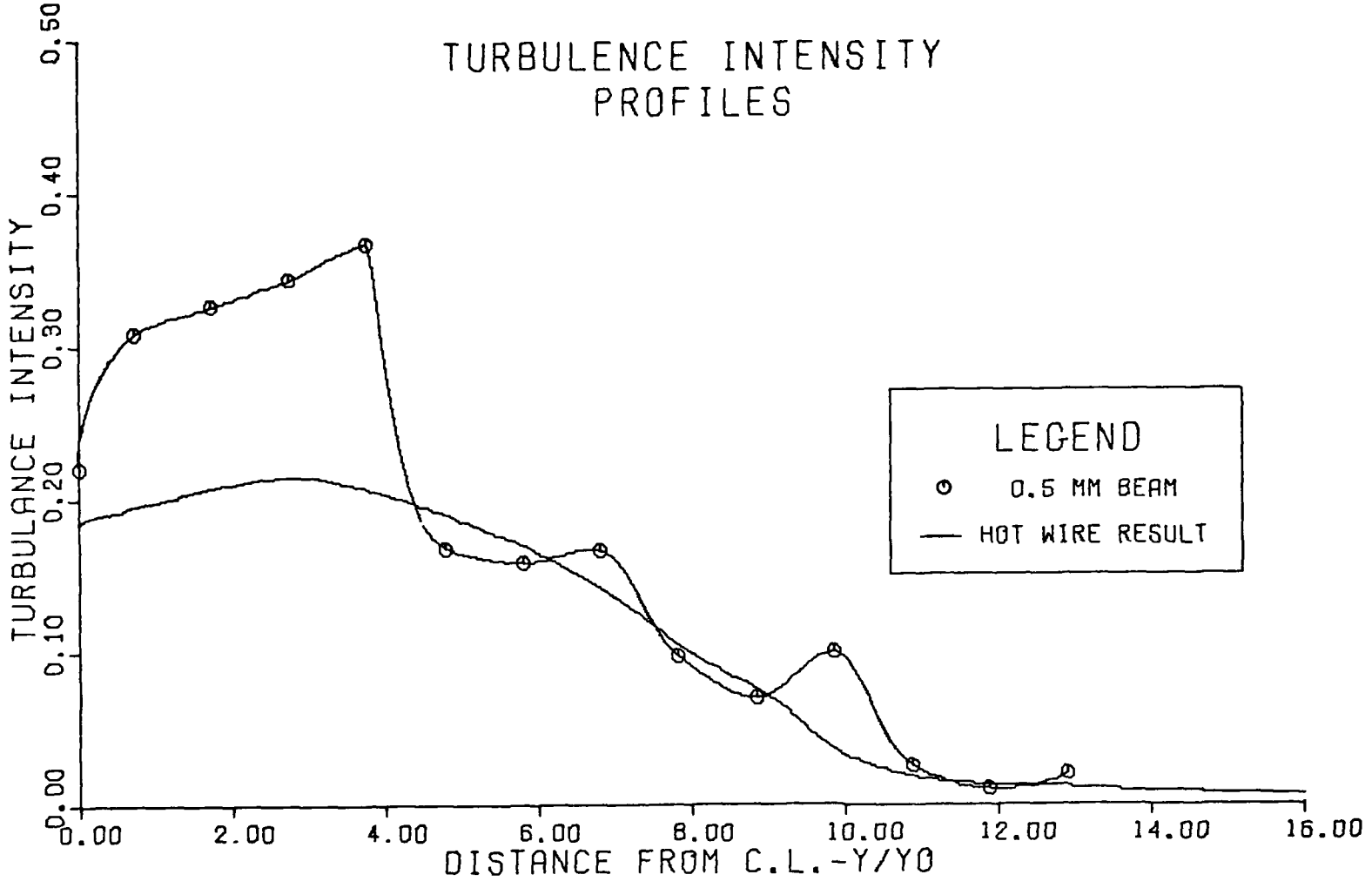

FIG. 44. TURBULENCE INTENSITY PROFILES USING 0.5 MM BEAM

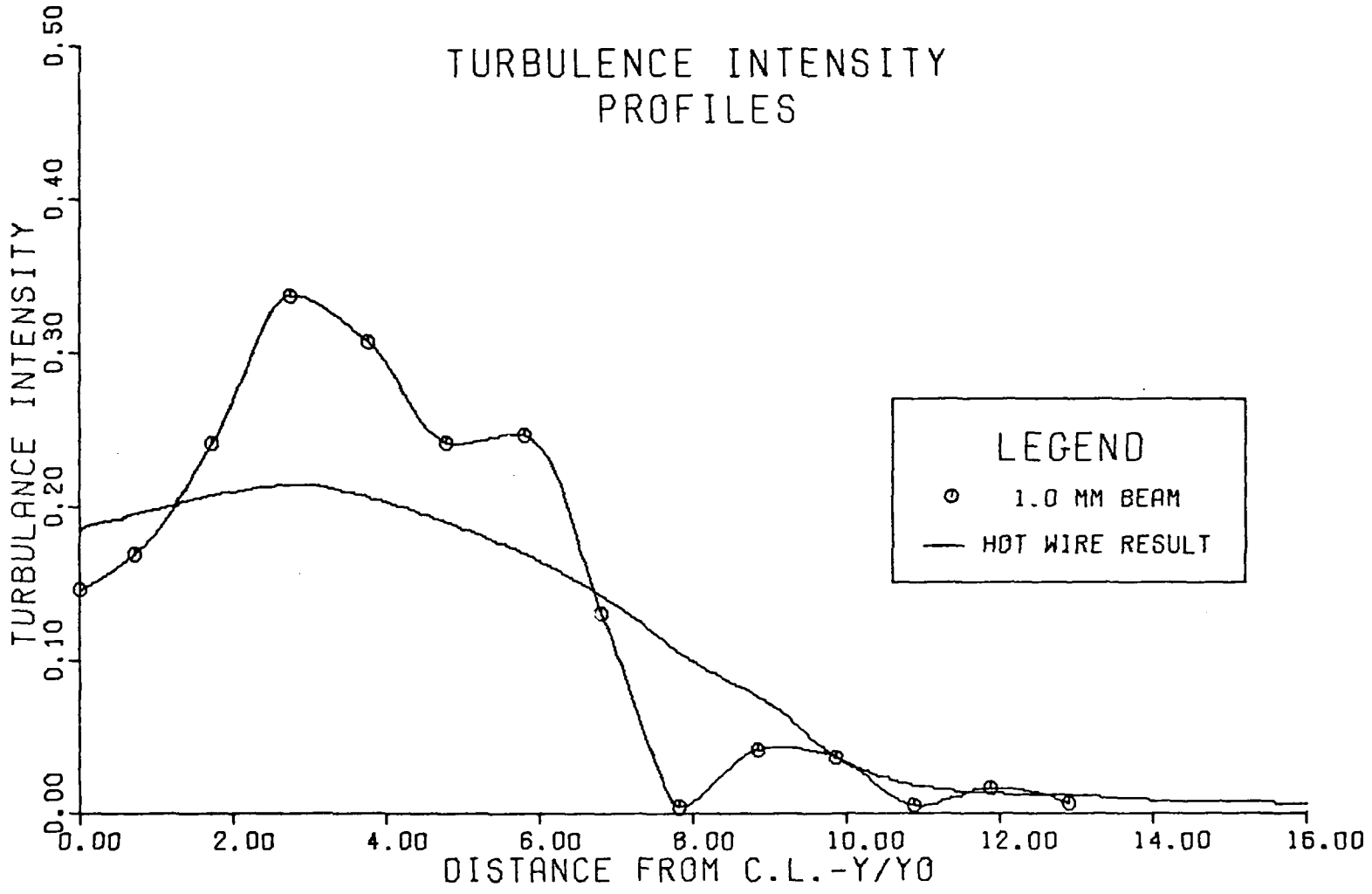

FIG. 45. TURBULENCE INTENSITY PROFILES USING 1.0 MM BEAM

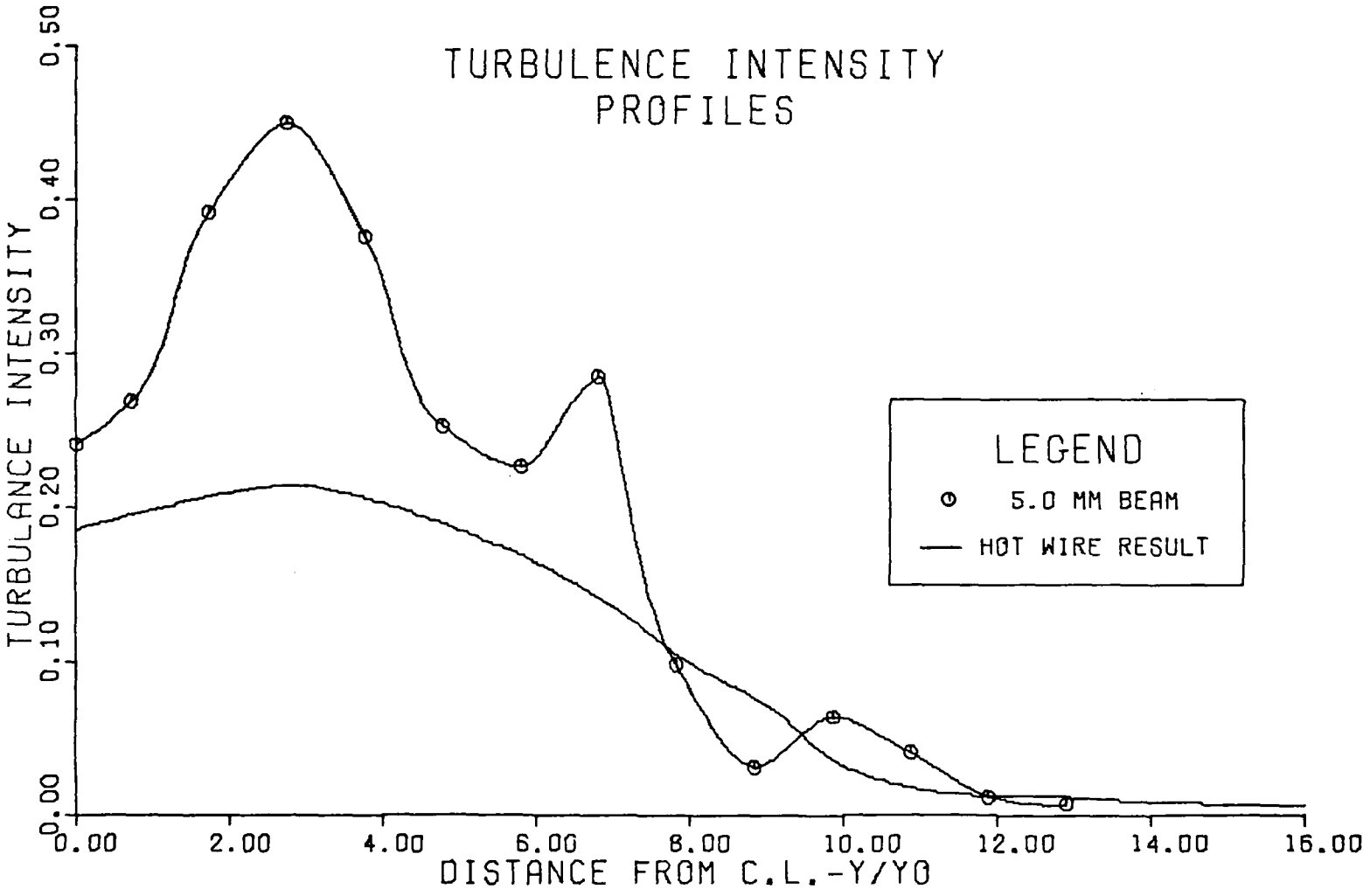

FIG. 46.TURBULENCE INTENSITY PROFILES USING 5.0 MM BEAM

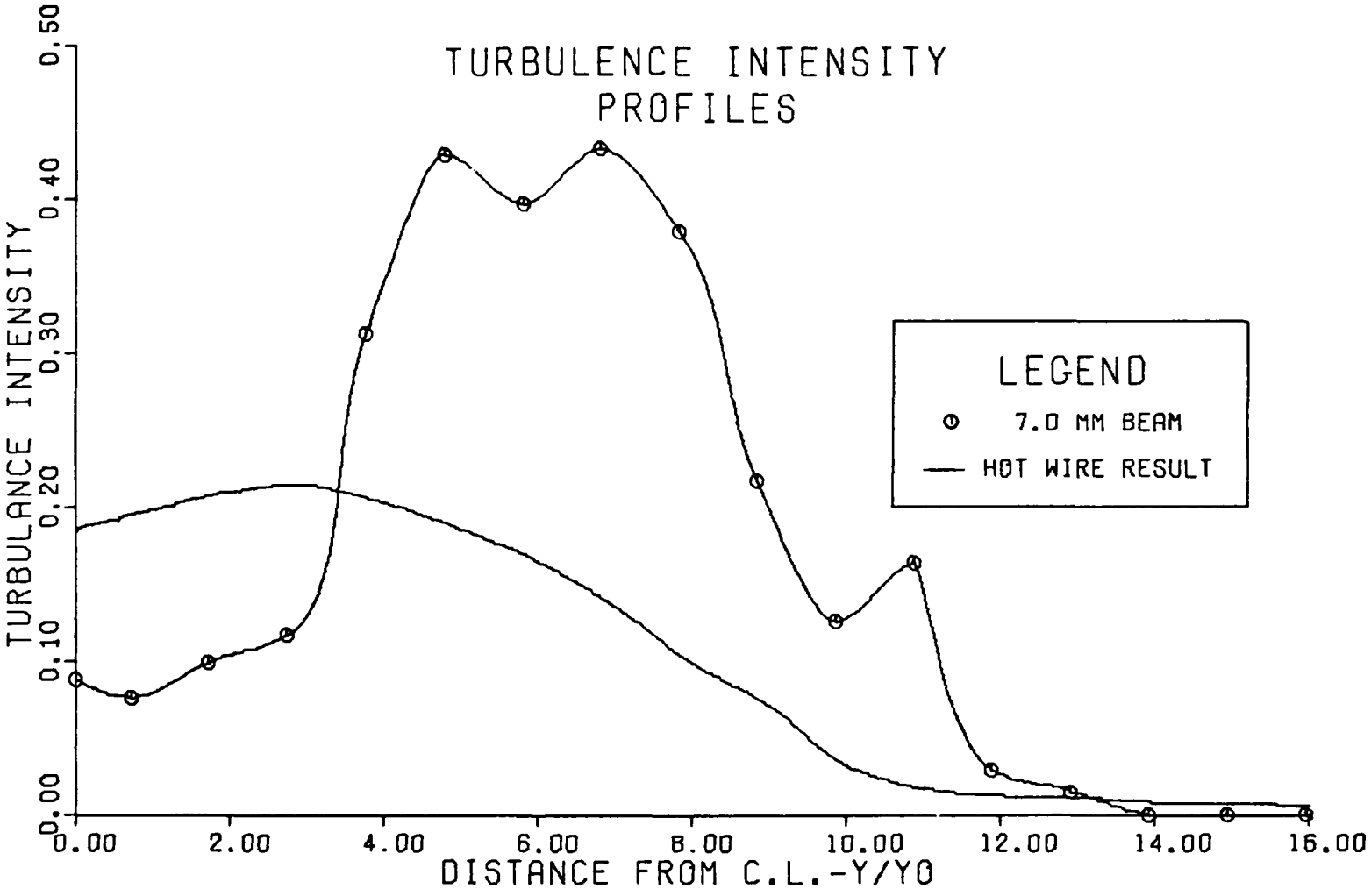

FIG.47. TURBULENCE INTENSITY PROFILES USING 7.0 MM BEAM

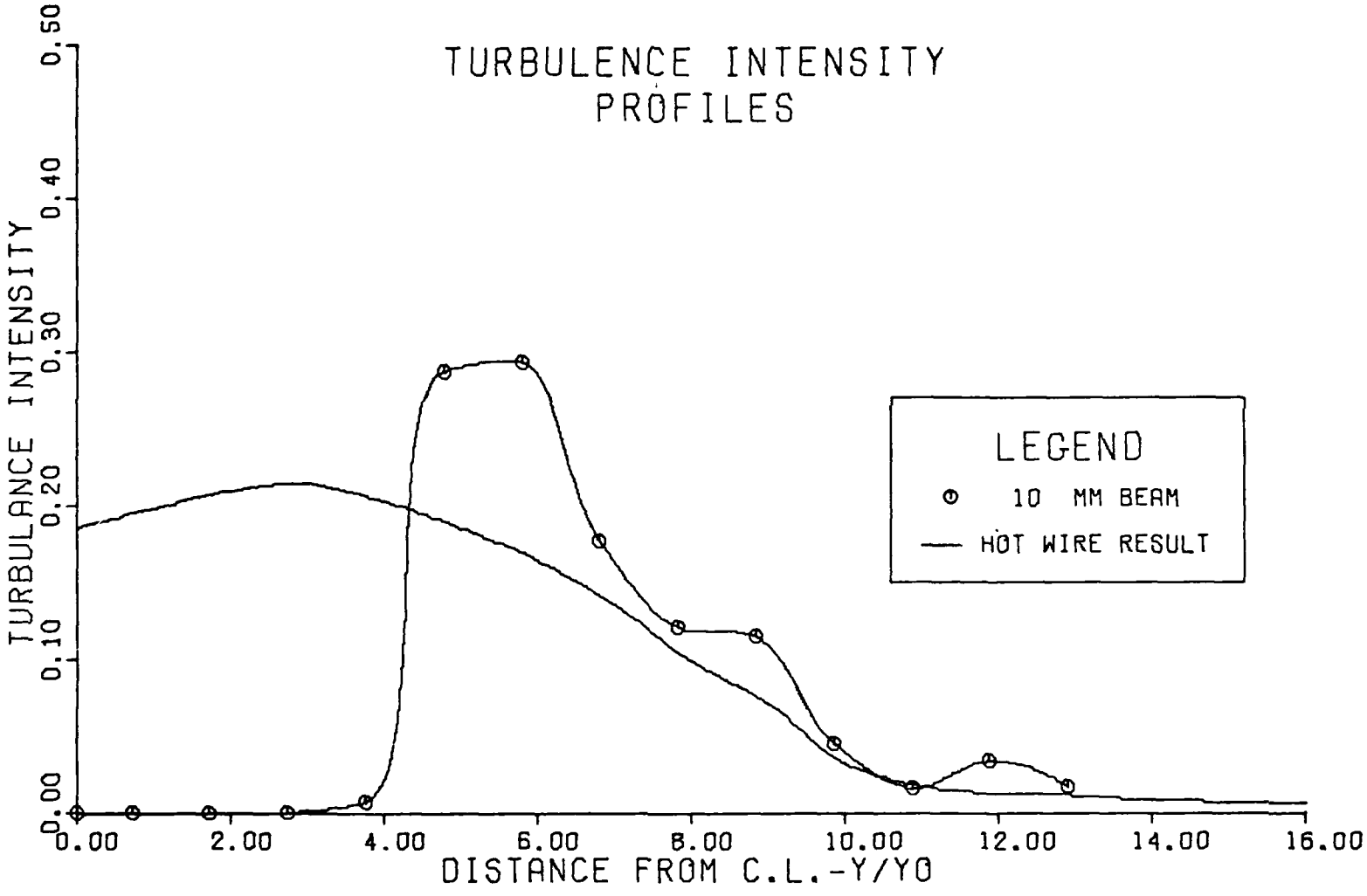

FIG. 48.TURBULENCE INTENSITY PROFILES USING 10 MM BEAM

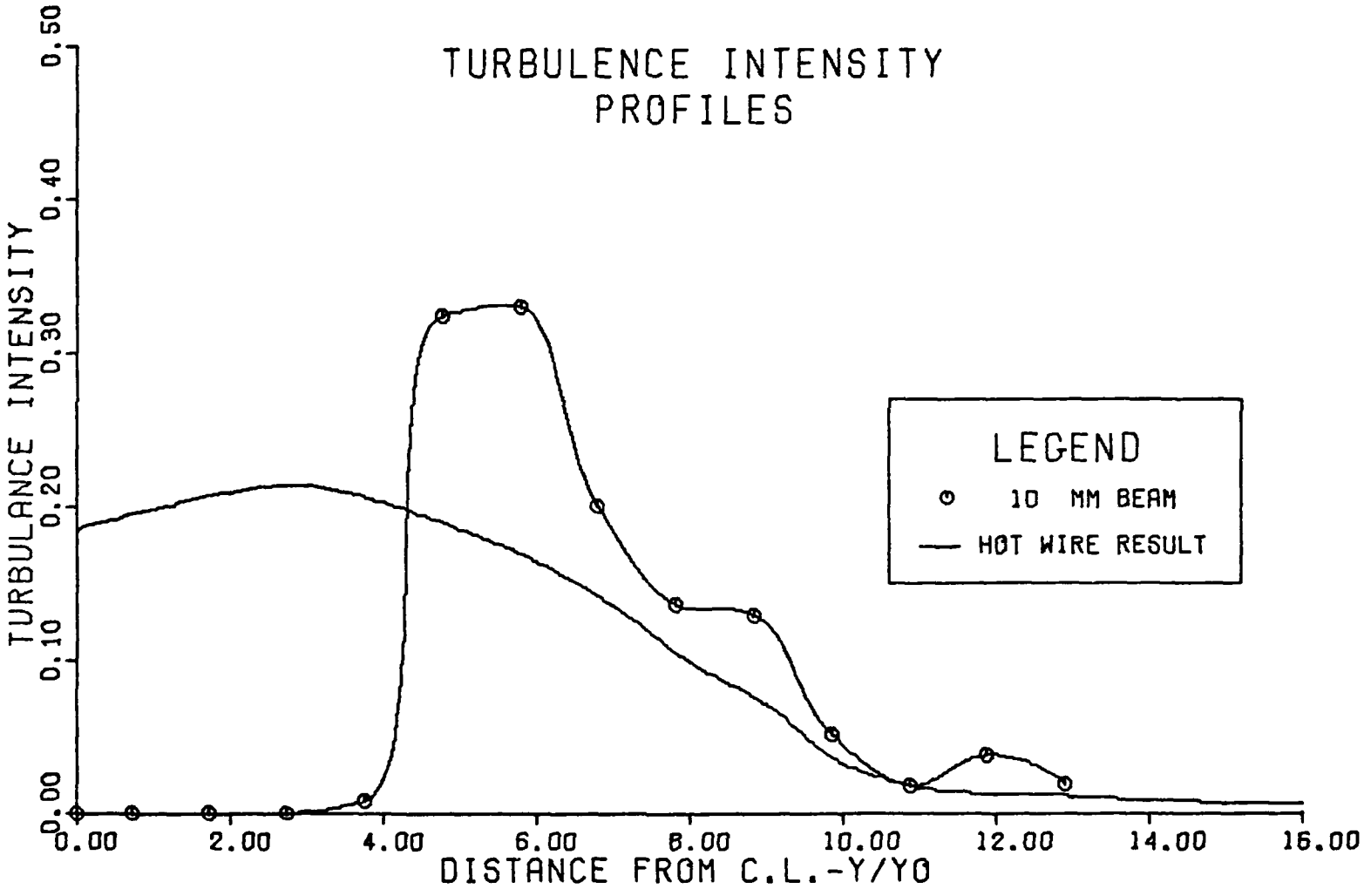

Figure 49. Turbulence Intensity Profiles Using 10 mm Beam and Corrected for U_{cen}

APPENDIX F

Experimental Data

TABLE V

Theoretical Curves Used for Comparison

of Velocity Similarity Profiles

Gortler's Solution		
$\eta = \sigma \frac{y}{x}$ and $\eta_{\frac{1}{2}} = \sigma \frac{y_{\frac{1}{2}}}{x} = 0.8813736$		
$\eta = \sigma \frac{y}{x}$	$\frac{y}{y_{\frac{1}{2}}} = \frac{\eta}{\eta_{\frac{1}{2}}}$	$\frac{U}{U_{cen}}$
0.00	0.00	1.000
0.25	0.284	.940
0.50	0.567	.786
0.75	0.851	.597
0.8814	1.00	.500
1.00	1.135	.420
1.25	1.418	.280
1.50	1.702	.181
1.75	1.986	.114
2.00	2.269	.071
2.25	2.553	.043
2.50	2.836	.027
2.644	3.000	.020

TABLE VI

Tollmien's Solution $\phi = \frac{y}{a_x}$ and $\phi_{1/2} = \frac{y_{1/2}}{a_x} = 0.959$		
$\phi = \frac{y}{a_x}$	$\frac{y}{y_{1/2}} = \frac{\phi}{\phi_{1/2}}$	$\frac{U}{U_{cen}}$
0.0	0.000	1.000
0.1	0.104	0.979
0.2	0.209	0.940
0.3	0.313	0.897
0.4	0.417	0.842
0.5	0.521	0.782
0.6	0.626	0.721
0.7	0.730	0.660
0.8	0.834	0.604
0.9	0.938	0.538
0.959	1.000	0.500
1.0	1.043	0.474
1.1	1.147	0.411
1.2	1.251	0.357
1.3	1.356	0.300
1.4	1.460	0.249
1.5	1.564	0.200
1.6	1.668	0.165
1.7	1.773	0.125
1.8	1.877	0.095
1.9	1.981	0.067
2.0	2.086	0.046
2.1	2.190	0.030
2.2	2.294	0.020
2.3	2.398	0.009
2.4	2.503	0.000

TABLE VII

1.1 mm Diameter Beam Without Using Beam Expanding Assembly

DATE: 28 Aug
L/D = 23.405341
S = 14.8109 x 10^{-6} meters

P_a = 29.39 in of Hg
P_c = 7.72 in of Marriam Fluid
T_c = 79° F

$y_{1/2}$ = 0.8554 in
P/P_o = 0.9457259
U_{cor} = 97.5534 m.p.s.

Y in	Sample Time (x 10^{-9} sec)	Peak Ch	g_1	g_2	g_3	U m.p.s.	R	n
0.0	50	8.0	156,070	163,723	157,108	59.244	1.1569	.0251
0.2	50	8.3	265,488	276,615	268,451	55.890	1.3629	.0579
0.4	50	8.7	205,788	214,035	210,843	51.968	2.5836	.2522
0.6	50	10	249,296	255,570	253,064	42.317	2.5036	.2394
0.8	50	12.4	189,353	192,617	190,581	31.513	2.5855	.2524
1.0	50	15	410,616	415,527	413,797	24.685	2.8387	.2928
1.21	100	10	1,084,365	1,088,611	1,086,464	21.158	1.9776	.1557
1.4	100	14	700,535	703,114	701,760	13.464	1.9047	.1441
1.6	200	11	2,092,216	2,097,453	2,094,081	9.257	1.5531	.0881
1.8	200	14	3,052,380	3,056,331	3,053,252	6.732	1.2832	.0452
2.0	300	16	2,579,498	2,583,731	2,581,967	3.798	2.3997	.2229
2.2	400	16	5,672,511	5,678,842	5,670,350	2.848	2.3008	.2071
2.4	400	25	3,900,343	3,904,551	3,902,361	1.683	2.9304	.3073
2.6	600	21	7,065,311	7,071,512	7,068,511	1.371	2.0663	.1698
2.8	800	20	8,492,590	8,498,914	8,494,426	1.089	1.4091	.0652
3.0	800	32	6,493,799	6,498,230	6,494,438	0.638	1.1685	.0269

TABLE VII (Cont'd)

0.5 mm Diameter Beam

DATE: 9 September | P_a = 29.26 in of Hg | $y_{1/2}$ = 0.932 in

L/D = 23.405341 | P_c = 8.80 in of Marriam Fluid | P/P_o = 0.9383434

S = 14.8109 x 10^{-6} meters | T_c = 77° F | U_{cor} = 103.927 m.p.s.

Y in	Sample Time (x 10^{-9} sec)	Peak Ch	g_1	g_2	g_3	U m.p.s.	R	n
0.00	50	7.7	1,530,522	1,583,529	1,561,247	63.025	2.3789	.2200
0.14	50	7.8	1,444,897	1,639,258	1,573,845	61.712	2.9713	.3143
0.34	50	8.0	831,988	845,570	841,289	59.244	3.1726	.3463
0.54	50	9.0	901,823	915,527	911,873	49.370	3.7504	.4383
0.74	50	10.5	1,049,978	1,081,314	1,074,589	39.496	4.6596	.5830
0.94	50	12.5	2,003,619	2,011,156	2,008,741	31.181	3.1209	.3381
1.14	50	17.0	808,299	830,892	825,177	21.158	3.9533	.4706
1.34	100	10.6	1,523,805	1,554,948	1,547,826	19.488	4.3726	.5373
1.54	100	15	941,878	963,608	958,318	12.342	4.1078	.4952
1.74	100	18	1,142,782	1,206,494	1,189,692	9.874	3.7919	.4449
1.94	200	13	1,077,354	1,130,534	1,122,121	7.405	6.3212	.8474
2.14	200	20	1,844,051	2,081,349	2,008,817	4.356	3.2716	.3621
2.34	400	13	1,234,238	1,278,188	1,256,383	3.703	2.0156	.1622
2.54	400	15	1,035,826	1,093,337	1,077,215	3.086	3.5672	.4091

TABLE VII (Cont'd)

1.0 mm Diameter Beam

DATE: 10 September | P_a = 29.32 in of Hg | $y_{1/2}$ = 0.8477 in

L/D = 23.405341 | P_c = 6.85 in of Marriam Fluid | P/P_o = 0.951436

S = 14.8109 x 10^{-6} meters | T_c = 76° F | U_{cor} = 91.924 m.p.s.

Y in	Sample Time (x 10^{-9} sec)	Peak Ch	g_1	g_2	g_3	U m.p.s.	R	η
0.00	50	8.2	1,431,829	1,475,466	1,452,659	56.965	1.9133	.1455
0.14	50	8.4	1,473,073	1,548,879	1,512,780	54.855	2.0999	.1752
0.34	50	8.6	1,391,922	1,467,159	1,438,561	52.896	2.6308	.2597
0.54	50	10.4	2,347,478	2,482,770	2,449,058	40.029	4.0132	.4797
0.74	50	12	1,493,465	1,673,833	1,632,188	32.913	4.3311	.5303
0.94	50	15	827,692	936,822	912,575	24.685	4.5008	.5573
1.14	50	18	1,043,391	1,211,825	1,180,899	19.748	5.4464	.7078
1.34	50	23	2,213,924	2,319,257	2,293,834	14.811	4.1432	.5004
1.54	100	20	3,624,320	3,666,632	3,629,614	8.712	1.1430	.0229
1.74	100	24	2,619,683	2,759,914	2,714,562	7.053	3.0921	.3331
1.94	100	32	1,943,323	2,075,581	2,038,074	5.107	3.5262	.4022
2.14	200	25	2,058,709	2,121,281	2,078,955	3.366	1.4785	.0763
2.34	200	29	1,917,184	2,109,978	2,046,714	2.848	3.0475	.3260
2.54	400	25	3,146,753	3,234,617	3,193,766	1.683	2.1508	.1833

TABLE VII (Cont'd)

3.0 mm Diameter Beam

DATE: 12 September P_a = 29.24 in of Hg $y_{1/2}$ = 0.91655 in

L/D = 23.405341 P_c = 6.17 in of Marriam Fluid P/P_o = 0.95593

S = 14.8109 x 10^{-6} meters T_c = 71° F U_{cor} = 87.086 m.p.s.

Y in	Sample Time (x 10^{-9} sec)	Peak Ch	g_1	g_2	g_3	U m.p.s.	R	n
0.00	50	8.4	2,863,911	2,891,694	2,877,830	54.855	2.0040	.1598
0.14	50	8.5	1,870,521	1,887,960	1,878,831	53.858	1.9103	.1449
0.34	50	9.5	2,456,159	2,491,675	2,477,716	45.572	2.5443	.2458
0.54	50	10.5	1,155,479	1,162,030	1,160,152	39.496	3.4883	.3960
0.74	50	12.5	4,433,872	4,489,717	4,476,171	31.181	4.1226	.4970
0.94	50	14	2,460,756	2,508,092	2,497,501	26.929	4.4695	.5522
1.14	50	18	1,428,510	1,495,512	1,482,218	19.748	5.0400	.6430
1.34	50	22	1,834,800	1,863,294	1,856,773	15.590	4.3696	.5363
1.54	50	30	2,446,988	2,468,256	2,459,535	10.971	2.4387	.2290
1.74	100	19	1,868,777	1,878,181	1,870,762	9.257	1.2676	.0426
1.94	100	25	2,043,559	2,080,753	2,069,832	6.732	3.4057	.3829
2.14	100	41	1,422,694	1,460,478	1,453,668	3.898	5.5483	.7239
2.34	200	28	1,031,421	1,069,249	1,061,131	2.962	4.6598	.5825
2.54	200	32	2,460,343	2,487,635	2,477,567	2.554	2.7108	.2723
2.74	400	20	3,107,887	3,144,505	3,129,624	2.178	2.4607	.2325

TABLE VII (Cont'd)

5.0 mm Diameter Beam

DATE: 17 September | P_a = 29.00 in of Hg | $y_{1/2}$ = 0.85 in

L/D = 23.405341 | P_c = 8.58 in of Marriam Fluid | P/P_o = 0.939285

S = 14.8109 x 10^{-6} meters | T_c = 67° F | U_{cor} = 102.1476 m.p.s.

Y in	Sample Time (x 10^{-9} sec)	Peak Ch	g_1	g_2	g_3	U m.p.s.	R	n
0.00	50	8	1,881,105	1,917,626	1,903,111	59.244	2.5161	.2413
0.14	50	8	1,684,698	1,723,352	1,708,973	59.244	2.6882	.2687
0.34	50	8.5	2,016,598	2,079,052	2,062,229	53.858	3.7124	.4317
0.54	50	9.5	1,869,238	1,895,350	1,889,763	45.572	4.6737	.5847
0.74	50	12	1,388,751	1,485,915	1,467,385	32.913	5.2436	.6754
0.94	50	14	1,443,965	1,509,474	1,494,891	26.929	4.4921	.5558
1.14	50	20	1,867,858	1,915,573	1,907,427	17.425	5.8575	.7731
1.34	50	23	1,385,680	1,499,880	1,485,894	14.811	8.1653	1.1404
1.54	100	19	1,497,835	1,512,015	1,509,137	9.257	4.9270	.6250
1.74	100	26	1,477,088	1,496,326	1,489,451	6.440	2.7982	.2862
1.94	100	38	2,477,585	2,540,436	2,530,979	4.232	6.6461	.8986
2.14	200	24	1,466,512	1,495,082	1,489,642	3.526	5.2518	.6767
2.34	200	28	1,652,206	1,670,311	1,663,128	2.962	2.5205	.2420
2.54	400	18	1,926,884	1,932,976	1,929,956	2.468	2.0172	.1619

TABLE VII (Cont'd)

7.0 mm Diameter Beam

DATE: 19 September | P_a = 29.40 in of Hg | $y_{1/2}$ = 1.0874 in

L/D = 23.405341 | P_c = 7.05 in of Marriam Fluid | P/P_o = 0.95022

S = 14.8109 x 10^{-6} meters | T_c = 68° F | U_{cor} = 92.394 m.p.s.

Y in	Sample Time (x 10^{-9} sec)	Peak Ch	g_1	g_2	g_3	U m.p.s.	R	n
0.00	50	8.7	2,905,046	2,929,258	2,913,679	51.968	1.5541	.0882
0.14	50	9.0	2,654,970	2,678,581	2,662,894	49.370	1.5051	.0804
0.34	50	9.0	1,462,456	1,484,868	1,471,339	49.370	1.6566	.1045
0.54	50	9.5	2,880,260	2,902,049	2,890,187	45.572	1.8369	.1332
0.74	50	10.6	3,158,617	3,293,706	3,256,292	38.976	3.6107	.4155
0.94	50	13	2,696,087	2,968,403	2,920,805	29.622	5.7212	.7514
1.14	50	15	2,298,427	2,514,027	2,479,487	24.685	6.2420	.8343
1.34	50	19.5	1,829,899	1,874,155	1,869,159	17.953	8.8583	1.2507
1.54	50	22	1,153,485	1,215,349	1,208,416	15.590	8.9231	1.2610
1.74	100	14	1,435,954	1,574,241	1,552,200	13.464	6.2740	.8394
1.94	100	22	1,288,329	1,407,209	1,388,248	7.795	6.2697	.8387
2.14	100	23	1,857,687	2,121,471	2,089,471	7.405	8.2433	1.1528
2.34	100	27	2,879,237	2,976,202	2,937,568	6.171	2.5098	.2403
2.54	200	19	2,118,763	2,191,308	2,156,547	4.628	2.0870	.1730
2.74	200	26	2,821,624	2,912,574	2,819,085	3.220	0.9728	0
2.94	300	22	3,076,629	3,128,458	3,072,315	2.598	0.9232	0
3.14	400	21	3,547,961	3,611,105	3,538,894	2.057	0.8744	0

TABLE VII (Cont'd)

10.0 mm Diameter Beam

DATE: 22 September | P_a = 29.1 in of Hg | $y_{1/2}$ = 1.106 in

L/D = 23.405341 | P_c = 5.32 in of Marriam Fluid | P/P_o = 0.96159

S = 14.8109 x 10^{-6} meters | T_c = 73° F | U_{cor} = 81.367 m.p.s.

Y in	Sample Time (x 10^{-9} sec)	Peak Ch	g_1	g_2	g_3	U m.p.s.	R	n
0.00	50	8.3	1,809,526	1,814,086	1,808,674	55.890	.8426	0
0.14	50	8.1	1,862,967	1,871,786	1,862,540	58.820	.9538	0
0.34	50	8.6	1,188,920	1,198,082	1,185,625	52.896	.7355	0
0.54	50	9	1,519,819	1,535,182	1,517,868	49.370	.8873	0
0.74	50	10	1,958,961	1,995,215	1,961,062	42.317	1.0615	.0098
0.94	50	12	1,881,406	1,969,513	1,947,838	32.913	4.0649	.4878
1.14	50	15	1,017,496	1,101,621	1,085,324	24.685	5.1620	.6624
1.34	50	23	1,399,223	1,484,346	1,467,995	14.811	5.2060	.6694
1.54	100	15	1,135,238	1,163,374	1,157,029	12.342	4.4344	.5466
1.74	100	21	1,326,797	1,352,703	1,348,311	8.228	5.8985	.7796
1.94	200	18	845,721	894,763	883,140	4.937	4.2194	.5124
2.14	200	28	971,004	997,808	988,486	2.962	2.8753	.2985
2.34	400	18	1,790,202	1,867,347	1,853,996	2.468	5.7782	.7605
2.54	400	22	1,673,799	1,697,417	1,691,540	1.949	4.0187	.4804

TABLE VII (Cont'd)

10.0 mm Diameter Beam (Corrected for Expected Value of $y_{1/2}$ and U_{cen})

DATE: 22 September
L/D = 23.405341
S = 14.8109 x 10^{-6} meters

P_a = 29.1 in of Hg
P_c = 5.32 in of Marriam Fluid
T_c = 73° F

$y_{1/2}$ = 0.88033 in
P/P_o = 0.96159
U_{cor} = 81.367 m.p.s.
U_{cen} = 49.525 m.p.s.

Y in	$\frac{y}{y_{1/2}}$	$\frac{U}{U_{cen}}$	$\frac{y}{y_o}$	$\eta \frac{U}{U_{cen}}$
0.00	0.000	1.129	0.000	0
0.14	0.159	1.188	0.711	0
0.34	0.386	1.068	1.727	0
0.54	0.613	.997	2.743	0
0.74	0.841	.854	3.759	.0084
0.94	1.068	.665	4.775	.3244
1.14	1.295	.498	5.791	.3299
1.34	1.522	.299	6.807	.2002
1.54	1.749	.249	7.823	.1361
1.74	1.977	.166	8.839	.1294
1.94	2.204	.100	9.855	.0512
2.14	2.431	.060	10.871	.0179
2.34	2.658	.050	11.887	.0380
2.54	2.885	.039	12.903	.0187

TABLE VII (Cont'd)

Average Values of the Turbulence Intensities

y/y_o	$\eta\ U/U_{cen}$					
	1.1 mm	0.5 mm	1.0 mm	3.0 mm	5.0 mm	Average
0.000	.0251	.2200	.1455	.1598	.2413	.1583
.711	.0450	.3077	.1687	.1423	.2687	.1865
1.727	.1710	.3256	.2413	.2043	.3924	.2669
2.743	.1850	.3432	.3372	.2851	.4496	.3200
3.759	.1430	.3655	.3065	.2823	.3755	.2946
4.775	.1250	.1674	.2413	.2711	.2529	.2115
5.791	.0750	.1581	.2456	.2315	.2273	.1875
6.807	.0390	.1660	.1301	.1523	.2851	.1545
7.823	.0180	.0971	.0035	.0458	.0975	.0524
8.839	.0060	.0699	.0413	.0072	.0312	.0311
9.855	.0130	.1000	.0362	.0471	.0638	.0520
10.871	.0110	.0250	.0045	.0514	.0406	.0265
11.887	.0100	.0096	.0163	.0315	.0121	.0159
12.903	.0060	.0200	.0055	.0128	.0068	.0102

Vita

Flight Lieutenant Insha Hamid was born on February 15, 1951 in Peshawar, Pakistan, the son of Fida Mohammad Khan. After completing the F.Sc. (pre-engineering) certificate from Edwarde's College, Peshawar, in July 1969, he joined the Pakistan Air Force as a cadet at the College of Aeronautical Engineering, Korangi Creek, Karachi. He graduated from the same college in January, 1974 with a degree of Bachelor of Engineering (With Distinction) in Aerospace Engineering and was commissioned in the Air Force as a Flying Officer. He was assigned various engineering and maintenance jobs in the operational units of the Pakistan Air Force. In May, 1979 he was selected for a master program in aeronautical engineering at the United States Air Force Institute of Technology, Wright-Patterson Air Force Base, Ohio.

Permanent Address: 1636-Kashmiry Street
Gung, Peshawar
Pakistan

(This thesis was typed by Sharon A. Gabriel)

UNCLASSIFIED

SECURITY CLASSIFICATION OF THIS PAGE *(When Data Entered)*

REPORT DOCUMENTATION PAGE	READ INSTRUCTIONS BEFORE COMPLETING FORM
1. REPORT NUMBER: AFIT/GAE/AA/80D-7	2. GOVT ACCESSION NO.: AD-A094 758
	3. RECIPIENT'S CATALOG NUMBER
4. TITLE *(and Subtitle)*: EFFECT OF TEST RHOMBUS SIZE ON PHOTON CORRELATION LASER VELOCIMETER DATA	5. TYPE OF REPORT & PERIOD COVERED: MS Thesis
	6. PERFORMING ORG. REPORT NUMBER
7. AUTHOR(s): Insha Hamid, Flt. Lt. PAF	8. CONTRACT OR GRANT NUMBER(s)
9. PERFORMING ORGANIZATION NAME AND ADDRESS: Air Force Institute of Technology (AFIT-EN) Wright-Patterson Air Force Base, Ohio	10. PROGRAM ELEMENT, PROJECT, TASK AREA & WORK UNIT NUMBERS
11. CONTROLLING OFFICE NAME AND ADDRESS	12. REPORT DATE: December 1980
	13. NUMBER OF PAGES: 124
14. MONITORING AGENCY NAME & ADDRESS*(if different from Controlling Office)*	15. SECURITY CLASS. *(of this report)*: Unclassified
	15a. DECLASSIFICATION DOWNGRADING SCHEDULE

16. DISTRIBUTION STATEMENT *(of this Report)*

Approved for Public Release; Distribution Unlimited.

17. DISTRIBUTION STATEMENT *(of the abstract entered in Block 20, if different from Report)*

18. SUPPLEMENTARY NOTES

Approved for Public Release IAW AFR 190-17

FREDERICK C. LYNCH, Major, USAF
Director of Public Affairs

30 DEC 1980

19. KEY WORDS *(Continue on reverse side if necessary and identify by block number)*

Laser Velocimeter
Test Rhombus Size
Beam Diameter Measurements
Mean Velocity
Turbulence Intensity

20. ABSTRACT *(Continue on reverse side if necessary and identify by block number)*

This thesis provides an experimental evaluation of the effects of test rhombus size on the photon correlation Laser Velocimeters. It also provides a method and results of laser beam expansion and beam diameter measurements. The study was carried out in the turbulent regime of a plane free jet 1 cm by 10 cm.

The flow field measurements were made at 25 jet widths downstream of the nozzle exit, at M = 0.3, using 0.5, 1.0, 1.1, 3.0, 5.0, 7.0 and 10.0 mm diameter laser beams. The measurements taken were mean velocities and turbulence

(Continued on Reverse)

DD FORM 1 JAN 73 1473 EDITION OF 1 NOV 65 IS OBSOLETE

UNCLASSIFIED

SECURITY CLASSIFICATION OF THIS PAGE *(When Data Entered)*

BLOCK 20: Abstract (Cont'd):

intensities which were then compared with the theoretical predictions and earlier experimental results.

The Laser Velocimeter System provided accurate results for mean velocities, but was found to be limited at higher turbulence levels (above 20%) for beam diameters up to and less than 5.0 mm.


DATE
FILMED
8